Clinical Applications of Calixarene based Sodium-Selective Electrodes

by

Suzanne Walsh B.Sc.

Thesis Submitted in Accordance with the Requirements for the Degree of

Doctor of Philosophy

to

Dublin City University

Ollscoil Chathair Bhaile Átha Cliath

School of Chemical Sciences

Supervised by: Dr. Dermot Diamond

September 1997

Declaration:

I hereby certify that this material, which I now submit for assessment on the programme of study leading to the award of DOCTOR OF PHILOSOPHY is entirely my own work and has not been taken from the work of others save and to the extent that such work has been cited and acknowledged within the text of my work.

Signed; Suzanne Walsh

I.D. Number ; 93700334

Date 11/09/1997

For Patricia Walsh

Acknowledgements

There are many people without whose help and support, this thesis could never have been possible.

- Firstly, I would like to thank Dr. Dermot Diamond for his guidance and encouragement over the last few years. Thanks also for the great nights out which wouldn't have been complete without his traditional music.

- I would like to thank Dr. Jim McLaughlin, Dr. Eric McAdams and Dr. Ming Zhou for all their help when I was in Jordanstown. Thanks also to Prof. David Woolfson, Dr. David Jones and Dr. Michael Bonner of Queens University, Belfast.

- Thanks to Dr. Gerry Canny, Dr. Des Kenny and Dr. John Brady of Our Lady's Hospital for Sick Children in Crumlin, for their advice and guidance on the CF project.

- On a more personal level, I must thank my family. I would like to dedicate this thesis to my mother who has supported me throughout everything. To her I owe more than I can ever express in a few lines. Thanks to Noelle and Donal for their love and encouragement. Many other family members including Eileen, Jim, Frances, Gertrude et al., deserve much thanks for their support both financially and otherwise.

- To Lester and Virginia Russell I would like to express my appreciation for all that they have done for me and my family.

- DCU Postgrads cannot be forgotten so I would like to thank all of them for their friendship and help. Thanks to Siobhan and Gemma for all the chats and good times over the years. Thanks to Patxi for getting me started, explaining things over and over again and being a friend throughout my research. Thanks to everyone in WG30, to Shane and Fran in J207 and our neighbours in J208.

- Several other friends also deserve a mention. John, Karen and Clodagh have always encouraged me and listened to my moaning and complaining when things were not going smoothly. Thanks to my friends in Belfast including the Postgrads in NIBEC and also to Sandra, Colin and Kerri for making my stay there so memorable.

List of Publications Presentations and Awards.

Publications :

1. S. Walsh and D. Diamond.
Talanta, 42 (1995) 561.

Non-linear Curve Fitting using Microsoft EXCEL Solver.

2. S. Walsh, F.J. Sáez de Viteri and D. Diamond.
Anal. Proc. Inc. Anal. Comm., 32 (1995) 365.

Analysis of Blood Sodium using Flow Injection Analysis with a Calix(4)arene Potentiometric Detector.

3. S. Walsh, D. Diamond, J. McLaughlin, E. McAdams, D. Woolfson, D. Jones and M. Bonner.

Accepted for publication in Electroanalysis.

Solid-State Sodium Selective Electrodes based on Screen Printed Ag/AgCl Reference Electrodes.

Presentations and Awards :

1. Poster Presentation at the 6th European Conference on Electroanalysis (ESEAC 96) held at the University of Durham from 25-29 March 1996.

Title : *Solid-State Sodium Selective Electrodes based on Screen-Printed Ag/AgCl Reference electrodes.*

Received prize from EG&G Instruments Ltd. for the best postgraduate poster presented.

2. Poster Presentation at the 1996 Royal Society of Chemistry postgraduate research colloquium held in the University of Limerick from 5-7 June 1996.

Title : *Solid-State Sodium Selective Electrodes based on Screen-Printed Ag/AgCl Reference electrodes.*

Received AGB gold medal for poster presentation.

Contents

Chapter 2 : *Characterisation of Ion-Selective Electrodes.*

Chapter 3 : ***Development of a Flow Injection Analysis System for the determination of Sodium in Blood samples.***

Chapter 4 : ***Solid-State Sodium Selective Sensors based on Screen Printed Ag/AgCl Reference Electrodes.***

Chapter 6 : *Computational Methods.*

Abstract

Since their beginnings in the late 1960's ion-selective electrodes have rapidly become one of the most important types of chemical sensor. They are commercially available for a large variety of ions, are widely used and have been characterised thoroughly by many investigators. Having attained this level of sophistication, research in this area today is often directed towards novel applications of such sensors. This thesis represents a study of certain clinical applications of sodium-selective electrodes.

As ion-selective electrodes possess the ability to directly sense analytes, they are well suited to whole blood, plasma and serum critical analyte testing. These critical analytes are major electrolytes, blood gases and some metabolites. Analysers based on ion-selective electrodes can provide fast turn-around time for critical care testing. With this in mind, a flow injection analysis system has been developed for the determination of sodium in blood samples. Here, the advantages of flow injection analysis and potentiometric detection were combined with those of computer control, to produce a blood analyser which has the potential to be user friendly, analytically reliable, portable and applicable to continuous monitoring.

Following this research, our attention turned to solid-state devices. Here, one opens up the possibility of mass fabrication of miniature, disposable, planar electrodes. Our efforts concentrated on the development of a potentiometric device, consisting of a solid-state sodium selective electrode and a solid-state chloride electrode. The device is based on a combination of screen printed Ag/AgCl electrodes and an ion-selective PVC membrane electrode. It was developed for use as a screening tool for Cystic Fibrosis, utilising the raised sodium level in sweat, which is a diagnostic indicator for the condition.

Theory of Potentiometry and Ion-selective Electrodes

1.1 Introduction.

Analytical Potentiometry involves deducing the concentration and/or activity of an analyte species from the potential difference measured between a selective electrode and a reference, such as a silver/silver chloride electrode. Ion-selective electrodes (ISEs) have the unique ability to sense and respond to changes in ion activity, which has led to their use in many industrial and clinical applications[1,2]. They are especially useful where an analytical technique is needed which is convenient, accurate, fast and inexpensive. For example, many ions that occur in vegetation, fruits, juices and oils can now be analysed with ion-selective electrodes. Several nitrate sensors are now commercially available, one being the Orion 92-07 liquid ion exchanger nitrate ISE which was first marketed in 1968[3]. In the food industry, ISEs have been used for estimating chloride and fluoride in milk[4,5] , sulfide in beer[6], sulfur dioxide in wine[7], sodium in smoked bacon[8], amongst others. Nitrogen oxides in air, exhaust gases and cigarette smoke[9,10,11], fluoride in air and stack gases[12] as well as sulfur dioxide in flue gases[13] have been monitored with ion-selective electrodes. They have also been successfully applied in water quality monitoring[14]. Here one major advantage of ISEs is the fact that they are not affected by colour or turbidity of samples. In the medical field, ISEs are used for the routine monitoring of pH and important blood electrolytes such as sodium, potassium and fluoride[15,16]. Many biological fluids are complicated mixtures of ions whose composition may vary considerably with respect to time. Ion-selective electrodes respond rapidly to ion activities and therefore are likely to develop further in the medical field where life processes are related to activities and not concentrations.

1.2 Potentiometry[17].

As mentioned previously, Analytical Potentiometry involves the measurement of a cell potential arising from spontaneous processes occurring at an ion-selective electrode and a reference electrode, from which the activity of an ion may be derived.

Activity and concentration.

Activity is defined as the effective concentration of an ion in the presence of an electrolyte and is defined by

$$a_i = c_i f_i \qquad \textbf{(1.1)}$$

a_i = The activity of ion i.

c_i = Concentration of ion i.

f_i = Activity coefficient.

The activity coefficient is a function of the total electrolyte concentration of the solution which is defined by ionic strength (I).

$$I = 0.5 \sum c_i z_i^2 \qquad \textbf{(1.2)}$$

I = Ionic strength.

z_i = Charge on each ion.

A theoretical expression known as the Davies equation[18] allows the calculation of activity coefficients in solutions of ionic strength up to approximately 0.6. The activity coefficient varies with the total number of ions in the solution and with their charge and it is basically a correction for inter-ionic attraction. In dilute solutions ($< 10^{-4}$ M), the activity coefficient of a simple electrolyte is near unity and activity is approximately equal to concentration. As the concentration of an electrolyte

increases, the activity coefficient generally decreases and the activity becomes less than the concentration.

$$-\log f_i = 0.5 z_i^2 \left[\frac{I^{1/2}}{1 + I^{1/2}} - 0.2I \right] \qquad \textbf{(1.3)}$$

In a potentiometric type of sensor, a membrane or sensing surface acts as a half cell generating a potential proportional to the logarithm of the analyte **activity**. This potential is measured relative to an inert reference electrode which ideally has a constant potential at a particular temperature, which is unaffected by changes in the sample composition. Therefore the potential difference is dependent only on the changes occurring at the ISE half cell and can be attributed to changes in analyte activity.

1.3 Ion Selective Electrodes[19].

Ion-selective electrodes (ISEs) are electrochemical sensors that allow potentiometric determination of the activity of certain ions in the presence of other ions. None of these electrodes is specific for any one ion, but each will possess a certain selectivity toward a given ion or ions. An ISE constitutes a galvanic half cell, consisting of an ion-selective membrane, an internal contacting solution or a solid contact and an internal reference electrode. The other half cell is given by an external reference electrode. The contact between the two half cells is maintained by a salt bridge in the form of an electrolyte within the reference electrode housing.

1.3.1 Potentiometric response of ion-selective electrodes.

Figure 1.1 shows the basic arrangement for potentiometric measurements involving ion-selective electrodes. The potential difference between the two electrodes is measured using a high input impedance voltmeter. The high input impedance ($> 10^{12}$ Ω) swamps the cell resistance. Hence the flow of electrons and therefore current becomes negligible. As the voltage drop across the meter is therefore effectively zero, the voltage recorded may be ascribed directly to the electrochemical cell.

Figure 1.1 : Typical ion-selective electrode set-up for potentiometric measurements.

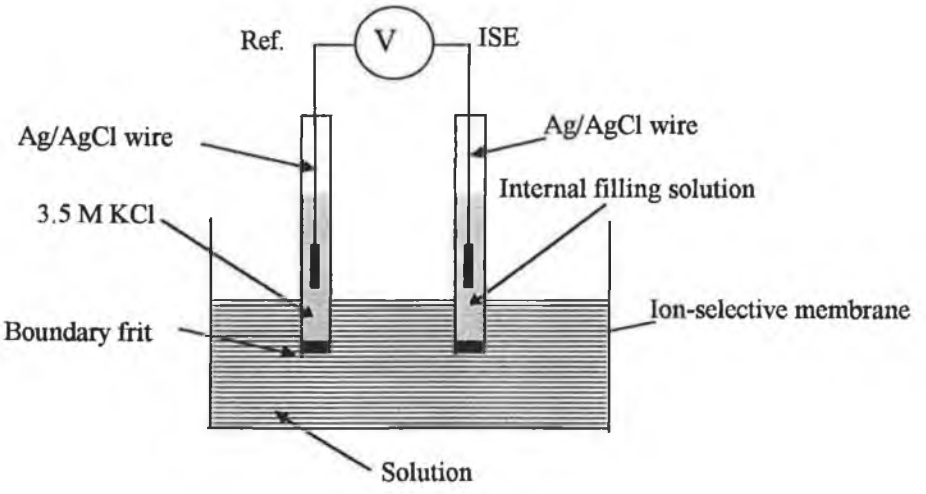

The overall cell potential may be represented;

$$E_{cell} = E_{ise} - E_{ref.} \qquad \textbf{(1.4)}$$

Where E_{cell} = The overall cell potential.

E_{ise} = Ion-selective electrode potential.

$E_{ref.}$ = Reference electrode potential.

In reality, the cell emf is composed of several local potential differences arising at solid-solid, solid-liquid and liquid-liquid interfaces. The major contributors to the cell potential are the membrane potential, the reference electrode potential and the junction potential. These contributions will be discussed later.

There is a relationship between the electrode potential of a galvanic cell and ion activity. This relationship, described by the Nernst equation may also be applied to ion-selective electrodes. For example, consider an electrode selective for a particular ion i, of charge z_i and activity a_i, then;

$$E_{ise} = E^0 + 2.303\frac{RT}{z_i F}\log a_i \qquad \textbf{(1.5)}$$

for R, T and F being the gas constant, absolute temperature and Faraday's constant respectively. E^0 is the standard electrode potential and should remain constant during use. Standard electrode potentials are assigned to half reactions and are calculated with respect to the standard hydrogen electrode (E^0 = 0V at 298K and 1 atm pressure). If the constants are multiplied into equation 1.5, it becomes clear that a change of one unit in the logarithmic term changes the value of the potential by $59.16/z_i$ mV. A system which behaves in this manner is said to be responding in a Nernstian fashion to changes in analyte activity.

1.3.2 Reference electrodes[20,21].

A reference electrode is an oxidation-reduction half cell of known and constant potential at a particular temperature. In this research the reference electrode used was the silver/silver chloride reference, which was first described by H. Jahn in 1900[22]. It has since been further developed not least in the replacement of Jahn's internal potassium cyanide solution with potassium chloride.

For a reference electrode incorporating a salt bridge, the main requirement is that it provides a stable liquid junction potential[23,24]. This liquid junction potential limits the accuracy of potentiometric measurements. The potential may be positive or negative

and arises from the unequal diffusion of the ions on each side of the boundary due to differences in ionic mobilities of the positive and negative ions which make up the bridge electrolyte.

A typical junction would be a sintered glass or ceramic frit, with two different solutions either side of it. The role of the junction is to provide an electronically conducting pathway between the ion-selective electrode (ISE) and the reference half cell, whilst functioning as a salt bridge. In potentiometry, one measures the cell emf, which includes a contribution from the reference electrode junction potential, the reference half cell potential and the ion-selective electrode potential. If the change in potential observed on changing sample solutions is to be attributed to the ion-selective electrode response, so that it may be related to analyte concentration, then contributions from the reference electrode must remain constant. The reference half cell potential is usually unaffected by transferring between solutions so the only other variable is the junction potential. Therefore, in order that the reference electrode fulfil its responsibilities, changes in the liquid junction potential must be reduced below the limits of significance. In a reference electrode the boundary frit is kept small to prevent bulk mixing of salt bridge and sample ions. The use of these small areas of contact means that the susceptibility to clogging can be high which causes stability problems. For this reason the junction material should have the following properties; low electrical resistance, low leakage rate of ions into the sample, no permeability of ions from sample to internal reference electrode element, the capability of using larger contact areas, resistance to temperature and pressure fluctuations and resistance to interference by troublesome samples such as blood. The junction potential is less if a concentrated bridge solution of ions that have nearly the same mobilities is used. For this reason KCl is commonly used in reference electrodes as the transference numbers for K^+ and Cl^- are almost the same at 0.49 and 0.51 respectively (when the filling solution is 3.5 M and the external electrolyte 0.1 M KCl).

The silver/silver chloride electrode works on the basis of the following reaction.

$$AgCl_{(s)} + e^- \rightleftharpoons Ag_{(s)} + Cl^-_{(aq)} \qquad \textbf{(1.6)}$$

$$E = E^0_{Ag/AgCl} + S\log a_{Cl^-} \qquad \textbf{(1.7)}$$

E^0 = Standard electrode potential (E^0 = 0.22V)*.

S = Electrode slope (mV/decade).

The exchange of electrons between the silver and silver chloride coupled with an exchange of Cl^- ions with the internal electrolyte provides the reference electrode with a constant potential. A slow diffusion of ions into the sample solution results in a stable liquid junction potential and an electronically conducting pathway between the ion-selective electrode and the reference half cell.

1.3.3 Theory of membrane potentials.

The phase boundary potential or Donnan potential.

An interface between two liquid or solid phases represents a potential generating system. The phase boundary potential arises mainly from the non-uniform distribution of electrically charged species between two phases. In real electrode systems various charge carriers are simultaneously involved in interfacial processes. However, the selectivity of ion-selective electrodes ensures that the transfer reactions are dominated by certain ions.

Virtually all ion-selective membrane electrodes exhibit reversible behaviour. The rate of electron transfer is fast in comparison to mass transport. In other words, ions traverse the membrane surfaces in rapid equilibrium. Both chemical and electrical potential contributions must be taken into consideration when describing ion transport or distribution. In ion-selective electrodes, phase boundary potentials arise between the ion-selective membrane and the internal filling solution and also between the membrane and the external sample solution. For an ion i of charge z_i exchanging

---

* Standard electrode potential quoted in CRC handbook of Physics and Chemistry, 77th edition, CRC Press Inc., 1996.

reversibly across such an interface, the work done in establishing equilibrium can be described by;

$$-\Delta G = z_i F E_B \qquad \textbf{(1.8)}$$

E_B = Boundary potential.

ΔG = Change in Gibbs free energy.

F = Faraday constant.

The change in Gibbs free energy is described as the difference between the partial molar free energy (μ_i) of the ion in the membrane (m) and aqueous (aq) phases.

$$-\Delta G = \mu_{i(aq)} - \mu_{i(m)} \qquad \textbf{(1.9)}$$

Under standard conditions of unit ion activities the change in Gibbs free energy is given by;

$$-\Delta G^0 = \mu^0_{i(aq)} - \mu^0_{i(m)} = z_i F E^0_B \qquad \textbf{(1.10)}$$

and the standard state ^{0} is related to other states by;

$$\mu_i = \mu_i^0 + RT \ln a_i \qquad \textbf{(1.11)}$$

By substituting into Equation 1.9: $-\Delta G = \mu^0_{i(aq)} - \mu^0_{i(m)} + RT \ln\left(\frac{a_{i(aq)}}{a_{i(m)}}\right)$ **(1.12)**

The electrical potential at the interface is given by;

$$E_B = \left(\frac{\mu^0_{i(aq)} - \mu^0_{i(m)}}{z_i F}\right) + \frac{RT}{z_i F} \ln\left(\frac{a_{i(aq)}}{a_{i(m)}}\right) \qquad \textbf{(1.13)}$$

Because E_B^0, the standard potential = $\frac{\left(\mu^0_{i(aq)} - \mu^0_{i(m)}\right)}{z_i F}$, the boundary potential at any particular membrane interface is given as a function of the activity ratios of exchangeable ions between the membrane surface and the aqueous solution.

$$E_B = E_B^0 + \frac{RT}{z_i F}\ln\left(\frac{a_{i(aq)}}{a_{i(m)}}\right) \qquad \textbf{(1.14)}$$

Because there are two interfaces, external ′ and internal ″, the complete equation for describing the phase boundary potential must include contributions from each;

$$E_B'' - E_B' = E_b^{0''} - E_B^{0'} + \frac{RT}{z_i F}\ln\left(\frac{a_{i(aq)}'' a_{i(m)}'}{a_{i(aq)}' a_{i(m)}''}\right) \qquad \textbf{(1.15)}$$

Assuming that the activity of ion i in the membrane, is the same at both interfaces(i.e. $a_{i(m)}' = a_{i(m)}''$, then;

$$E_B'' - E_B' = E_B^{0''} - E_B^{0'} + \frac{RT}{z_i F}\ln\left(\frac{a_{i(aq)}''}{a_{i(aq)}'}\right) \qquad \textbf{(1.16)}$$

Diffusion Potential.

The diffusion potential is produced by the diffusion of ions within the membrane. Even though the membrane is considered to be a uniform phase, the free energies of the different membrane components undergo variation with space and time and this results in diffusional fluxes of ions within the membrane. A membrane diffusion potential then develops to maintain a zero net current state.

The diffusion potential may be represented by the Henderson equation;

$$E_D = \left[\left(\frac{\left(\sum z_i u_i a_i\right)' - \left(\sum z_i u_i a_i\right)''}{\left(\sum z_i^2 u_i a_i\right)' - \left(\sum z_i u_i a_i\right)''}\right) \times 2.303\frac{RT}{F}\log\left(\frac{\left(\sum z_i^2 u_i a_i\right)'}{\left(\sum z_i^2 u_i a_i\right)''}\right)\right] \qquad \textbf{(1.17)}$$

u_i = Mobility of membrane component i.

Z_i = Charge on membrane component i.

a_i = activity of membrane component i.

(') and (") = The inner and outer membrane boundaries.

If one considers a membrane of thickness D and assumes that there is a negligible drop in primary ion activity across the membrane ($a_i' = a_i''$) and there is practically no penetration of the membrane by interfering ions then according to equation 1.17 the diffusion potential is approximately zero. Therefore the total membrane potential is overwhelmingly determined by the phase boundary potentials.

1.4 The Components of the Ion-selective Membrane.

1.4.1 Ionophore.

Ionophores are lipophilic complexing agents with the ability to reversibly bind ions and transport them across organic membranes by carrier translocation. Among the ionophores, the electrically neutral ones have found a particularly wide field of application as components in ion-selective electrodes[25]. Neutral carrier ionophores are uncharged lipophilic molecules capable of selectively transporting metal ions across a hydrophobic membrane. The first reference to neutral carriers was made by Moore and Pressman in 1964[26]. In this case the molecule involved was a neutral carrier antibiotic, Valinomycin. Although not studied in the context of ion-selective electrodes by Moore and Pressman, it was not long before the analytical potential of these molecules was recognised. Valinomycin has an electron rich pocket into which K^+ ions are selectively extracted. The first membrane electrodes incorporating Valinomycin were studied in 1966 by W. Blaedel et al.[27]

Other molecules which are finding increasing application as neutral carrier ionophores are the calixarenes[28,29]. Calixarenes are a group of macrocyclic phenol-formaldehyde condensates. The term calixarene was coined in 1975 by David Gutsche[30], who perceived a similarity between the shape of a Greek vase called a calix crater and the molecular model of the above cyclic condensates. The "arene" term refers to the

presence of aryl groups, the number of which is denoted by [n] in calix[n]arene. The general structure of a calixarene is shown in figure 1.2.

Figure 1.2; General structure of a calixarene.

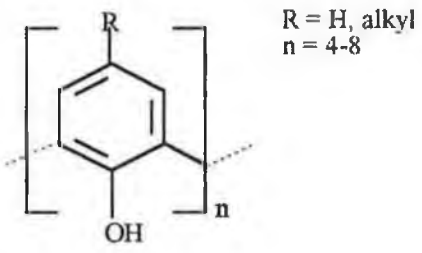

Two calixarenes were used throughout this research as ionophores[31,32]. Both were calix[4]arenes i.e. cyclic tetramers. Evidence for different conformations of these calix[4]arenes was found via x-ray crystallography[30], and the possible conformers have been confirmed as, cone, partial cone, 1,2 alternate and 1,3 alternate. These are shown in figure 1.3.

Figure 1.3; Possible conformers of a calix[4]arene.

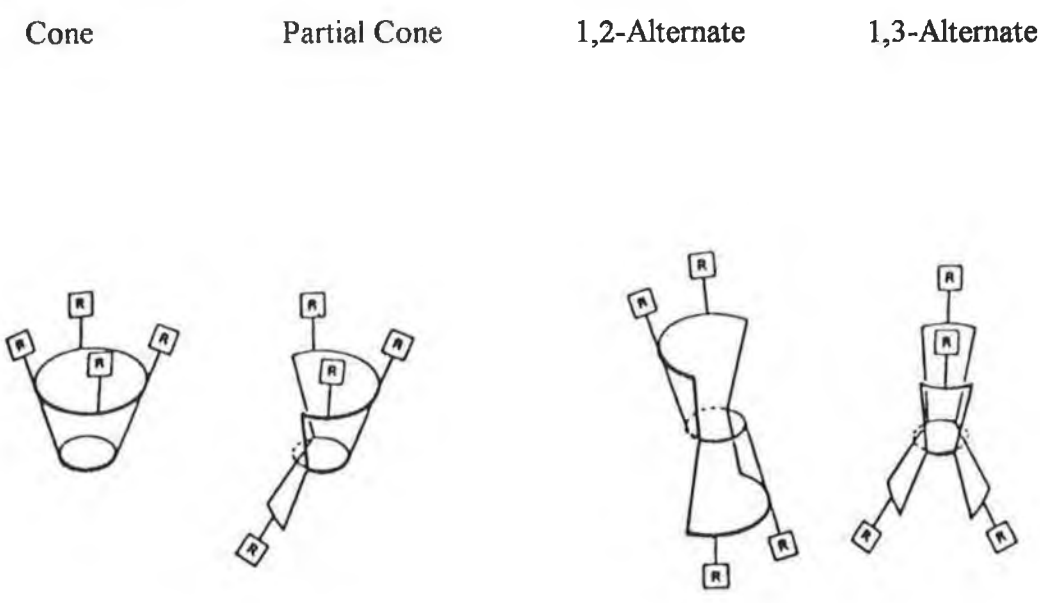

In solution it is known that the calixarenes can change from one conformation to another. In doing so the aryl group rotates so that the phenolic hydroxyl group passes through the centre of the molecule. By replacing the hydrogen with a larger group, rotation becomes more restricted preventing a conformational change. Therefore, "fixing" the calixarene will create a cavity of constant size. Functional group modification of the calixarene allows the selectivity of the host-guest interaction to be controlled. The tenacity of the interaction which occurs between alkali metal cations and certain modified calixarenes is determined by the overall macrocyclic structure, mostly the cavity size and the nature of the functional groups which act as the binding sites within the molecule. It has been shown that while the cavity size is the most influential factor in determining electrode selectivity, considerable fine tuning of the selective response is possible by variation of the pendant groups attached to the phenolic oxygen atoms of the parent calixarene. The calix(4)arenes used in this research are shown in figures 1.4a and b[♦] .

♦ Energy minimised structures were calculated via molecular modelling which was performed by P. Kane at Dublin City University, using Hyperchem 4.0.

Figure 1.4a; Tetra methoxy ethyl p-t butyl calix(4)arene tetracetate[31].

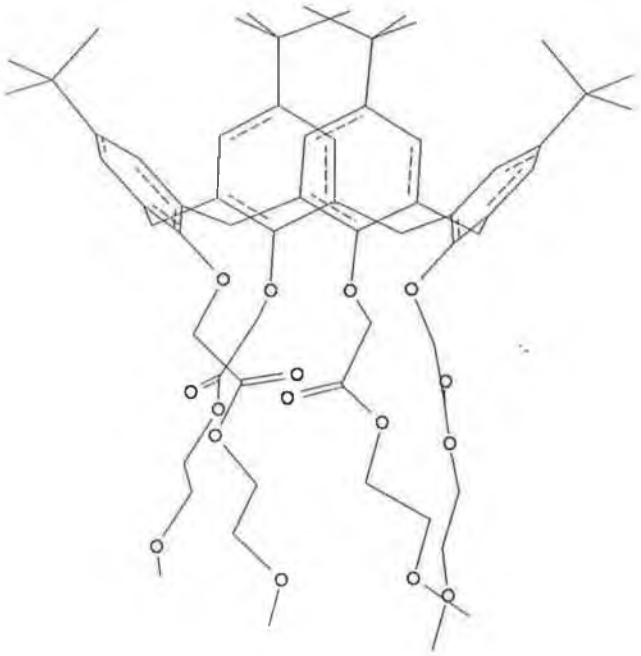

Figure 1.4b; Crown ligand Cone 5b:ET[32].

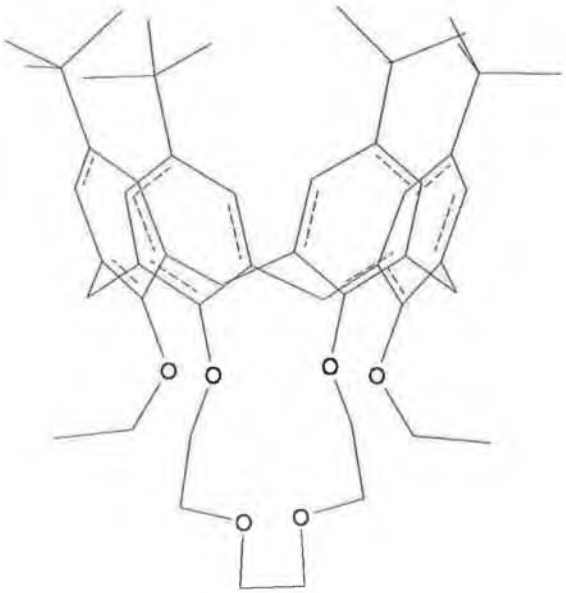

1.4.2 Ion-Exchanger.

The ion-exchanger, otherwise known as the anion excluder serves to repel sample anions from the membrane phase of cation selective electrodes. It also boosts the cation selectivity for singly or multiply charged ions, by increasing the membrane polarity and reducing the membrane resistance. Added sites reduce the interference of lipophilic counter anions[33], decrease the electrical resistance of the membrane bulk[34], shorten response times, help control the ion selectivity and lower the activation barrier for the primary ion transfer at the solution | membrane interface[35]. In effect, the slope, drift and general stability of the electrode can be improved. A commonly used ion-exchanger is Potassium tetrakis 4-chloro phenyl borate (KTpClPB). Tetra phenyl borate ions are highly lipophilic and so are trapped within the organic phase by virtue of their poor water solubility. Variation in the amount and type of ion-exchanger has a significant effect on the membrane selectivity. This will be discussed later in section 1.4.6.

1.4.3 Plasticiser.

The Plasticiser used throughout this research was 2-nitrophenyl octyl ether (2-NPOE).

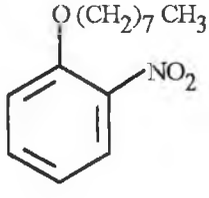

2-Nitrophenyl Octyl ether

This organic compound was included in the membrane to act as a plasticiser for the poly(vinyl chloride), (PVC) polymeric support. It also functions as a solvent for the ligand. The type of plasticiser used effects the polarity of the membrane. If the

polarity of the membrane is increased, a preference for divalent ions over monovalent ions is exhibited. 2-NPOE has a higher dielectric constant making it one of the more polar plasticisers.

1.4.4 Matrix support.

PVC is typically used as a support matrix for liquid membranes. Its main functions are to give mechanical strength to the membrane and immobilise the sensing agent. PVC also reduces the leaching of sensing agent and plasticiser by virtue of its hydrophobic nature. Despite this, reduction in the operative lifetimes of PVC based systems is principally caused by the loss of active components from the polymer matrix, especially at the membrane | solution interface.

1.4.5 Selectivity.

Equation 1.5 describes the potentiometric response of an ion-selective electrode responding to changes in activity of the primary ion i. In practice an ideal electrode behaviour such as that described in equation 1.5 can usually not be attained. One has to consider additional contributions to the total measured activity that result from the presence of interfering ions j in the sample matrix. The effect of interfering ions on the electrode potential is described by the semi-empirical extension of the Nernst equation known as the Nikolskii-Eisenmann equation.

$$E_{ise} = E_i^0 + S\log\left(a_i + \sum K_{ij}^{pot} a_j^{z_i/z_j}\right) \qquad \textbf{(1.18)}$$

Where

K_{ij}^{pot} = The potentiometric coefficient of the electrode against the j^{th} interfering ion.

a_j = The activity of any interfering ion j.

z_i and z_j = The charges on the analyte (i) and any interfering ion (j).

$\sum K_{ij}^{pot} a_j^{z_i/z_j}$ = The net contribution of all interferents.

Therefore it may be deduced that the most useful ISE's are those that are selective against a wide range of common interfering ions. The summation factor $\sum K_{ij}^{pot} a_j^{z_i/z_j}$ then tends to zero and changes in the electrode potential may be related with confidence to variations in the analyte activity via the Nernst equation.

1.4.6 The effect of membrane additives on the potentiometric response.

Ionophore selectivity is only one of the crucial parameters determining the performance of neutral carrier ion-selective electrodes. The effect of the lipophilicity of the ligand, plasticiser and the presence of lipophilic salt additives has been studied by Simon et al.[35] Their research has shown that leaching of the plasticiser from the membrane will finally result in an increase in membrane resistance and loss of ion sensitivity. For this reason plasticisers of higher lipophilicity are to be favoured. It was also shown that electrode performance depends strongly on the amount of ionic sites trapped within the membrane phase. Some of these sites have been introduced deliberately in the form of ion exchangers as mentioned in section 1.4.2, while others are introduced as impurities associated with membrane components. Membranes which do not have ligands added have been shown to behave as low level ion-exchangers[36]. This cation permselectivity has been attributed to the impurities associated with membrane components. For example, commercially available plasticisers 2-NPOE and dioctyl sebacate have been shown to have impurity concentrations high enough to lead to small emf responses. Van den Berg et al. have suggested that the anionic sites may arise from ionic components of the PVC polymer[37] such as polymer bound initiating groups (e.g. RSO_3^- groups probably are present in the PVC which were generated by a persulfate anion radical initiator). These sites are thought to be present in the form of emulsifier residues and are not bound to the polymer matrix. The possibility that carboxyl groups attached to the PVC might provide immobile anionic groups in PVC was also investigated, but a comparison of the bulk resistivity of COOH-PVC, (carboxylated PVC with 1.4 wt %

COOH) with that of high molecular weight PVC caused this theory to be rejected as the difference in resistivity observed was not significant[37]. Other researchers, for example Thoma et al have taken a different approach to explaining cation permselectivity[38]. They assumed that there are no impurities in the membrane capable of ion exchange. Their ion-exchange theories are based on water clusters. Solvent polymeric membranes are susceptible to water uptake and water permeability. Therefore it was reasoned that the dominant anions in the membrane originate from proton exchange reactions involving water. These reactions stem from the OH^- formed by;

$$X^-_{(aq)} + H_2O_{(m)} \rightleftharpoons X^+_{(m)} + OH^-_{(m)} + H^+_{(aq)} \qquad \textbf{(1.19)}$$

for X^+ being the analyte ion. The OH^- ions were thought to be immobilised in water clusters within the organic phase while the protons diffused away into the aqueous phase. The mobility of these anionic sites is likely to be low. One major flaw in this theory is that it is assuming that ion exchange sites could only be created once diffusion of analyte into the membrane phase took place. This is unlikely as AC impedance experiments performed by Horvai et al. suggest otherwise[39]. It was shown that the charge trapping cannot be caused exclusively by spontaneous water droplet formation. Little change in resistance measurements was noted when the hydrophilic areas were removed by filtration.

However, it must be noted that the effect of impurities on electrode performance becomes negligible when ionic sites are deliberately added in the form of ion exchangers such as KTpClPB. Nowadays the inclusion of ion exchangers in the membrane can be taken for granted. This will guarantee the fast exchange of charge carriers between the electrode and the aqueous phase necessary to provide stable and reproducible potentiometric responses.

Another effect of additives is on the water distribution within the membrane[40]. The surface region of plasticised PVC can be highly enriched in water relative to the bulk and this effect is strongly dependent on the additives present in the membrane. Harrison et al. have shown that water uptake in PVC based membranes occurs as a two stage process with an initial rapid uptake associated with water freely dissolved in

the membrane matrix[41]. During this step, water transport obeys Ficks laws of diffusion. A second much slower stage then begins that is associated with the formation of light scattering centres. Using NMR it was shown that these centres are due to the formation of water droplets within the polymer matrix[42]. Experiments show that the water distribution within the membrane does not necessarily become uniform, even after many days soaking. Instead a water rich surface region develops, the thickness of which depends on the nature and concentration of additives in the membrane. It has been proposed that the absorption of substantial amounts of water in polymers arises due to the inclusion of salts and is driven by osmotic forces. Thomas et al. used this assumption to explain water uptake in polymers[43]. It is generally accepted that water diffuses through the membrane phase in which it is slightly soluble and forms droplets of saturated aqueous solution at impurity sites containing water soluble salts. Equilibrium water uptake is reached when the osmotic pressure difference between the droplet solution and the external solution balances the restraining elastic stresses acting on the droplet. Therefore it seems to be driven by osmotic pressure. The equilibrium water content of membranes was shown to increase with salt content. Also changes in the membrane plasticiser or plasticiser content, as well as the casting solvent evaporation conditions, were shown to adjust water uptake rates[44,45].

It can be concluded that only the careful selection of each membrane component will guarantee a highly selective and sensitive electrode which will exhibit a stable and reproducible potential response.

1.5 Solid-State Electrodes.

A major stumbling block impeding the further development of ion-selective electrodes has been the requirement for an internal reference electrolyte solution (part 3 in figure 1.5). The role of this electrolyte is to stabilise the internal reference potential at the internal reference electrode (almost always an Ag/AgCl electrode) and to stabilise the internal boundary potential of the ion-selective membrane, which for the electrodes

studied in this research is a poly(vinyl chloride) (PVC) membrane with the sensing agent dispersed in the plasticiser. In addition, the electrolyte provides mobile charge carriers (hydrated ions) which enable charge to pass through the bulk solution. In order to stabilise these potentials the internal electrolyte is almost always a chloride (stabilises the Ag/AgCl potential) and the cation is that for which the ligand in the PVC is selective (stabilises the internal PVC membrane boundary potential).

The situation is summarised in figure 1.5. In this case we are using a sodium selective ligand dispersed in PVC. Thus sodium ions are exchanged at the sample/PVC boundary and the mobile Na-ligand complexes provide charge transfer across the PVC membrane (4) to the internal electrolyte (3). Na^+ ions are thus able to exchange freely at the internal PVC/electrolyte boundary, while the Cl^- ions can exchange at the Ag/AgCl electrode, coupled with an exchange of electrons between the AgCl (2) and Ag (1) phases of the internal reference electrode.

Figure 1.5; The charge transfer process occurring in a conventional electrolyte filled Na^+ selective electrode.

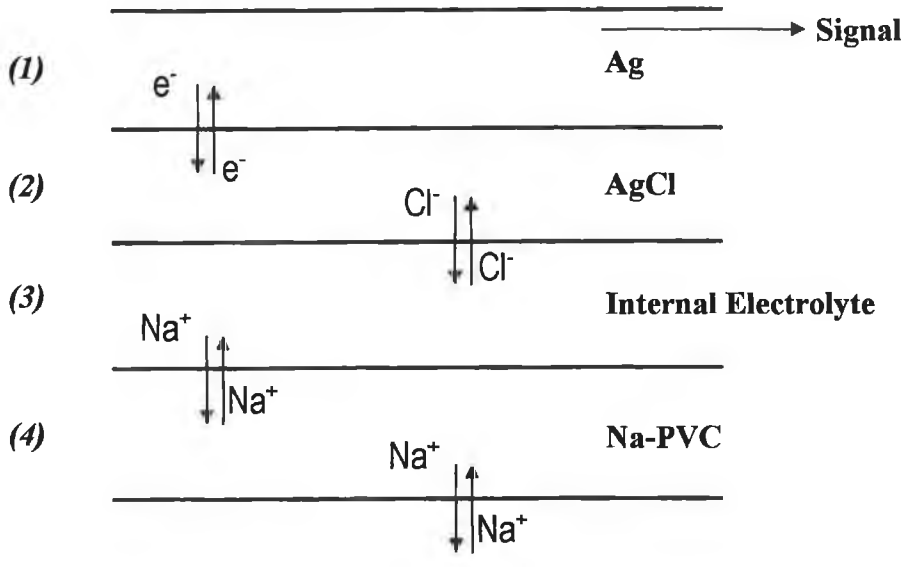

While the use of an internal electrolyte is an elegant solution to the electrochemical problem of providing stable reference potentials it requires that the electrode be used in an upright position unless a gel-filled configuration is used, limits miniaturisation prospects and prevents the development of mass produced planar ion-selective electrodes. Hence there is great interest in solid state versions of these sensors[46,47,48].

The first solid state ion-selective sensors were coated wire electrodes (CWEs). These were first described by Cattrall and Freiser in 1971[49]. They consist of a film of a suitable polymeric matrix substrate (such as the ligand doped PVC already mentioned) dip cast onto a substrate such as a metal or Ag/AgCl wire[50,51]. In coated wire electrodes the cell configuration may be written;

Internal reference electrode | ion-selective membrane | sample solution | external reference electrode.

This arrangement has met with considerable critical comment. The main issue has been the nature of the processes which might operate at the internal reference | membrane interface to maintain this junction at constant potential. Figure 1.6 illustrates this problem schematically. As with the conventional electrolyte filled electrode shown in figure 1.5, the PVC membrane (3) can exchange Na^+ ions with the sample solution but there is no mechanism for exchange of charge at the internal membrane boundary and the AgCl reference element (2). This interface is termed "blocked" because a continuous flow of charge is not possible.[52,53]

Figure 1.6; The charge transfer processes occurring in a solid-state Na^+ selective PVC membrane electrode with no un-blocking mechanism at the interface between the Ag/AgCl electrode and the PVC membrane.

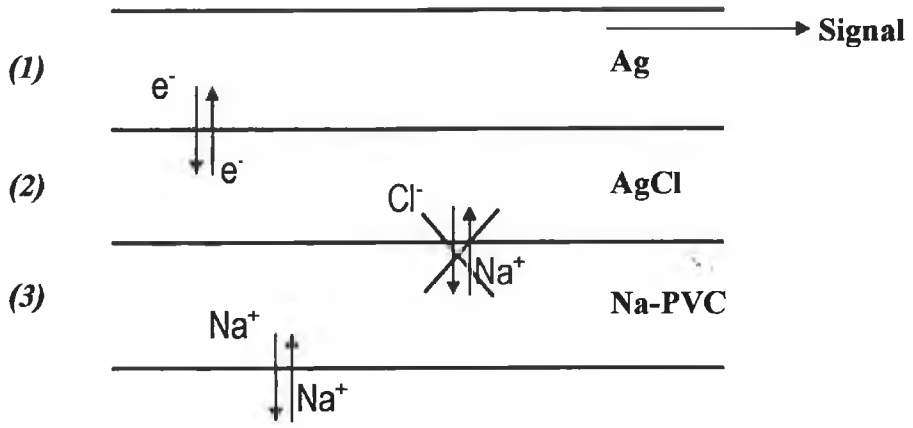

In a conventional ion-selective electrode, the membrane composition near the internal reference solution remains practically constant, controlled by the composition of this internal electrolyte. The composition of the membrane near the sample solution will reflect the exchange behaviour of ions at this interface. For coated wire electrodes, the equilibrium composition of the membrane will be determined only by the behaviour of ions at the sample | membrane interface. No ionic concentration gradient will develop across the membrane and therefore there will be no diffusion potential. This suggests that once at equilibrium the selectivity of coated wire devices may possibly be superior to that of traditional ion-selective electrodes. However it also means that this selectivity will depend on the length of time the electrode is allowed to condition as it will take a certain amount of time for the system to equilibrate. The lack of a stabilising internal reference electrolyte may also mean that coated wire electrodes are more prone to drift associated with the leaching of reagents into the sample solution. It has been shown that the potential observed for CWEs depends on the mole fraction of lipophilic ions present in the membrane[54]. Ion-selective PVC membranes will absorb water to a substantial extent. In conventional electrodes, with an aqueous internal reference, the water content of the membrane will remain

essentially constant. As the membrane of a coated wire electrode absorbs water the mole fraction of lipophilic ion in the membrane will alter and the potential of the electrode will drift until the membrane becomes saturated with water. Despite many reservations, the large number of reports detailing the successful construction and application of coated wire electrodes indicates that they can work satisfactorily. Therefore many researchers have turned their attentions to devise a model to explain the mechanism behind the electron or ion exchange occurring at the internal reference | membrane interface. One such attempt was made by Cattrall et al[55]. In this case, a calcium selective electrode with a platinum internal reference was studied. It was suggested that an oxygen electrode was set up at the interface. Schindler et al[56] observed the dependence of the potential of a Valinomycin electrode on oxygen partial pressure and showed how the potential shifted to more negative values when oxygen was replaced with hydrogen. However, others have claimed that the oxygen electrode is not very reversible and therefore is unlikely as such to provide the equilibrium needed to maintain a stable internal potential. Another possible theory involves oxidisable impurities in the membrane. Tetrahydrofuran is a solvent commonly used for casting PVC membranes. Because of problems with peroxide formation on storage of THF, the solvent is frequently supplied with a percentage of a stabiliser, e.g. 0.1% hydroquinone. Hydroquinone is well known as one half of the reversible couple in the classical quinhydrone electrode used for pH measurement. A quinhydrone electrode consists of a smooth platinum wire dipped in a solution saturated with quinhydrone. The properties of this half cell can be related to that of a hydrogen electrode[57]. It has been proposed that residual hydroquinone in the membrane is oxidised at the reference | membrane interface by oxygen dissolved in the membrane. In this way a stable internal reference potential develops, so long as the pH within the membrane remains stable.

During the late 1970's conductive epoxy based ion-selective electrodes began to develop. Epoxy resins[58] are produced by cyclopolymerisation of suitable epoxide compounds with phenols and the addition of hardening catalytic or co-reactive agents such as polyamines, which promote further cross-linking between the residual epoxide groups. The addition of fillers of a metallic or carbonaceous nature increases the electrical and heat conductivities of epoxies, providing materials that combine the high

conductivity of metals with the ease of processing of plastics. The construction of PVC membrane electrodes with silver filled epoxy supports has been well documented[59]. In these, silver filled conductive epoxy resins play a dual role, working both as a physical support for holding the membrane and as an internal contact for collecting the electrical signal transduced by the membrane[60,61,62]. Parallel studies of epoxy based and conventional ISEs have shown that the performance of the two electrode types are quite similar, however the epoxy based electrodes are slightly less stable and display a more irregular behaviour with temperature[60,63]. Alegret et al. focused on the stability of the potential response of a perchlorate electrode[61]. His research compared a commercially available perchlorate ISE (Orion) with a perchlorate ISE with internal filling solution and a perchlorate ISE based on a silver-epoxy composite substrate. The electrodes displayed similar sensitivity to perchlorate and similar reproducibility over time. However Alegret also showed how the epoxy based electrodes are less stable, with particular reference to an inert nitrogen atmosphere. Results obtained suggested that PVC membrane electrodes with conductive epoxy resin supports are not stable for long periods in a nitrogen atmosphere with continuous de-aeration. This research supports the theory, already discussed with reference to coated wire electrodes, that electrodes with metal contacts and no internal filling solution achieve a stable internal reference potential due to an oxygen half cell[55,64]. However in a review by Machado[60], it was also stated that the effect of oxygen depended strongly on the type of epoxy support chosen and therefore can only go so far in explaining the mechanisms involved in maintaining a stable internal reference potential in coated wire and epoxy based ion-selective electrodes. Construction of such electrodes is likely to be worthwhile because, while they are less than perfect, construction is simple, inexpensive and produces functional electrodes.

Another approach to the design of solid-state electrodes has been in the form of ion selective field effect transistors (ISFETs)[65,66,67]. Here, one sees the product of the integration of two seemingly diverse technologies, solid-state device physics and electrochemistry. In an ISFET, ion-selective polymeric membranes are placed directly on the gate insulator of an FET. Field effect transistors are based on semi-conductor technology. In a semi-conductor, electron energy levels do not entirely overlap as in a

metal, neither is there as large a gap between the valence and conduction bands as exists in an insulator. Therefore a certain number of electrons may be excited from the valence band (lowest occupied band) to the conduction band (outer levels). Electrons in the conduction band are delocalised and can conduct electricity. When an electron is promoted to the conduction band it leaves behind a positive hole in the valence band. These holes may also conduct charge. In semi-conductors impurities are incorporated into the crystal which will either donate or accept electrons making the semi-conductor either more positive (p-type) or more negative (n-type). Therefore the electrical properties of the crystal can be manipulated. The junction between a p-type region and an n-type region in the same semi-conductor single crystal is referred to as a pn-junction. Electrons will tend to flow from the n to the p regions until an equilibrium is reached. If an ion-selective membrane is attached to the pn-junction of a semi-conductor any changes in membrane potential will shift the equilibrium potential of the junction and this may be related back to the sample solution composition.

ISFET's have a number of potential advantages over conventional electrodes because of their rapid response, small size, low output impedance, suitability for temperature and noise compensation and the possibility of manufacturing small combined multi-sensors including a reference electrode. The main problem which has been encountered with these devices is the poor adhesion of the membrane to the surface of gate materials such as Si_3N_4 and Al_2O_3. This leads to drift and short lifetimes. Any water getting between the membrane and the sensing surface will tend to short circuit the device. Some attempts to include intermediate layers between the membrane and the surface have been discussed. Layers used include hydrated poly(vinyl)alcohol and dextran gels. It was also shown that the high drift rates associated with ion-selective field effect transistors can be reduced if the sensors are used as part of a flow system[68].

Despite the reasonable behaviour of many of the above electrode types , random failure is still common and the devices are prone to drift. Therefore, there have been attempts to introduce a thermodynamically stable reference system. For example, other solid contact ion-selective electrodes have been developed in which the transfer from ionic to electronic conductivity is provided by a solid contact, having mixed

ionic and electronic properties, between the reference element and the sensing membrane[69]. Recently, several polymers such as polyaniline[70], poly(ethyleneoxide)[71], poly(3-octylthiophene)[72], poly(vinyl ferrocene)[73] and poly(pyrrole)[74,52] have been used as solid contacts in an attempt to solve the problems of instability related to the "blocked" interface. Poly(pyrrole) is one of the most widely studied conducting polymers due to its ease of preparation, high conductivity and relative stability[75]. Lewenstam et al. have designed an alternative to the traditional glass pH electrode, based on platinum covered with hexanoferrate doped poly(pyrrole) and a PVC membrane incorporating a tri-n-dodecylamine ligand[74]. It was found that a conducting poly(pyrrole) solid contact improved the stability of the electrode in comparison to an electrode without the poly(pyrrole) layer. Selectivity against sodium and potassium was sufficient to make measurements in commonly used buffer solutions as well as in biological fluid samples possible. Log $K^{pot}_{H,Na}$ values of -11.9 for the solid-state electrode and -12.8 for traditional glass electrode (Radelkis, OP-711-I/A, Budapest, Hungary) were recorded. Similarly Log $K^{pot}_{H,K}$ values of -10.8 (solid-state electrode) and <-13.7 (glass electrode) were quoted. Lewenstam[74] amongst others[76,77] reported that a long conditioning time was needed for poly(pyrrole) based electrodes, (> 50 hours). This may be due to the process of establishing an equilibrium between the PVC and the poly(pyrrole) layers. Another solid-state reference has been developed by Diamond et al.[78] based on a KCl doped vinyl ester resin known as Refex. Here, the solid-state reference was fabricated by placing an Ag/AgCl wire in the salt doped monomer and leaving it to polymerise overnight. It was found that the Refex electrode was able to function very well without the conventional internal reference electrolyte and AC impedance measurements showed that the Refex constitutes an unblocked interface in terms of charge transfer[79]. The resin prevented a large scale uptake of water, provided a solid support and prevented a large loss of dissolved KCl to the aqueous phase. Poly(ethylene oxide) has been used as a polymer support for a sodium selective ISE[71]. The sodium selective material used here was NASCION ($Na_3Zr_2Si_2PO_{12}$), which is a solid ionic conductor. Another sodium electrode was developed based on $NaBF_4$ doped poly(pyrrole) and a sodium selective PVC membrane[52].

In general, it has been concluded that the inclusion of such polymers helps alleviate some of the drift which has been associated with the solid-state electrodes discussed. It is likely that there will be an increase in demand for solid-state sensors as current research leads to improvements in their performance and reliability.

1.6 Bibliography.

[1] P.L. Bailey; Ion-selective electrode reviews, 1 (1979) 81.

[2] G. Rumpf, L. Dürselen, H. Bühler, W. Simon; *Contemporary Electroanalytical Chemistry*, Plenum Press, New York, 1990.

[3] J. Paul, R. Carlson; J. Agr. Food Chem., 16 (1968) 766.

[4] A.W.M. Sweetsur; Analyst, 99 (1974) 690.

[5] J.L. Stuart; Analyst, 95 (1970) 1032.

[6] J. Owades, R. Block, S. Owades; Am. Soc. Brewers Chem. Proc., 75 (1967).

[7] E. Hansen, H. Filho, J. Ruzicka; Anal. Chim. Acta, 71 (1974) 225.

[8] J. H. Halliday, F.W. Wood; Analyst, 91 (1966) 802.

[9] R. DiMartini; Anal. Chem., 42 (1970) 1102.

[10] L.A. Dee, H.H. Martens, C.I. Merill, J.T. Nakamura, F. Jaye; Anal. Chem., 45 (1973) 1477.

[11] G.G. Barna, R.J. Jasinskii; Anal. Chem., 46 (1974) 1834.

[12] L.A. Elfters, C.E. Decker; Anal. Chem., 40 (1968) 1658.

[13] J.N. Driscoll, K. Mahoney, M. Young; Anal. Chem., 45 (1973) 2283.

[14] K.N. Andrew, N.J. Blundell, D. Price, P.J. Worsford; Anal. Chem., 66 (1994) 917A.

[15] **S. Walsh,** F. J. Sáez de Viteri, D. Diamond; Anal. Proc. Inc. Anal. Comm., 32 (1995) 365.

[16] F. Muldowney, R. Freaney, E. Spillane, P. O'Donohoe; Irish J. Med. Sci., 142 (1973) 223.

[17] E. Serjeant ; *Potentiometry and Potentiometric titrations*, J. Wiley & Sons Inc., New York, 1984.

[18] C. Davies; *Ion Association*, Butterworth, London, 1962.

[19] W. Morf ; *The principles of ion-selective electrodes and of membrane transport*, Elsevier Press, New York, 1981.

[20] G.J. Janz, H. Taniguchi; Chem. Review, 53 (1953) 397.

[21] D.J. Ives, G.J. Janz; *Reference electrodes, theory and practice*, Academic Press, New York, 1961.

[22] H. Jahn; Z. Physik. Chem., 33 (1900) 545.

[23] D. Diamond, A. Lewenstam; Electroanalysis, 6 (1994) 962.

[24] A.K. Covington, M. Rebelo; Ion-selective electrode reviews, 5 (1983) 93.

[25] I. Kolthoff; Anal Chem., 51 (1979) 1R.

[26] C. Moore, B. Pressman; Biochem. Biophys. Res. Commun., 15 (1964) 562.

[27] W.J. Blaedel, D.B. Easty, L. Anderson, T.R. Farrell; Anal. Chem., 43 (1971) 890.

[28] T. Kappe; Journal of Inc. Phenomen. and Mol. Recog. in Chem., 19 (1994) 3.

[29] D. Diamond; Journal of Inc. Phenomen. and Mol. Recog. in Chem., 19 (1994) 149.

[30] C. Gutsche; *Calixarenes*, The Royal Society of Chemistry, Cambridge, U.K., 1989.

[31] K. Cunningham, G. Svehla, S.J. Harris, M.A. McKervey; Analyst, 118 (1993) 341.

[32] H. Yamamoto, S. Shinkai; Chemistry Letters, (1994) 1115.

[33] W.E. Morf; Analytical letters, 7 (1974) 9.

[34] M. Oehme; Anal. Chim. Acta, 86 (1976) 21.

[35] W. Simon, M. Huser; P.M. Gehrig, W.E. Morf, E. Lindner, J. Jeney, K. Toth, E. Pungor; Anal. Chem., 63 (1991) 1380.

[36] P. Bühlmann, S. Yajima, K. Tohda, Y. Umezawa; Electrochimica Acta, 40 (1995) 3021.

[37] A. Van Den Berg, P. Van der Wal, M. Skowronska-Ptasinska, E. Sudhölter, D. Reinhoudt, P. Bergveld; Anal. Chem., 59 (1987) 2827.

[38] A. Thoma, A. Viviani-Nauer, S. Arvanitis, W. Morf, W. Simon; Anal. Chem., 49 (1977) 1567.

[39] G. Horvai, E. Graf, K. Toth, E. Pungor, R. Buck; Anal. Chem., 58 (1986) 2735.

[40] Z. Li, X. Li, S. Petrovic, D.J. Harrison; Analytical Methods and Instrumentation, 1 (1993) 30.

[41] X. Li, S. Petrovic, D.J. Harrison; Sensors and Accuators, B1 (1990) 275.

[42] A. Chan, D.J. Harrison; Anal. Chem., 65 (1993) 32.

[43] A. Thomas, K. Muniandy; Polymer, 28 (1987) 408.

[44] Z. Li, X. Li, S. Petrovic, D.J. Harrison; Anal. Chem., 68 (1996) 1717.

[45] Z. Li, X. Li, M. Rathmaier, D.J. Harrison; Anal. Chem., 68 (1996) 1726.

[46] I Lundström and C. Svensson; *Solid state chemical sensors*, Academic Press inc., San Diego, 1985.

[47]M. Madou and S. Morrison; *Chemical sensing with solid state devices*, Academic Press inc., San Diego, 1989.

[48] J. Janata; *Contemporary Electroanalytical Chemistry*, Editor A. Ivaska et al., Plenum Press, New York, 1990.

[49] R. Cattrall and H. Freiser; Anal. Chem., 43 (1971) 1905.

[50] L. Cunningham and H. Freiser; Anal. Chim. Acta, 180 (1986) 271.

[51] R. Cattrall and I. Hamilton; Ion-selective electrode reviews, 6 (1984) 125.

[52]A. Ivaska, A. Cadogan, Z. Gao, A. Lewenstam, D. Diamond; Anal. Chem., 64 (1992) 2496.

[53] R.P. Buck; *Ion selective electrodes in analytical chemistry*, H. Freiser ed. Plenum Press, New York, 1 (1980) 58.

[54] R. Cattrall, I. Hamilton; Ion-selective electrode reviews, 6 (1994) 125.

[55] R. Cattrall, D. Drew, I. Hamilton; Anal. Chim. Acta, 76 (1975) 269.

[56] J. Schindler, G. Stork, H. Struh, W. Schmid, K. Karaschinski, Z. Fresenius; Anal. Chem., 295 (1979) 248.

[57] W. Göpel, J. Hesse, J. Zemel; *Sensors a comprehensive survey*, Vol. 2, VCH publishers Inc., New York, 1991.

[58] M. Dekker; *Epoxy Resins, Chemistry and Technology*, C. May ed., New York, 1988.

[59] J.L.F.C. Lima, A.A.S.C. Machado; Analyst, 111 (1986) 799.

[60] A.A.S.C. Machado; Analyst, 119 (1994) 2263.

[61] S. Alegret, A. Florido; Analyst, 116 (1991) 473.

[62] J.L.F.C. Lima, A.A.S.C Machado; Analyst, 111 (1986) 799.

[63] M.T.S.D. Vasconcelos, A.A.S.C. Machado; Analyst, 113 (1988) 49.

[64] A. Hulanicki, M. Trojanowicz; Anal. Chim. Acta., 87 (1976) 411.

[65] H. Van den Vlekkert, C. Francis, A. Grisel, N. de Rooij; Analyst, 113 (1988) 1029.

[66] Y. Miyahara, W. Simon; Electroanalysis, 3 (1991) 287.

[67] U. Oesch, S. Caras, J. Janata; Anal. Chem., 53 (1981) 1983.

[68] P.L. Cobben, R.J. Egberink, J.G. Bomer, E. Sudhölter, P. Bergveld, D. Reinhoudt; Anal. Chim. Acta, 248 (1991) 307.

[69] B. Nikolskii, E. Materova; Ion-selective electrode reviews, 7 (1985) 3.

[70] J. Bobacka, T. Lindfors, M. McCarrick, A. Ivaska, A. Lewenstam; Anal. Chem., 67 (1995) 3819.

[71] P. Fabry, C. Montero-ocampo, M. Armand; Sensors and Actuators, 15 (1988) 1.

[72] J. Bobacka, M. McCarrick, A. Lewenstam, A. Ivaska; Analyst, 119 (1994) 1985.

[73] P. Hauser, D. Chiang, G. Wright; Anal. Chim. Acta, 302 (1995) 241.

[74] A. Lewenstam, A. Michalska, A. Hulanicki; Analyst, 119 (1994) 2417.

[75] G. Evans; *Advances in Electrochemical Science and Engineering,* Ed. H. Gerischer, C. Tobias, VCH Press, New York, 1990.

[76] S. Dong, G. Che; Talanta, 38 (1991) 111.

[77] A. Cadogan, A. Lewenstam, A. Ivaska; Talanta, 39 (1992) 617.

[78] D. Diamond, D. Rehm, E. McEnroe; Anal. Proc. Inc. Anal. Comm., 32 (1995) 319.

[79] D. Diamond, E. McEnroe, A. Lewenstam, M. Mc Carrick; Electroanalysis, 6 (1994) 962.

Characterisation of Ion-selective electrodes.

2.1 Potentiometric Characterisation.

In chapter 1 the origins of the potential of an ion-selective electrode were established and discussed. Before deciding on the suitability of a particular electrode for an application, certain features need to be considered. For example, electrodes need to be calibrated under conditions that relate closely to those existing in the analyte solutions. Also, each type of ion-selective electrode will only function to an analytically acceptable level within a certain concentration range. Ideally, an ion-selective electrode will respond in a Nernstian fashion to only the analyte ion. However, in reality it has been found that these electrodes are selective not specific and therefore are susceptible to physical interferences caused by the presence of other ions in sample solutions.

With these factors in mind, before the establishment of any method utilising ion-selective potentiometry one must consider cell calibration, determination of the response range and selectivity values.

2.1.1 Cell Calibration.

Proper calibration of any instrument is necessary to obtain accurate analyses. The choice of a calibration method depends on the instrumental method, sample composition and also on the number of samples to be analysed. Some of the most commonly used techniques for the evaluation of ion activity are the analytical or working curve and the method of standard additions.

When the ***analytical curve method*** is used in the calibration of ion-selective electrodes, a series of standard solutions are prepared containing known amounts of the analyte species. The solutions should cover the concentration range of interest and have matrix compositions as similar to the sample matrix as possible. The electrode is exposed to each solution in turn and potentiometric data is collected for each sample. A plot of analyte activity versus steady state potential then yields a calibration curve such as that shown in figure 2.1. This theoretical calibration curve was prepared assuming a singly charged analyte ion under Nernstian conditions.

Unknown sample solutions may then be compared to the calibration curve and their concentration deduced. The calibration curve must be checked periodically to detect and adjust for changes in electrode response.

Figure 2.1; Theoretical calibration curve for a singly charged analyte ion (a_i). The steady state potentials were calculated using the Nernst equation where $E = S \log a_i$. This yields a slope of 59.2 mV/decade change in activity. Activity values correspond to solutions having an analyte concentration from 10^{-1} M to 10^{-5} M.

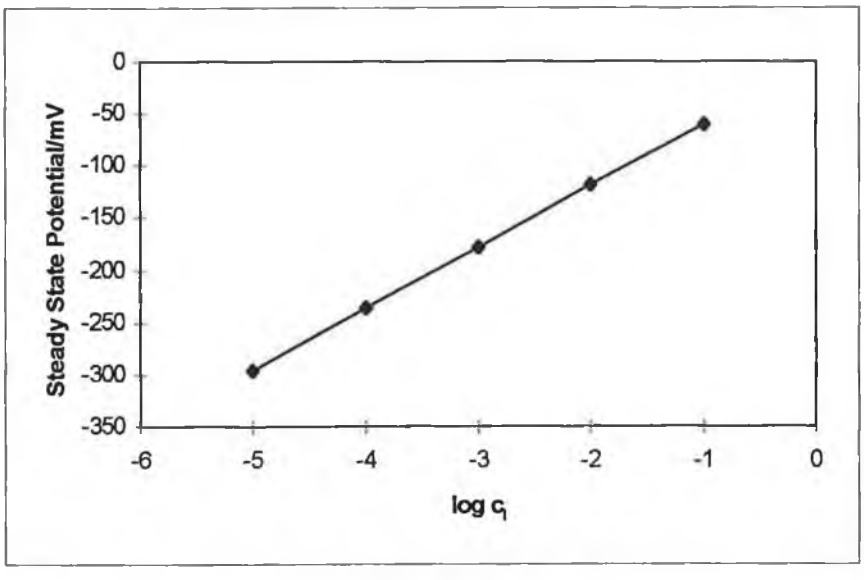

The ***method of standard additions*** is used where it is impossible to suppress physical or chemical interferents. A small amount of analyte solution of known concentration is added to a portion of a previously analysed sample solution and the analysis is repeated using identical reagents and experimental procedures. In other words the initial analyte ion concentration is deduced by measuring the change in E_{cell} that results from the addition of a known concentration of analyte ion to the unknown sample solution. If this method is used then the electrode response must be a linear function of the analyte concentration over the range of interest. The Nernst equation is used to deduce an equation which can be applied to the standard additions method.

The electrode is first exposed to a sample solution and the concentration of the analyte ion may be described by;

$$E^1_{cell} = \text{Constant} + S\log c_i f_i \qquad \textbf{(2.1)}$$

where;

Constant = contributions from liquid junction potentials and the standard cell potential when activity is unity.

E^1_{cell} = Cell potential in solution 1.

S = Electrode slope.

c_i = Analyte concentration (unknown).

f_i = Activity coefficient of the analyte ion.

If the volume of the sample solution is V_i and a known volume of a standard solution V_s of concentration C_s is added, then the potential of the cell may now be described as;

$$E^2_{cell} = \text{Constant} + S\log f_i\left(\frac{V_iC_i + V_sC_s}{V_i + V_s}\right) \qquad \textbf{(2.2)}$$

where;

$\left(\frac{V_iC_i + V_sC_s}{V_i + V_s}\right)$ refers to the total analyte ion concentration after spiking.

In chapter 1, the relationship between concentration and ionic strength was introduced (see equation 1.2). If the ionic strength of all solutions is held constant, the activity coefficient of the test substance remains constant for all concentrations and therefore the term $S\log f_i$ in the following equation may be considered constant.

$$S\log c_i f_i = S\log f_i + S\log c_i \qquad \textbf{(2.3)}$$

If E^1_{cell} refers to the potential before the addition and E^2_{cell} refers to the potential after the addition and f_i remains constant, then the change in cell potential ΔE may be related to the unknown concentration C_i by;

$$\Delta E = S\log\left(\frac{V_i C_i + V_s C_s}{C_i(V_i + V_s)}\right) \qquad \textbf{(2.4)}$$

or

$$C_i = \frac{\frac{C_s V_s}{V_s + V_i}}{10^{\Delta E/S} - \left(\frac{V_i}{V_i + V_s}\right)} \qquad \textbf{(2.5)}$$

Thus the only unknown is the concentration of the analyte ion in the original sample.

2.1.2 Dynamic Range.

The dynamic or response range defines the range of concentrations of analyte ion within which the ion-selective electrode will produce an analytically useful signal. All instrumental methods have a degree of noise associated with signal measurement that limits the amount of analyte that can be detected. This limit of detection may be described as the lowest concentration level that can be determined to be statistically different from an analyte blank. It is generally taken to be that concentration which gives a signal which is three times the standard deviation of the background noise. The general limit of detection of an ion-selective electrode in direct potentiometry is approximately 10^{-4} M of the analyte ion.

2.1.3 Selectivity.

An ion-selective electrode will selectively target a particular analyte ion. However it cannot always be assumed that the effect of ions other than the primary ion will be negligible. Correction for the contribution of interferents is highly desirable for an

accurate analyte determination. Despite attempts by various researchers over the years to synthesise more selective ligands there is still a fairly limited number of highly selective ionophores. Some have approached the problem of interferents by trying to separate them. For example in the detection of NH_4^+ ions[1], separation of the primary ion from interferents was achieved by the use of ion chromatography followed by post-column NH_4^+ detection with neutral carrier based ion-selective electrodes. Another approach by Meyerhoff et al[2,3], involved the transformation of NH_4^+ into gaseous ammonia at high pH, followed by its separation from the sample matrix through a gas-diffusion membrane.

Where such an approach is not desirable or feasible, it is possible to generally determine the effect of interferents by calculating selectivity coefficients for each interfering ion using an extended form of the Nernst equation known as the Nikolskii-Eisenman equation (see Chapter 1). In this equation a quantity K_{ij}^{pot} is described. This is known as the selectivity coefficient. Two methods are commonly used to determine selectivity coefficients. These are the separate solutions[4] and the mixed solutions[5] methods.

Separate Solutions Method; This is the simplest way to determine selectivity coefficients. Calibration curves are prepared for each ion being tested. Parallel curves should ideally result as shown in figure 2.2. The selectivity coefficient can then be related to the difference in potential between the two curves. When the activity of the primary and interfering ions are equal and where z_i and z_j are also equal, then

$$\log K_{ij}^{pot} = \frac{E_i - E_j}{S} \qquad \textbf{(2.6)}$$

or $K_{ij}^{pot} = \frac{a_i}{a_j}$ at a selected potential, for $z_i = z_j$. **(2.7)**

K_{ij}^{pot} = Selectivity coefficient for the primary ion over the interfering ion.

E_i = Potential recorded at an activity a_i of the primary ion.

E_j = Potential recorded at an activity a_j of the interfering ion (where $a_i = a_j$).

S = Electrode slope (59.2 mV/decade change in activity for a singly charged ion at 25°C.

Selectivity coefficients recorded by this method are not regarded as completely reliable. This is because the response of an electrode in separate solutions of the primary and interfering ion does not closely model the real situation where the interferent is present in a sample containing the primary ion.

Figure 2.2; Parallel curves resulting from the separate solutions method for determining selectivity. E_i refers to the potential obtained for a positively charged analyte ion. E_j refers to the potential obtained for a positively charged interfering ion.

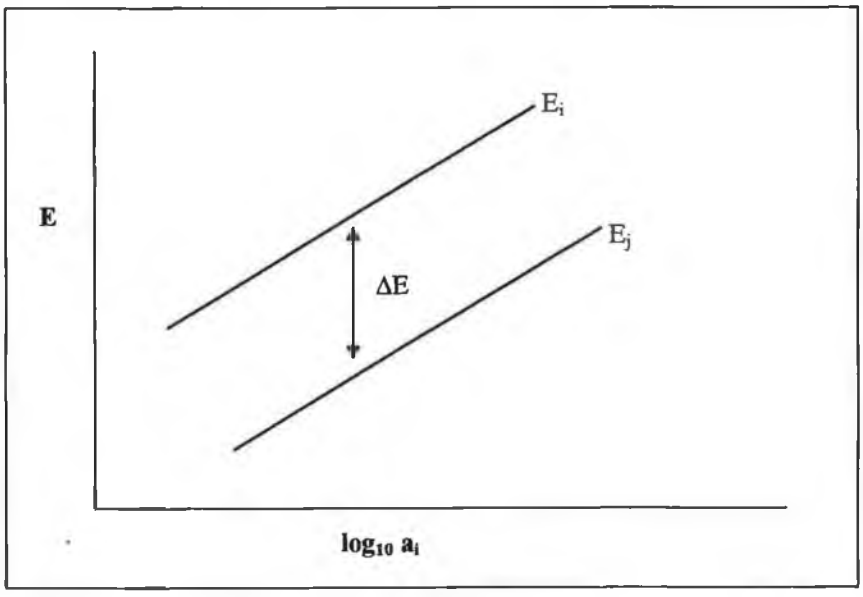

Mixed Solution Method; Using this method, potential measurements are made in solutions where the activity of the primary ion varies in the presence of a constant background of interfering ion. In other words an electrode is calibrated in the presence of a fixed background of interfering ion. A plot such as that shown in Figure 2.3 results. In the upper portion of the curve where the analyte concentration is higher, the electrode responds in a Nernstian manner. As the analyte concentration

decreases the electrode response is increasingly affected by the presence of the interfering ion. From the graph a point can be found where the electrode is responding equally to both ions. This corresponds to the activity of primary ion, (from the extrapolated linear portion of the curve) at which the potential is equal to the background potential due to the interferent. This is clearly shown in figure 2.3.

At this point $K_{ij}^{pot} = \frac{a_i}{a_j^{z_i/z_j}}$ for z_i and z_j representing the charge on the primary and interfering ions respectively. The mixed solution method more closely resembles the situation in real samples and therefore is generally preferred over the separate solutions method.

Figure 2.3; Example of the mixed solution method for the determination of selectivity.

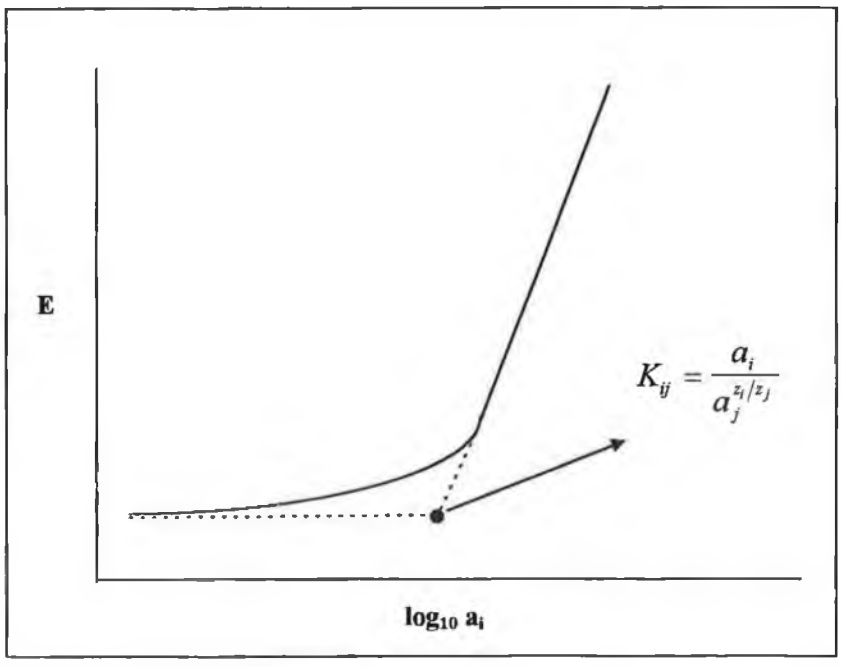

In recent times, the type of selectivity coefficients resulting from the above methods are said to be merely an indication of the selectivity and do not qualify as an exact quantification of the ability of an electrode to respond primarily to the analyte ion in

the presence of interferents[6,7]. It is believed that the coefficients obtained by the separate or mixed solutions methods are accurate indicators of electrode selectivity only for the very restricted conditions under which they are generated (i.e. separate pure solutions of ions for the separate solutions method). Selectivity coefficients defined and calculated on the basis of the Nikolskii-Eisenman equation are often criticised because this definition of selectivity does not tend to deal with situations where $z_i \neq z_j$[8]. When $z_i \neq z_j$ the selectivity coefficient becomes a function of the interfering ion activity. Also, as sample solutions can have an unknown and varying background ion composition, measured potentials would contain an unknown but significant error in the summation factor of the Nikolskii-Eisenman equation. In the separate solutions method, equal charges do not always mean that K_{ij}^{pot} may be simply determined from the ratio of primary and interfering ion activities because the slope of the interferent is often less than that of the primary ion and therefore the resulting curves are not parallel. In the mixed solutions method it may be difficult to graphically locate the point where $K_{ij} = \frac{a_i}{a_j^{z_i/z_j}}$. A decision must be made as to which portions of the response curve are linear, thus making the method subjective. Also, it has been shown that potentials in the plateau region of the plot are subject to an unacceptable level of irreproducibility and drift[9].

In dealing with these problems researchers are tending to define their selectivity coefficients as applicable only within the range of the experimental conditions used[7]. Non-linear modelling approaches based on multivariate calibration and simplex optimisation have been presented in a series of papers by Diamond et al.[7,8,10]. Their approach allowed the determination of potentiometric selectivity coefficients in mixed solutions containing up to four interfering ions. However, these methods are not very easy to implement as even with partial factorial design, 32 solutions were needed to characterise a four electrode array. Another approach describes a very simple method of obtaining experimental data and fitting them to a Nikolskii-Eisenman model to obtain electrode characteristics[11]. Here the interfering ion concentration was kept constant and the primary ion concentration varied by means of small volume spikes into the solution. The cell potential was measured after each addition. The electrode

characteristics were taken as those values which provided the best fit to the experimental data through minimisation of a least squares error. The non-linear analysis was carried out using the *Solver* optimisation add-on available in Microsoft Excel for Windows 95. Recently, Davey et al.[12] used a flow analysis approach to plot peak heights obtained Vs log of the primary ion activity at a constant concentration of interfering ion. They then used values in the curved region of the plot to determine potentiometric selectivity coefficients using a data linearisation technique based on the Nikolskii-Eisenman equation. However their method does not yield a value for the Nernst slope factor.

In all cases it is advised that much caution be exercised when experimental values for selectivity coefficients valid for definite conditions are extrapolated to different conditions.

2.2 Flow Injection Analysis[13,14].

Ion-selective electrodes are commonly used as detectors in flow injection analysis (FIA) systems. Flow injection analysis is a type of continuous flow analysis, which utilises an unsegmented carrier stream, into which highly reproducible volumes of sample are injected. It was initially developed by Ruzicka and Hansen[15] in Copenhagen and correspondingly by Stewart et al[16] in Washington DC.

In a flow injection analysis system, the carrier stream is continuously pumped around the analytical manifold. At selected intervals a liquid sample is injected into the carrier stream via an automatic injection valve which loads the sample. The valve is then switched and the carrier stream is directed through the valve to sweep out the sample. At this point the sample may or may not be moved into a reaction manifold where it is reacted with a number of reagents, incubated, dialysed, distilled or extracted. The reaction product (or unreacted sample) is then passed to the flow through cell of an appropriate detector, for example an ISE. Here, the sample generates an analogue signal which generally takes the form of a sharp peak, the height of which is related to the concentration of analyte.

Where ion-selective electrodes are used as detectors in flow systems, four distinct geometries are possible as shown in figure 2.4. These are flow through, flow past[17], tangential[18] and wall jet[19]. The ion-selective electrode components and configuration remain the same in each arrangement, the only difference being the way in which the samples are presented to the detector[20].

Figure 2.4; The four distinct geometries available for ion-selective electrodes in flow systems; (i) flow through, (ii) flow past, (iii) tangential and (iv) wall jet.

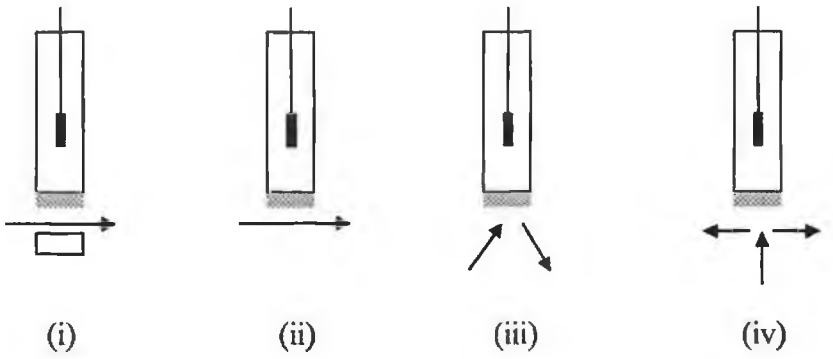

In flow through and flow past designs the sample crosses the electrode through a small piece of tubing in which part or all of the electrode body is replaced with the membrane. In the tangential system the sample makes contact with the membrane at an angle between 0° and 90°. In a wall jet system the sample approaches the membrane from a 90° angle and then is pushed out at the sides.

2.2.1 Theory of the flow injection response.

The success of a flow injection analysis system depends on the reproducibility of sample injection, reproducible timing and controllable sample dispersion.

To ensure precision one needs to pay attention to the timing throughout the system. This applies especially to the injection port and the pumping mechanism. The operation of the injection valve must be regulated to ensure injection of precise sample volumes. Similarly the residence time of the sample in the analytical manifold should be the same for each sample. Therefore, the pump must be capable of generating reproducible flow rates.

In any flow system, the injected sample forms a zone which, between the points of injection and detection will have been dispersed to some extent. This is reflected in the peak detected as shown in figure 2.5.

Dispersion is defined according to a dispersion coefficient D. The dispersion coefficient is the ratio of the concentration of the sample solution before (C^0) and after (C^{max}) the dispersion or mixing process has taken place

$$D = \frac{C^0}{C^{max}} \qquad \textbf{(2.8)}$$

Dispersion may be considered as limited (D = 1-3), medium (D = 3-15) or large (D > 15). Limited dispersion is useful to feed detectors such as electrodes and atomic absorption spectrometers. In other words, if the purpose of the flow system is simply to transport the sample toward a detector then dispersion should be minimised to preserve the integrity of the sample plug and avoid dilution. Where some chemical reaction must take place, medium dispersion is to be preferred as some mixing of sample and reagents must take place. Finally, large dispersion is used when a longer residence time is required to allow a slow reaction to proceed to some degree of completeness. This is generally achieved using a mixing chamber. One of the key features of FIA is the fact that since all conditions are reproduced, dispersion is very

controlled. By changing the flow parameters, the dispersion can be easily manipulated to suit the requirements of a particular analytical procedure so that optimum response is obtained at minimum time and reagent expense[21].

Figure 2.5: A typical flow injection analysis peak. The sample zone prior to injection (left) is homogenous and therefore yields a square readout while the zone following injection (S) is dispersed and is composed of a continuum of changing concentrations up to a maximum (C_{max}).

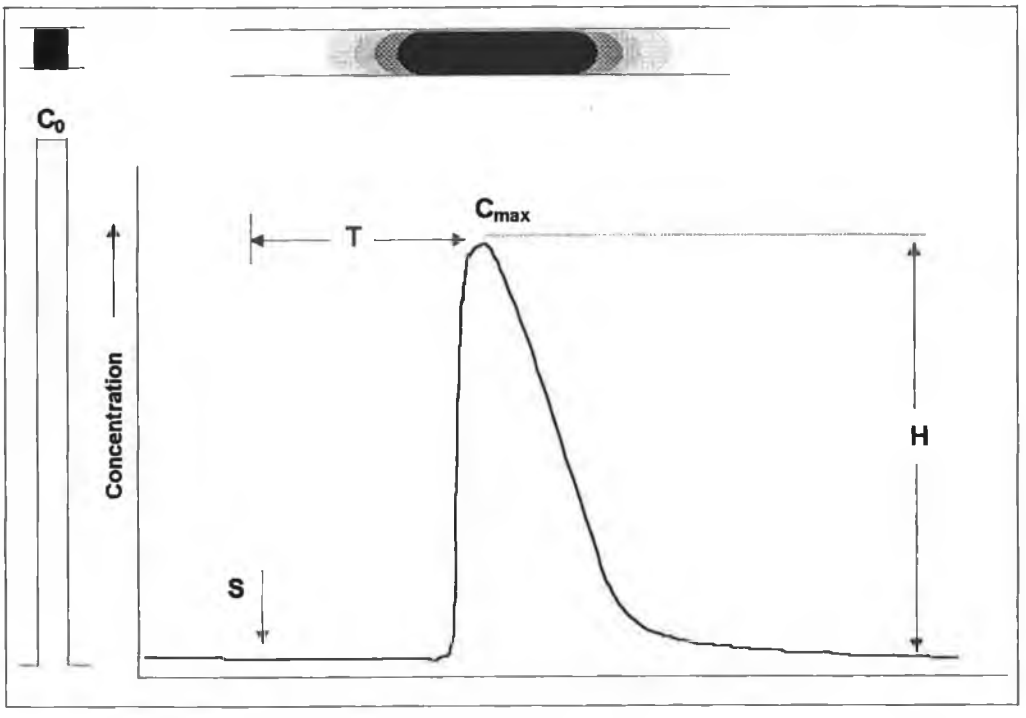

2.2.2 Dispersion Models.

Several research groups have attempted to mathematically define the dispersion process.

Flow injection analysis systems operate under laminar flow conditions, therefore

Taylor[22] based his description on laminar flow equations.

In laminar flow, as the sample is swept along the narrow bore tubing, the velocity at the centre of the sample plug is twice the mean velocity, while the velocity at the tube walls is practically zero, resulting in a parabolic velocity profile. The first molecules to arrive at the detector are those in the centre of the sample plug. Molecules at the edges will theoretically arrive much later. However, this feature of laminar flow will tend to cause large dispersion as the sample plug would have an infinitely long tail. Therefore some mechanism must exist to limit the effects of laminar flow on the peak profile. This mechanism is provided by radial diffusion. In radial diffusion, molecules which were originally in the centre of the tube move towards the walls where they are transported at a lower velocity. Similarly, molecules in the almost stagnant layer at the wall will tend to move towards the centre where they will move at a higher velocity. When the molecules reach the detector each molecule will have spent the same fraction of time in each streamline and therefore the average velocity for all molecules is almost the same. Thus a greatly reduced dispersion is observed. Radial diffusion or secondary flow tends to offer an efficient scrubbing mechanism as the molecules move toward and away from the tube walls, which leads to low carryover between samples. Taylor explained that while both laminar flow and radial diffusion occur, dispersion by longitudinal diffusion also occurs. Longitudinal diffusion occurs in the direction of flow and is due to the molecules gaining some longitudinal motion as they move towards and away from the tube walls. However, Taylor concluded that longitudinal diffusion may be ignored relative to that caused by the main flow pattern but that radial diffusion is always important in narrow tubes. The relative importance of the radial diffusion and laminar flow processes depends on the flow rate, the radius of the tube, the time of the analysis and the magnitude of the diffusion coefficient[23,24]. This is described mathematically by Taylor's equation;

$$C_x = M\left(\frac{1}{r^2\pi}\right)\left(\frac{1}{2(\pi\delta L^2)^{1/2}}\right)e^{-(L-x)^2/L4\delta^2} \qquad \textbf{(2.9)}$$

for;

C_x = Concentration at distance x.

M = Mass of material injected at a point L = 0 at time t = 0.

r = Radius of the tubing.

δ = Dispersion number (dimensionless), where $\delta = D\left(\frac{t}{L^2}\right)$.

D = Axial dispersion coefficient (cm^2 $sec.^{-1}$).

T = Mean residence time.

Taylor's equation is valid where;

$$T \geq \frac{r^2}{3.8^2 D_c} \qquad \textbf{(2.10)}$$

D_c = Molecular diffusion coefficient (cm^2 $sec.^{-1}$).

Under diffusion controlled conditions the peak shape is gaussian. F.I.A. is generally carried out just outside Taylor conditions (i.e. equation 2.10), but Taylor's argument leads to some conclusions such as, mixing will be complete without recourse to mechanical stirring, the concentration gradients in a given sample plug are both reproducible and predictable and the peak shape will be influenced by differences in the sample and carrier matrices because the whole of the plug, matrix and analyte is diffusing into the carrier.

Another approach to dispersion was made by Ruzicka and Hansen[25]. Here it was proposed that the distance between the points of injection and detection consists of a number of imaginary tanks (N). The tanks are theoretically formed by the injection valve, flow cell, analytical conduits and connectors. If the injection valve and connectors have a zero dead volume as is ideal and the flow cell is of a sufficiently small volume, then the tanks can be ascribed to the passage of components through the tubing. The mathematical models used to account for the distribution of a sample introduced into the first tank can be used to account for the physical dispersion of a sample as a function of time.

$$C_x = \frac{1}{t_i}\left(\frac{t}{t_i}\right)^{N-1}\left(\frac{1}{(N-1)!}\right)e^{-t/t_i} \qquad \textbf{(2.11)}$$

C_x = Concentration at distance x.

t = Time (sec.).

t_i = Mean residence time in one tank (sec.).

N = Number of tanks.

This model works well for large values of N but for values of N =1 a gaussian peak shape is not found. The mean residence time of the sample in the system (T) is related to N through the individual residence times t_i by;

$$T = Nt_i \qquad \textbf{(2.12)}$$

For values of $N \geq 10$ the dispersion number δ is related to the mean residence time T and the number of tanks N by;

$$\delta = \frac{1}{2}\left(\frac{T^2}{N}\right) \qquad \textbf{(2.13)}$$

Therefore for increasing N, the dispersion will decrease and in contrast if N is small, asymmetrical concentration profiles will result. As a short residence time is needed to minimise dispersion and save reagents narrow bore tubing is to be preferred. Based on the above tanks in series equation it was calculated that the optimum diameter for F.I.A. tubing is 0.5 ± 0.2 mm i.d.[14] as in this range a reasonable flow rate can be maintained without difficulty, reagent consumption is not excessive and a variety of chemistries is available to the analyst.

2.2.3 Advantages of ISE detectors for FIA systems.

The incorporation of ion-selective electrodes as detectors in flow systems has attracted much attention in recent years because it offers several advantages when compared to batch procedures.[26,27]

Electrodes must be conditioned on a regular basis to ensure stable interface potentials. The carrier solution in a flow injection system will typically contain a low concentration of the analyte ion. Hence the electrode is continuously conditioned as the carrier solution washes through the flow cell.

It has been proposed that ion-selective electrodes in flow systems display enhanced selectivity[28,8]. Diamond and Forster[8] have shown that during the rising portion of a typical flow injection peak (0.5 - 5 sec. after injection) the selectivity towards the primary ion is enhanced. The response kinetics of the ion-selective electrode to the primary ion is usually faster than to the interferents. Also, at this time the interfering ions are below their final equilibrium concentrations in the membrane. This allows for improvements in selectivity, as the time in which the sample segment passes the sensor surface is too short to establish the full equilibrium potential for the interfering ions. It was also shown that % error values on analyte concentrations obtained by analysis of potential values on the rising portion of the peak were very similar to % error values obtained in steady state measurements. It was concluded that as the errors were similar and the rising portion of a peak can be difficult to reproduce exactly an enhanced kinetic selectivity must be present to counteract an expected larger error in the pre steady state analysis. In batch measurements one has to wait for the signal to reach a steady state and so these procedures cannot benefit from such enhanced kinetic selectivity.

Further advantages of using ion-selective electrodes in flow systems include simplified sample handling, small sample sizes (typically 25-100µl) and a high sample throughput (> 100 samples/hour possible). A certain control on carryover can be exerted. In FIA a second injection is not made until the first sample has been completely washed out, indicated by a return to baseline. Finally, as the hydrodynamics in front of the sensing surface are controlled and stable, the response time and potential generated are also

reproducible.

2.2.4 Multiple sensor arrays.

The ability to perform multi-component analysis is very attractive as it reduces both analysis time and expense and also presents a more realistic result as contributions from various components in the same sample can be investigated simultaneously. Flow injection potentiometry at limited dispersion offers the possibility of sequential detection of different species by the use of an array of ion-selective electrodes.[29,30] Ion-selective electrodes are ideal detectors for use in such arrays because of their excellent selectivity and stability[31]. For example, Diamond et al. have used an array of ISEs to determine electrode parameters[29]. Here, multivariate calibration and simplex optimisation was used to obtain accurate and precise values for each electrode in the array. A knowledge of the precise values of these parameters enables an "intelligent" detector or sensing system to be developed which can recognise the presence of interferents and correct for them. In addition to opening up the possibility of the sequential detection of different species, sensor arrays have also proven useful where sufficiently selective ISEs are not available. Other research describes the simultaneous determination of sodium, potassium and calcium in an FIA system[10]. This array consisted of three highly selective electrodes and a fourth which responded to differing degrees to each species. The response surface of each electrode within the array was determined using mixed calibration solutions and this response modelled using simplex optimisation.

Sensor arrays are likely to be further developed during the remainder of the 1990's as the cost of computing power continues to fall and more high quality, easily manufactured reproducible arrays become available.

2.3 AC Impedance spectroscopy.

The concept of electrical impedance was first introduced by Oliver Heaviside in the 1880's. In more recent times AC impedance methods are being increasingly applied to the investigation of electrochemical systems[32]. The interface between two liquid or solid phases represents a potential generating system. In real electrode systems various charge carriers are simultaneously involved in interfacial processes. However, the selectivity of ion-selective electrodes ensures that the transfer reactions are dominated by certain ions. AC Impedance is proving a very useful technique for studying the charge transfer characteristics of ion-selective electrode processes. For example, Brand and Rechnitz have used steady state AC impedance methods as a means of studying the kinetics of ion transfer at membrane|solution interfaces[33,34]. Covington et al. have more recently applied the AC impedance method to liquid membrane ISEs incorporating valinomycin as the neutral carrier ionophore.[35,36]

2.3.1 AC Impedance Theory.

Impedance is a more general concept than resistance because it takes phase difference and frequency into account.

In an AC impedance experiment a small amplitude sinusoidal voltage is applied to an electrode system;

$$v(t) = V_m Sin(\omega t) \qquad \textbf{(2.14)}$$

v(t) = Voltage applied.

V_m = Maximum voltage amplitude.

ω = Angular frequency ($2\pi f$ / Hertz, for f = frequency / Hertz).

The resulting current is measured. It is of the same frequency but different in

amplitude and phase. It may be represented;

$$i(t) = I_m Sin(\omega t + \theta) \qquad (2.15)$$

i(t) = Current measured.

I_m = Maximum current amplitude.

θ = Phase difference.

The shift in phase occurs because an electrode behaves equivalent to an electrical circuit which contains capacitances as well as resistances and capacitance is frequency dependent. The system impedance (Z) is then defined by Ohms law as;

$$Z(\omega,t) = \frac{v(t)}{i(t)} \qquad (2.16)$$

And is of magnitude $|Z| = \frac{V_m}{I_m}$ **(2.17)**

Impedance is represented by a vector quantity with real (Z') and imaginary (Z") parts and appears as a point in the complex plane as shown in figure 2.6.

$$Z = Z' - jZ'' \qquad (2.18)$$

Where j equals the complex number $\sqrt{-1}$.

Figure 2.6; Impedance is represented by a vector quantity and appears as a point in the complex plane.

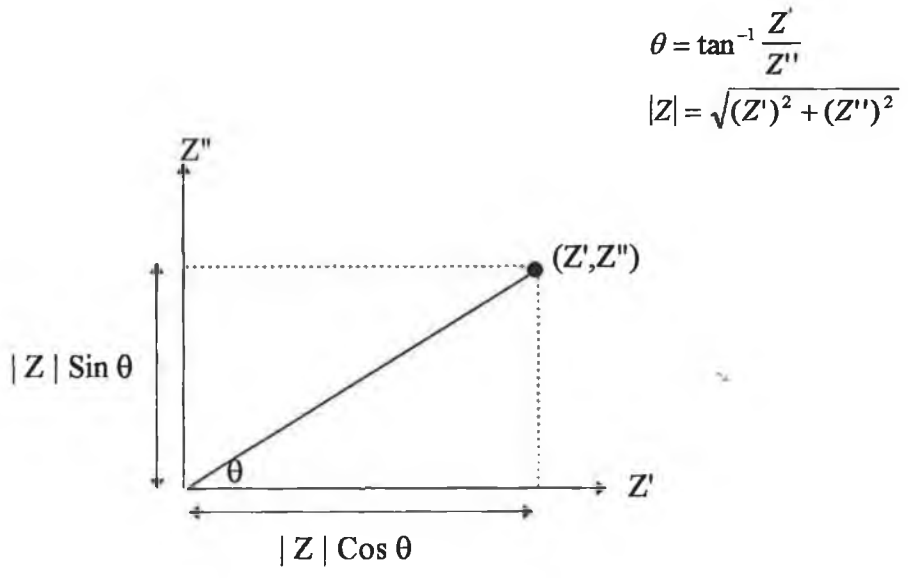

θ and | Z | are both functions of the applied frequency ω and so, for every frequency measured one gets a different point on the complex plane. Distance of a point from the origin corresponds to the magnitude of the impedance and the angle formed with the real axis corresponds to the phase difference θ between voltage and current.

Impedance may be modelled by an equivalent circuit consisting of discrete electrical components, such as capacitances and resistances. The complex planes of a resistor, a capacitor and their combination in series and in parallel are shown in figure 2.7. Interpreting the results of AC impedance experiments relies on finding this equivalent circuit and extracting values for the individual components which are then related to the electrochemical system.

Figure 2.7; The equivalent circuit models and complex plane representation of a resistor(i), a capacitor(ii) and their combination in series(iii) and in parallel(iv).

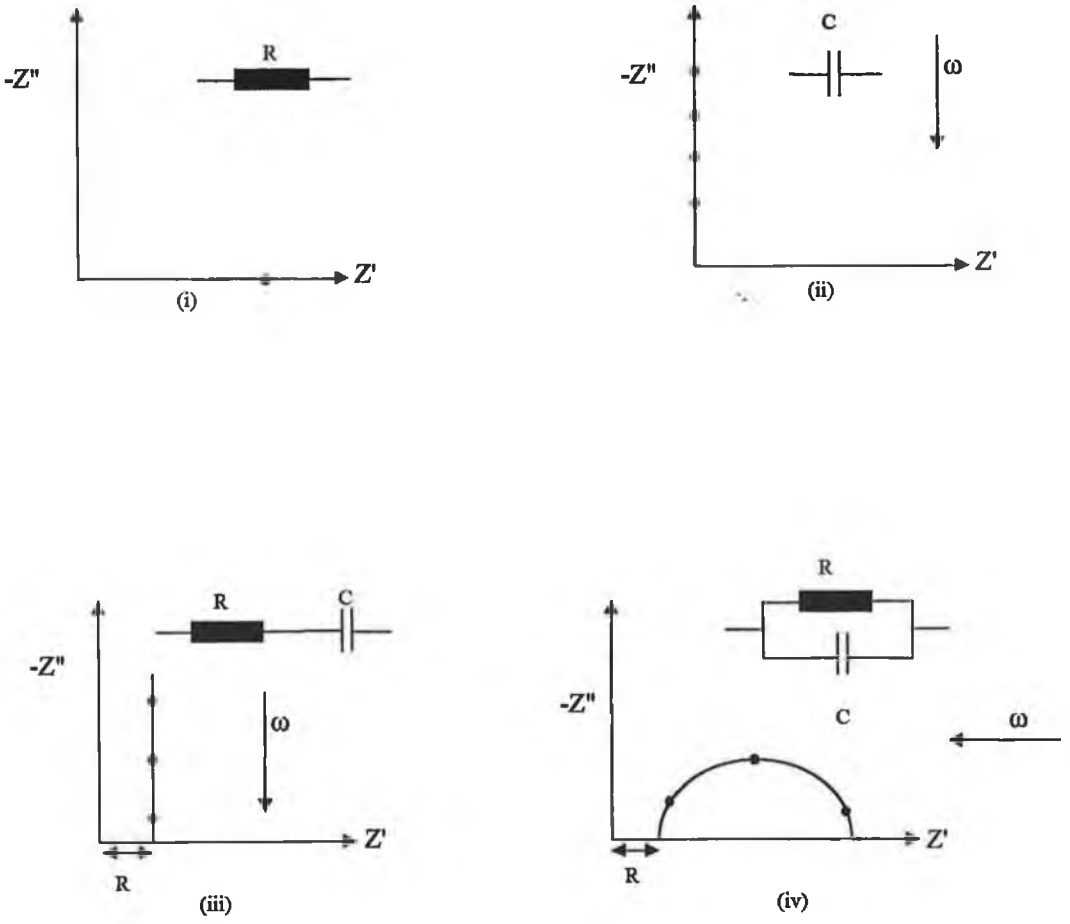

2.3.2 Using AC Impedance to study Electrochemical Systems.

A theory of reaction rates at electrode surfaces was developed in the early 20th Century by Butler and Volmer.[37,38] The resulting Butler-Volmer equation is a fundamental equation of electrode kinetics as it shows the way in which current density varies with exchange current density, over-potential and the transfer coefficients[39].

Butler-Volmer equation;

$$i = i_0\left[\exp(\alpha nF\eta / RT) - \exp((1-\alpha)nF\eta / RT)\right] \qquad \textbf{(2.19)}$$

i = Magnitude of the current at a given over-potential.

i_0 = Exchange current density.

α = Transfer coefficient for the electrode reaction.

n = Number of electrons involved in the reaction.

F = Faradays constant.

R = Gas Constant.

η = Over-potential i.e. a deviation of the electrode from the equilibrium potential.

The exchange current density (i_0) is a measure of the number of ions that flow in opposite directions across an interface and therefore represents a quantitative measure of the rate of ion exchange. The Butler-Volmer equation shows that the rates of elementary reaction steps are exponentially dependent upon the potential, therefore indicating that electrochemical processes are inherently non linear. The AC theories that are most fully developed are all linear theories, so in order to use them to study electrochemical processes the amplitude of the exciting signal must be kept small[40]. Selective ISEs tend to display relatively large exchange currents (ca. 10^{-3} A/cm^2), given that the potential determining process arises form the rapid exchange of the analyte ion at the membrane surface[41]. The exchange current has also been shown to provide a semi-quantitative means of elucidating the identity of the potential determining ion, to characterise the selectivity of the membranes and gain some insight into the mechanism of the potential generating response in PVC membranes[41].

Studies have also shown that Nernstian behaviour can be directly correlated with a high exchange current density which leads to low over-potential values due to a rapid ion exchange.[42,43]

Applying small voltages, as in AC impedance spectroscopy, only slightly alters reactions occurring at the electrode/electrolyte interface. At small potentials the Butler-Volmer equation may be linearised and simplified to;

$$i = i_0 \frac{nF\eta}{RT} \qquad \textbf{(2.20)}$$

Therefore, the impedance method may be used to study reaction kinetics at electrode surfaces.

One example of an equivalent circuit is shown in figure 2.8 and is known as the Randles equivalent circuit[44]. Randles studied rapid metal/metal ion and redox reactions in which the time averaged concentrations at the electrode surface obey the Nernst equation. His work began the application of impedance methods to electrode processes. This famous equivalent circuit combines the elements of charge transfer (R_{ct}), diffusion (W), double layer capacitance (C_{dl}) and electrolyte conductivity (R_s).

Figure 2.8; Randles equivalent circuit for a simple electrochemical system.

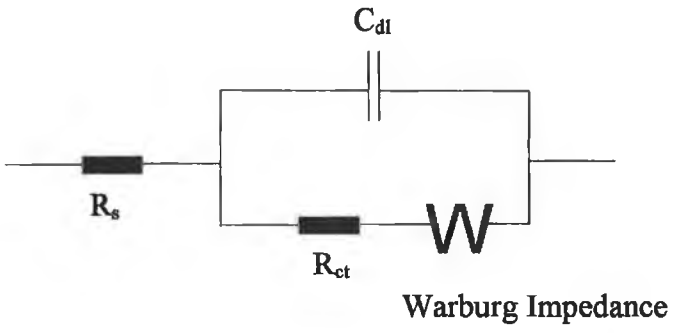

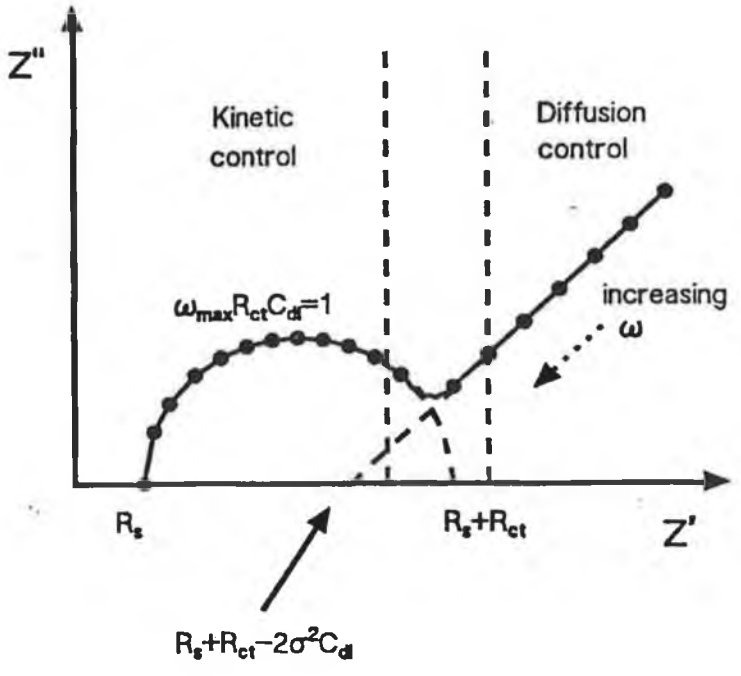

For the Randles equivalent circuit, the real and imaginary components of the impedance may be represented;

$$Z' = R_s + \frac{R_{ct} + \sigma\omega^{-1/2}}{(C_{dl}\sigma\omega^{-1/2} + 1)^2 + \omega^2 C_{dl}{}^2 (R_{ct} + \sigma\omega^{-1/2})^2} \quad \textbf{(2.21)}$$

$$Z'' = \frac{\omega C_{dl}(R_{ct} + \sigma\omega^{-1/2})^2 + \sigma\omega^{-1/2}(\omega^{1/2} C_{dl}\sigma + 1)}{(C_{dl}\sigma\omega^{1/2} + 1)^2 + \omega^2 C_{dl}^2 (R_{ct} + \sigma\omega^{-1/2})^2} \quad \textbf{(2.22)}$$

R_s = Solution resistance.

R_{ct} = Charge transfer resistance.

C_{dl} = Double layer capacitance.

σ = Warburg coefficient.

ω = Frequency.

Figure 2.8 results from the consideration of two limiting cases.

(1) Where charge transfer is important. This occurs at high frequency or where diffusion is unimportant. Equations 2.21 and 2.22 may be simplified to;

$$Z' = R_s + \frac{R_{ct}}{1 + \omega^2 C_{dl}^2 R_{ct}^2} \quad \textbf{(2.23)}$$

$$Z'' = \frac{\omega C_{dl} R_{ct}^2}{1 + \omega^2 C_{dl}^2 R_{ct}^2} \quad \textbf{(2.24)}$$

Eliminating ω from equations 2.23 and 2.24 yields;

$$(Z'-R_s - R_{ct}/2)^2 + (Z'')^2 = (R_{ct}/2)^2 \quad \textbf{(2.25)}$$

This refers to a semi-circle centred on $Z' = R_s + R_{ct}/2$ of radius $R_{ct}/2$.

At the maximum of the semi-circle $C_{dl} = \dfrac{1}{\omega_{max} R_{ct}}$ **(2.26)**

ω_{max} = Frequency at which the imaginary component of the impedance reaches a maximum.

(2) At lower frequencies and where charge transfer resistance is small compared to diffusion, the impedance is given.

$$Z' = R_s + R_{ct} + \sigma\omega^{-1/2} \quad \textbf{(2.27)}$$

$$Z'' = \sigma\omega^{-1/2} + 2\sigma^2 C_{dl} \quad \textbf{(2.28)}$$

Eliminating ω gives $Z'' = Z' - (R_s + R_{ct} - 2\sigma^2 C_{dl})$ **(2.29)**

which is a straight line of unit slope.

There is no frequency dependence at this point, but there is a linear correlation of Z' and Z" which is indicative of a diffusion controlled process. Warburg pioneered the study of diffusional phenomena and therefore, this diffusion controlled impedance is termed the Warburg Impedance (W).

$$W = \frac{\sigma}{\sqrt{\omega}} - j\frac{\sigma}{\sqrt{\omega}} \quad \textbf{(2.30)}$$

This equation (2.30) implies that at any frequency ω, the real and imaginary

components of the impedance are equal and proportional to $\frac{1}{\omega}$ where σ represents the Warburg coefficient and $\sigma = Z'' \sqrt{\omega}$. At high frequencies the term $\frac{1}{\omega}$ is small and consequently the Warburg impedance is only observed at lower frequencies.

2.3.3 AC Impedance of Ag/AgCl electrodes.

The potential of silver/silver chloride electrodes has been found to be relatively small and stable, leading to their use as reference electrodes in potentiometric systems[45]. An Ag/AgCl interface will readily exchange electrons according to the equation;

$$AgCl_{(s)} + e^- \rightleftharpoons Ag_{(s)} + Cl^-_{(aq)} \qquad \textbf{(2.31)}$$

When a DC current (Faradic current) is passed through such a system, charge is transferred across the interface with relative ease and little voltage is lost. Therefore silver/silver chloride electrodes are said to be fairly non-polarisable, where polarisation is defined as the departure of the electrode potential from its reversible value by the passage of Faradic current. Owing to the large value of the exchange current density in Ag/AgCl electrodes, small currents caused by the measuring circuit will have a negligible effect on the measured potential. In other words Ag/AgCl electrodes display over-potentials which tend to zero. Ag/AgCl electrodes have a low general impedance which increases as the frequency is lowered[46]. It has been shown that in systems where Ag/AgCl electrodes are used as reference electrodes, their impedance is several orders of magnitude less than that of the measuring electrode and therefore may be ignored relative to the latter[47].

The Ag/AgCl electrode/electrolyte interface impedance may be represented by a double layer capacitance (C_{dl}) in parallel with a charge transfer resistance (R_{ct})[48]. In addition, there is also a resistance associated with contact of the AgCl surface with the electrolyte (R_s), which is in series with the above. The basic equivalent circuit model for an Ag/AgCl reference electrode is shown in figure 2.9.

Figure 2.9; The Equivalent circuit model attributed to an Ag/AgCl reference electrode.

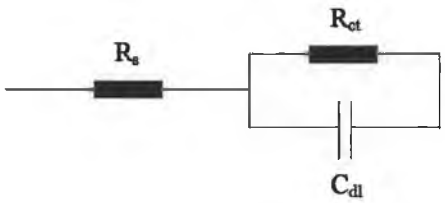

$$Z_{Ag/AgCl} = R_{ct} + R_s + j\frac{1}{\omega C_{dl}} \qquad (2.32)$$

Figure 2.10 shows a typical impedance spectrum obtained for a screen printed Ag/AgCl electrode in contact with a 0.1 M chloride solution.

Figure 2.10; The AC Impedance spectrum of a screen printed Ag/AgCl electrode in 0.1M chloride solution. The frequency range scanned was from 10 KHz to 1Hz and a 10 mV sinusoidal exciting voltage was used.

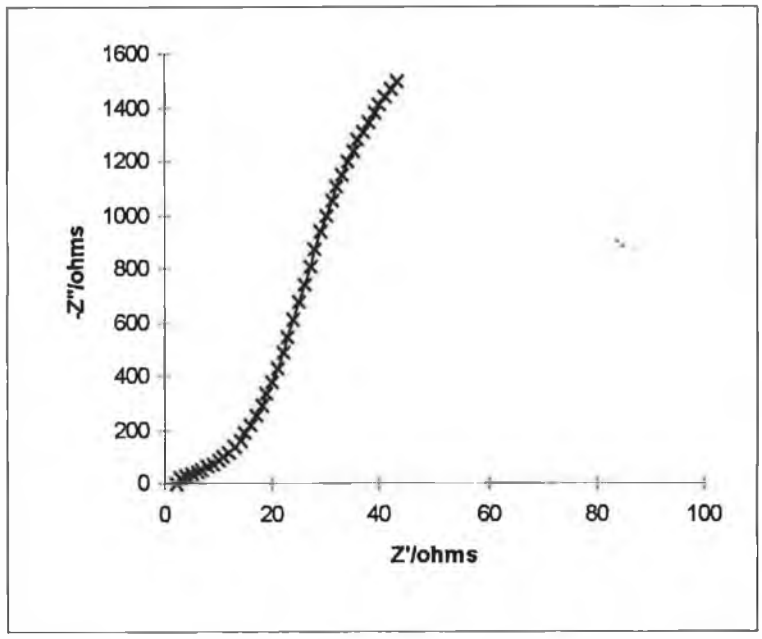

As mentioned previously, charge is transferred across the Ag/AgCl interface with relative ease leading to a low value of charge transfer resistance[49]. At high frequencies (> 10 kHz) the interface impedance is dominated by that of the double layer capacitance. It follows therefore that Ag/AgCl electrodes have very low interface impedances. It has been shown that there is an optimal amount of deposited chloride which will yield the lowest impedance available for a given electrode[48,50]. AgCl is itself a poor conductor having a resistivity of around 10^6 Ω cm[51], however a very light layer of AgCl will tend to decrease the series resistance (R_s) due to the effect of a rougher surface. As the layer thickness increases the series resistance will increase and will eventually outweigh the decrease in interface impedance due to its presence in the first place.

2.3.4 AC Impedance of PVC membranes[52].

AC Impedance may be used to investigate ion transport in PVC membrane electrodes. Impedance plane plots of -Z" Vs Z' generally present at least one semi-circle as shown in figure 2.11. This arises in the high frequency region of the spectrum and therefore is likely to be associated with the rapid exchange of ions at the membrane | bathing solution interface. It may be described as a parallel resistance and capacitance[53] in series with a resistance associated with contact with the electrolyte (R_s). The capacitance (C_b) refers to the bulk geometric capacitance i.e. the capacitance defined by the external solution surface charge, membrane thickness and the membrane dielectric constant. The external solution surface charge refers to a double layer of charge which tends to form near the surface of such membranes due to the selective exchange of analyte ions. The high frequency resistance is a function of the membrane bulk resistance (R_b). If a semi-circle is fitted to the spectrum data, its diameter corresponds to bulk resistance (R_b).

Figure 2.11; High frequency semi-circle associated with PVC membrane electrodes.

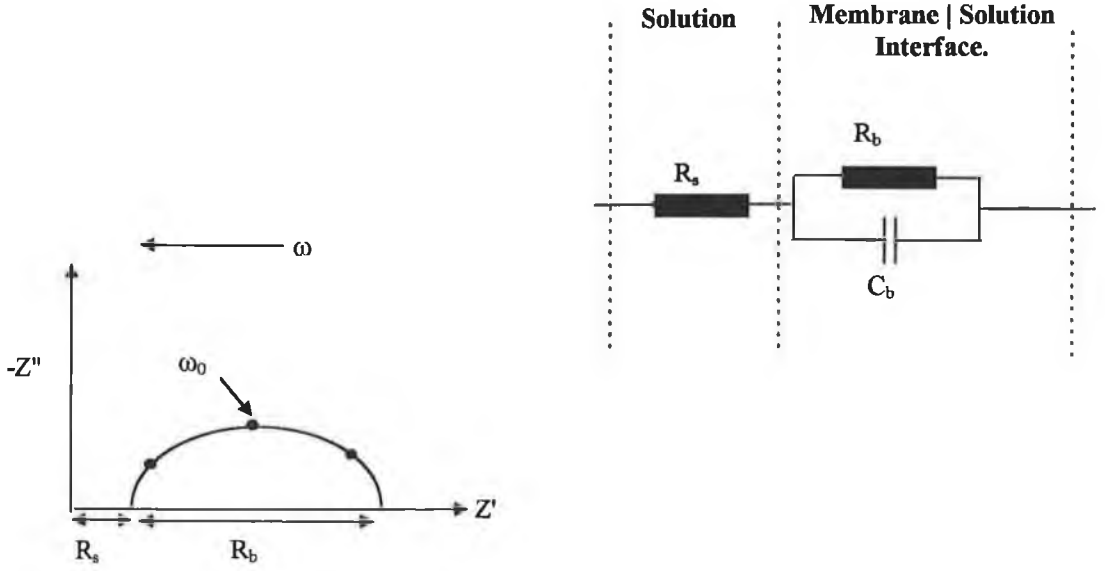

The frequency at the semi-circle maximum (ω_0) is given by;

$$\omega_0 = \frac{1}{R_b C_b} \qquad \textbf{(2.33)}$$

Therefore the bulk capacitance can be easily calculated.

This capacitance depends on membrane dimensions and its dielectric constant[53,54,55] according to;

$$C_b = \frac{\varepsilon A}{d} \qquad \textbf{(2.34)}$$

for ε = dielectric constant.

A = area.

d = membrane thickness.

The dielectric constant is an indication of the number of dissociated charge carriers and is larger in PVC membranes (~ 15) than in pure PVC or plasticiser (~ 5), which is related to the increased polarity of the former.

The bulk resistance R_b is affected by membrane dimensions and conductance.[54,55] Bulk resistance tends to decrease with increasing concentration of bathing solution as more analyte ion is available for complexation. Also, as soaking time increases, so does water uptake until the membrane attains its equilibrium water content. Membranes bathed in water will show continuous resistance increases, whereas membranes bathed in aqueous analyte solutions will show a slight increase in resistance which tends to become constant over time[53].

$$R_b = \frac{d}{\upsilon A} \qquad \textbf{(2.35)}$$

for υ = conductance (i.e. reciprocal of resistance).

In addition to the high frequency semi-circle, one may also observe a second semi-circle or other more complex form on the mid to lower frequency end of the spectrum[56]. This semi-circle is often known as a kinetic semi-circle and develops due to either a slow charge transfer of ions which is potential dependent (an electrochemical "activation" over-potential) or a slow potential dependent transfer of ions through a high resistance surface film (i.e. high resistance relative to the bulk). Second semi-circles are also thought to be related to the development of site free surface films, perhaps where a slow loss of membrane components tends to cause a build up at the surface as it tends to increase with soaking time[53]. Once again, this region may be described in terms of a parallel resistor | capacitor arrangement (R_2,C_2), where R_2 may be attributed to a surface resistance and C_2 to a low frequency capacitance approximating the double layer at each membrane | electrolyte interface. The semi-circle will be more easily observed where its time constant (τ) does not lie beyond the lower frequency limit of the measuring device;

$$\tau = R_2 C_2 \qquad \textbf{(2.36)}$$

In general, a second semi-circle tends to disappear when surface rates become fast compared with bulk bathing electrolyte transport rates. It has been shown[53] that surface resistance disappears when argon or air is blown onto the submerged surface of the electrode, i.e. it had the same effect as removing the bathing solution or the electrode.

The inclusion of charge carriers (i.e. KTpClPB) in the membrane will tend to cause this surface rate semi-circle to shift into the frequency range by decreasing film resistance and the time constant.

Figure 2.12; Impedance plane plot showing a high frequency semi-circle and second semi-circle at the mid to lower frequency end of the spectrum.

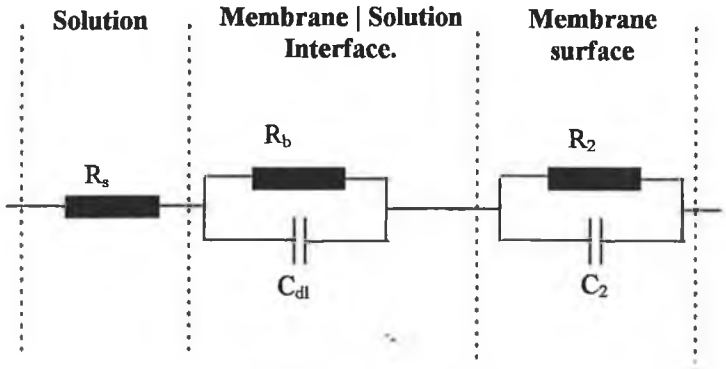

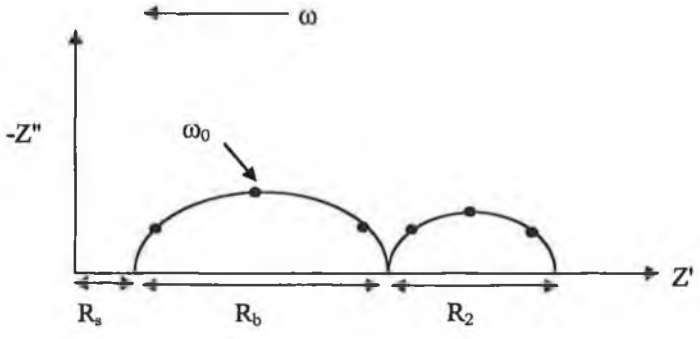

Finally, a Warburg impedance may also be observed. This will occur where current is controlled by diffusion of a charge carrier or metal-ligand complex. In fixed site carrier containing membranes, current may be controlled by the back diffusion of free carriers even though the actual charge carriers the metal-ligand complex is carrying the current[56]. This type of Warburg impedance would be expected to occur at low concentrations of charge carriers. At higher carrier concentrations, this type of concentration polarisation is not likely to occur because current will be limited by bulk resistances and not by the back diffusion of carriers. For this reason, Warburg impedances, observed as a line 45° to the Z' axis, are not usually observed for normal PVC membranes except at very low frequencies ($\cong$ 0.001 Hz)[57].

2.4 Bibliography.

[1] K. Suzuki, H. Aruga, T. Shirai; Anal. Chem., 55 (1993) 2011.

[2] M. Meyerhoff, D. Pranitis; Anal. Chem., 59 (1987) 2345.

[3] M. Meyerhoff, Y. Fraticelli; Anal. Chem., 53 (1981) 992.

[4] G. Guilbault, R. Durst et al; Pure and Applied Chemistry, 48 (1976) 127.

[5] R.P. Buck, E. Lindner; Pure and Applied Chemistry, 66 (1994) 2527.

[6] C. Macca; Anal. Chim. Acta, 321 (1996) 1.

[7] D. Diamond, F.J. Sáez de Viteri; Analyst, 119 (1994) 749.

[8] D. Diamond, R.J. Forster; Anal. Chim. Acta, 276 (1993) 75.

[9] G.J. Moody, J.D.R. Thomas; *Selective Ion Sensitive Electrodes,* Marrow, Watford, 1971.

[10] D. Diamond, R.J. Forster; Anal. Chem., 64 (1992) 1721.

[11] D. Diamond, P. Kane; Talanta, in Press.

[12] D.E. Davey, D.E. Mulcahy, G.R. O'Connell; Electroanalysis, 8 (1996) 274.

[13] C.B. Ranger; Anal. Chem., 53 (1981) 20A.

[14] D. Betteridge; Anal. Chem., 50 (1978) 832A.

[15] J. Ruzicka, E.H. Hansen; Anal. Chim. Acta, 78 (1975) 145.

[16] K.K. Stewart, G. Beecher, P. Hare; Anal. Biochem., 70 (1976) 167.

[17] M. Meyerhoff, P. Kovach; J. Chem. Edu., 60 (1983) 766.

[18] J. Vanstanden; Anal. Proc., 24 (1987) 331.

[19] J. Douglas; Anal. Chem., 61 (1989) 922.

[20] D.E. Davey, D.E. Mulcahy, G.R. O'Connell; Electroanalysis, 5 (1993) 581.

[21] W.E. Van der Linden; Trends in Anal. Chem., Vol. 1, 8 (1982) 188.

[22] G. Taylor; Proc. Roy. Soc. Ser. A, 219 (1953) 186.

[23] D. Betteridge; Anal. Chem., 50 (1978) 832A.

[24] J. Vanderslice, K. Stewart, A. Rosenfeld, D. Higgs; Talanta, 28 (1981) 11.

[25] J. Ruzicka, E.H. Hansen; Anal. Chim. Acta., 99 (1978) 37.

[26] K. Cammann; Fresenius Z Anal. Chem., 329 (1988) 691.

[27] M. Telting Diaz, D. Diamond, M.R. Smyth; Anal. Chim. Acta., 251 (1991)149.

[28] M. Trojanowicz, W. Matuszewski; Anal. Chim. Acta, 151 (1983) 77.

[29] D. Diamond, F. J. Sáez de Viteri; Electroanalysis, 6 (1994) 9.

[30] T. Dimitrakopoulos, P.W. Alexander, D.B. Hibbert; Electroanalysis, 8 (1996) 438.

[31] D. Diamond; Electroanalysis, 5 (1993) 795.

[32] Sluyters-Rehbach and Sluyters; Electroanalytical Chem., 4 (1970) 1.

[33] M.J.D. Brand, G.A. Rechnitz; Anal. Chem., 41 (1969) 1185.

[34] M.J.D. Brand, G.A. Rechnitz; Anal. Chem., 42 (1970) 478.

[35] A.K. Covington ,R. Armstrong, G.P. Evans; J. Electroanal. Chem., 159 (1983) 33.

[36] A.K. Covington, R.D. Armstrong,, G.P. Evans, T. Handyside; Electrochim. Acta, 29 (1984) 1127.

[37] J. Butler; Trans. Faraday Soc., 19 (1924) 729.

[38] M. Volmer, T. Erdey-Gruz; Z. Phys. Chem. (Leipzig), 150 (1930) 203.

[39] A. Bard and J. Faulkner; *Electrochemical methods*, Wiley, New York, 1980.

[40] Southampton Electrochemistry Group; *Instrumental Methods in Electrochemistry*, Chapter 8, Ellis Horwood series in Physical Chemistry, J. Wiley & Sons, Sussex, U.K. 1985.

[41] C.D. Crawley, G.A. Rechnitz; J. Memb. Sci., 24 (1985) 201.

[42] K. Cammann, G.A. Rechnitz; Anal. Chem., 48 (1976) 856.

[43] K. Cammann; Anal. Chem., 50 (1978) 936.

[44] J.E.B. Randles; Discuss. Faraday Soc., 1 (1947) 11.

[45] G.J. Janz, H. Taniguchi; Chem. Rev., 53 (1953) 397.

[46] L. Geddes, L. Baker, A. Moore; Med. Biol. Eng., 7 (1969) 49.

[47] Y.J. Kingma, J. Lenhart, N.G. Durdle, K.L. Bowes, M.M. Chambers; Med. Biol. Eng. Comput., 21 (1983) 351.

[48] E.T. McAdams, P. Henry, J. McC Anderson, J. Jossinet; Clin. Phys. Physiol. Meas., 13 (1992) 19.

[49] Y.J. Kingma, J. Lenhart, K.L. Bowes, M.M. Chambers, N.G. Durdle; Med. Biol. Eng. Compt., 21 (1983).

[50] L. Geddes; *Electrodes and the measurement of bioelectric events*, J. Wiley & Sons Ltd., New York, 1972.

[51] G.J. Janz, D. Ives; Ann. NY. Acad. Sci., 148 (1968) 210.

[52] R.P. Buck; Ion Sel. Electrode Rev., 4 (1982) 3.

[53] R.P. Buck, G. Horvai, E. Gráf, K. Tóth, E. Pungor; Anal. Chem., 58 (1986) 2735.

[54] U. Oesch, W. Simon; Anal. Chem., 52 (1980) 692.

[55] U. Oesch, W. Simon; Helv. Chim. Acta., 62 (1979) 754.

[56] R.P. Buck, G. Horvai, E. Gráf, K. Tóth,, E. Pungor; Anal. Chem., 58 (1986) 2741.

[57] R.D. Armstrong, J. Lockhart, M. Todd; Electrochim. Acta, 31 (1986) 591.

Development of a Flow-injection Analysis System for the determination of Sodium in Blood Samples

3.1 Introduction.

Sodium has been determined in biological specimens by several techniques, including atomic absorption spectrometry (AAS), flame photometry and potentiometry[1]. Although AAS may be the method of choice for many metal ions, it is not ordinarily used for sodium determination because the simpler and readily available flame emission methodology is entirely adequate. An ideal method for sodium determination requires, in addition to accuracy and precision, speed, simplicity of operation and safety.

The use of combustible gases in flame emission makes the method less attractive from the safety point of view and also restricts analysis to laboratory areas. Analysis by ion-selective electrode has become the method of choice for the determination of electrolytes in body fluids, as the technology is simple, portable, adaptable for continuous monitoring and compatible with multi-component tests performed by large chemical analysers.

The development of a sodium polymeric ion-selective membrane electrode would provide an ideal method of analysis, particularly if it were to utilise the inherent advantages of flow injection analysis. As already described in Chapter 2, these include controlled sample dispersion, variable flow rates, high sample throughput, enhanced kinetic selectivity and small reagent consumption.

3.2 Experimental Details.

It has been demonstrated that certain calix[4]arene derivatives can be successfully used as ionophores in sodium ion-selective electrodes[2,3,4]. In the past few years, a new series of calix[4]arene derivatives have been synthesised which, on the basis of steady-state measurements, demonstrate excellent selectivity against a wide range of interferents in blood, such as potassium and calcium[5]. This chapter describes the application of one of these ionophores to the analysis of blood sodium using flow injection potentiometry[6].

3.2.1 Equipment and materials.

Reagents:

2-nitrophenyl-octylether (2-NPOE), tetrahydrofuran (THF), high molecular weight poly(vinyl)chloride and potassium tetrakis(4-chlorophenyl)borate (KTpClPB) were Selectophore® grade purchased from Fluka. Tris(hydroxymethyl)methylamine (Tris) was GPR grade from BDH and Tris(hydroxymethyl)aminomethane-hydrochloride (Tris-hydrochloride) was BioChemika grade from Fluka. NaCl was reagent grade, purchased from Riedel-de Haën.

Ionophore:

The ionophore used was a calix[4]arene derivative (see Chapter 1, figure 1.4b) known as Cone 5b-Et, which was provided by Professor Seiji Shinkai and Dr. Hiromasa Yamamoto of the Research and Development Corporation of Japan[5].

Membrane composition:

The membrane was prepared as follows:

10 mg ionophore and 2 mg ion exchanger (KTpClPB) were dissolved in 1 g plasticiser (2-NPOE). 0.5 g of high relative molecular mass PVC was added to give a slurry. Tetrahydrofuran (THF) was added dropwise until a clear solution was obtained and the resulting solution was poured into a 10 cm diameter, glass Petri dish and left covered with a loosely fitting lid until dry (approximately three days). Evaporation of the THF left clear PVC membranes from which the sensing membranes were cut.

Blood Samples[♦]:

The samples were centrifuged at 3200 rpm for six minutes to separate the cells. The plasma samples were then analysed prior to receipt using an Hitachi 747 clinical chemistry analyser with indirect reading electrodes. Lithium-Heparin was used as the anti-coagulant.

Flow injection analyser:

This consisted of a single channel, wall jet type, flow through cell (EDT Instruments Ltd., Dover, Kent, UK) into which the working and reference electrodes were placed. The body of the working electrode was made from PVC onto which the membrane of about 3 mm diameter was "glued" using a small amount of THF. The reference electrode utilised a Ag/AgCl wire immersed in KCl. A four channel peristaltic pump (Minipuls 3, Gilson Medical Electronics, Middleton, WI, USA) was used to pump the carrier stream and sample at a flow rate of 1.0 ml/min. The injection port consisted of a set of three-way switching valves (Lee, Westbrook, CT, USA). They were configured so that it was possible to inject manually using a syringe into a 150 uL sample loop. The entire system was interfaced with a PC-486DX by means of an input/output (I/O) AT-MIO-16DL card (National Instruments, Austin, Texas, USA). The software used was written in-house using LabVIEW 3.0, which is a graphical programming environment specifically designed for applications involving laboratory data acquisition and analysis within the WINDOWS environment[7]. Data processing was carried out using Microsoft Excel 5.0. A diagram of the entire system is shown in Figure 3.1.

♦ Blood samples were provided and analysed prior to receipt by, Dr. Peter Gaffney at the Central Pathology Laboratory, St. James' Hospital, Dublin.

Figure 3.1; Flow injection analysis system.

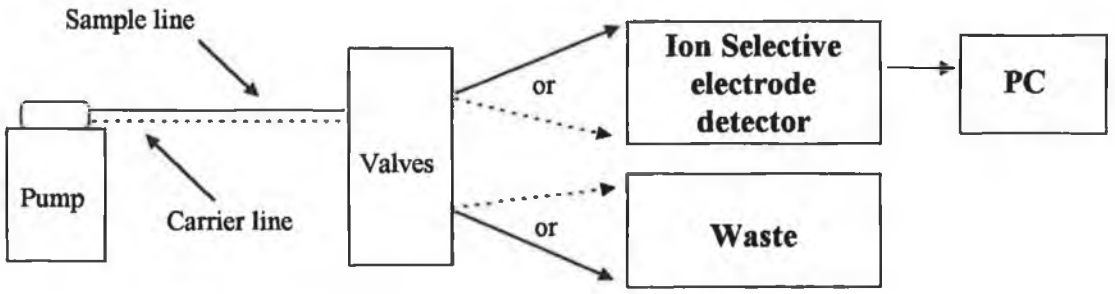

Carrier and standard solutions:

The carrier used consisted of 100 mM Na^+ diluted 5 fold with a Tris/Tris-HCL buffer solution to give a final sodium concentration of 20 mM, an ionic strength of 50 mM and a pH of 7.4. Tris and Tris-HCl refer to solutions of the compounds Tris(hydroxymethyl)aminomethane and Tris(hydroxymethyl)aminomethane hydrochloride respectively. These compounds can be blended to produce any desired pH between 7 and 9 and have been thoroughly established as an excellent biochemical buffer[8]. However, before any experiments were carried out involving the blood samples, it was confirmed that the ion-selective electrode did not respond to changes in Tris/Tris-HCl concentration. This was done by making several injections of 22 mM Tris/Tris-HCl onto a constant background carrier concentration of 50 mM Tris/Tris-HCl. As can be seen in Figure 3.2, the only fluctuations in potential are due to the valves switching over and therefore the ISE does not respond to changes in buffer concentration.

Figure 3.2; Establishing the fact the ISE will not respond to changes in buffer concentration.

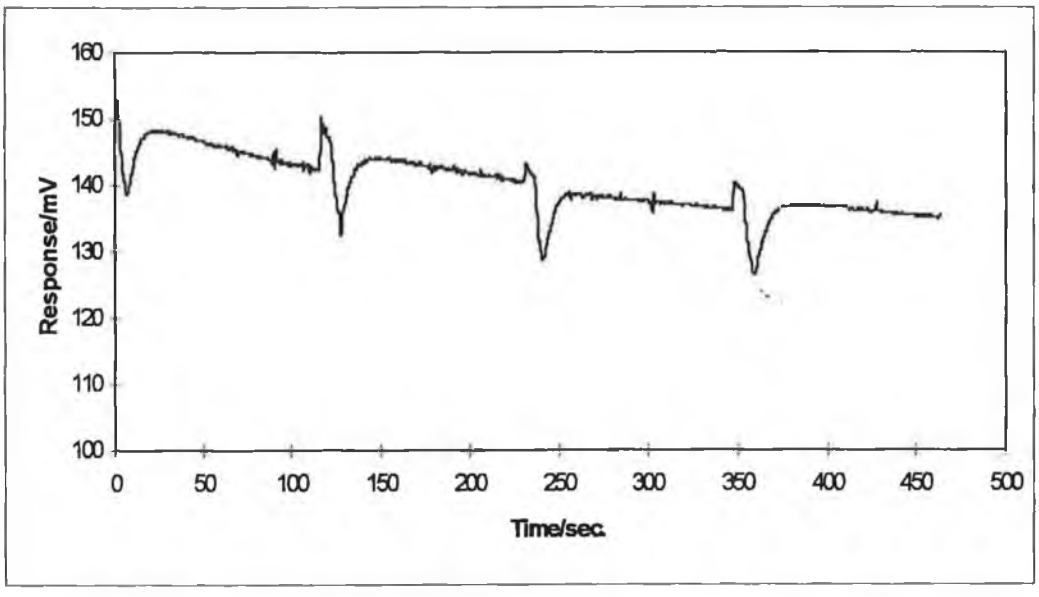

Once Tris/Tris-HCl was established as a suitable buffer, calculations were carried out based on the following equations, in order to establish the exact quantities of Tris/Tris-HCl necessary to give the required pH 7.4 and an ionic strength of 50 mM in both samples and standards:

$$Tris\text{-}H^+ \rightleftharpoons Tris + H^+ \qquad \textbf{(3.1)}$$

where "Tris-H^+" refers to the hydrochloric acid form and "Tris" to its conjugate base.

An equilibrium constant expression may be written for this reaction;

$$Ka = \frac{[H^+][Tris]}{[Tris - H^+]} \qquad \textbf{(3.2)}$$

The pH of a solution of the acid and conjugate base is given by the Henderson-Hasselbalch equation;

$$pH = pKa - \log\frac{[Tris - H^+]}{[Tris]} \qquad \textbf{(3.3)}$$

and pH = pKa if [Tris] = [Tris-H^+]. As the pKa = 8.1 at 25°C, in order to decrease the pH to 7.4 the equilibrium must shift to make [Tris < Tris-H^+].

With this in mind, equation 3.3 was used to calculate the number of moles of acid and base needed to reach a pH of 7.4 and add the necessary 30 mM to bring the final carrier ionic strength to 50mM after a 5 fold dilution in the buffer.

Sodium concentration in blood typically ranges from 135-155 mM while the pH ranges from 7.2-7.6 with 7.4 being the most common[1]. The standards were therefore prepared in the range of 120 to 160 mM Na^+. The final quantities weighed out for the carrier and standard solutions are shown in Table 3.1.

Table 3.1; Composition of carrier and calibration solutions, pH = 7.4, Ionic strength = 50 mM in both the carrier and each calibration solution.

[Na+] (M / L)	Tris-HCL (g /100 ml)	Tris (g / 100 ml)
0.020 (Carrier)	0.4728	0.0458
0.024	0.4098	0.0397
0.026	0.3782	0.0366
0.027	0.3625	0.0351
0.028	0.3467	0.0336
0.029	0.3310	0.0320
0.030	0.3152	0.0305
0.032	0.2837	0.0275

3.3 Discussion of Results.

Each blood sample and standard was diluted 5 fold with the buffer solution and injections were made directly into the injection loop using a 1 ml syringe. Each sample was assumed to contain approximately 140 mM Na^+ prior to analysis and buffer was added accordingly. An example of some of the peaks obtained is shown in Figure 3.3. The data have been zeroed on the background carrier potential. Figure 3.4 shows the calibration data obtained using all seven calibration solutions. Each point on the graph represents the mean of five injections made at each concentration. Peak heights were determined using LabVIEW software which was written in house♠ and is capable of automatically locating flow injection peaks and displaying the peak height in mV.

Figure 3.3: An example of some of the flow injection peaks obtained during electrode calibrations.

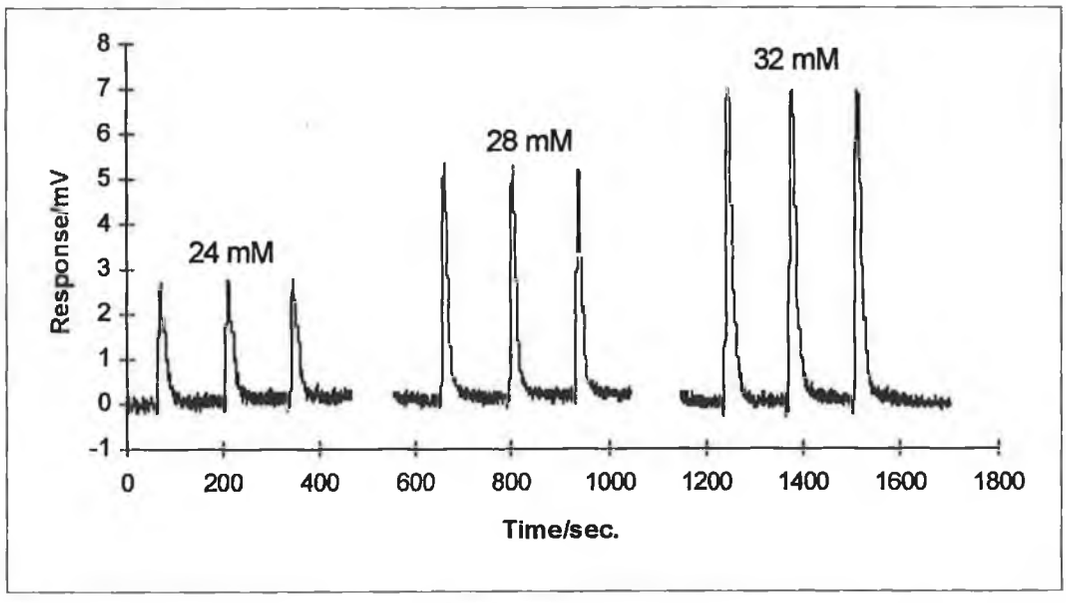

♠ LabVIEW software was written by Dr. F. J. Sáez de Viteri at Dublin City University.

Figure 3.4; The calibration curve obtained using sodium solutions ranging in concentration from 24 mM to 32 mM after a 5 fold dilution with buffer. Standard deviation values based on a sample population of 5 are shown as y-error bars.

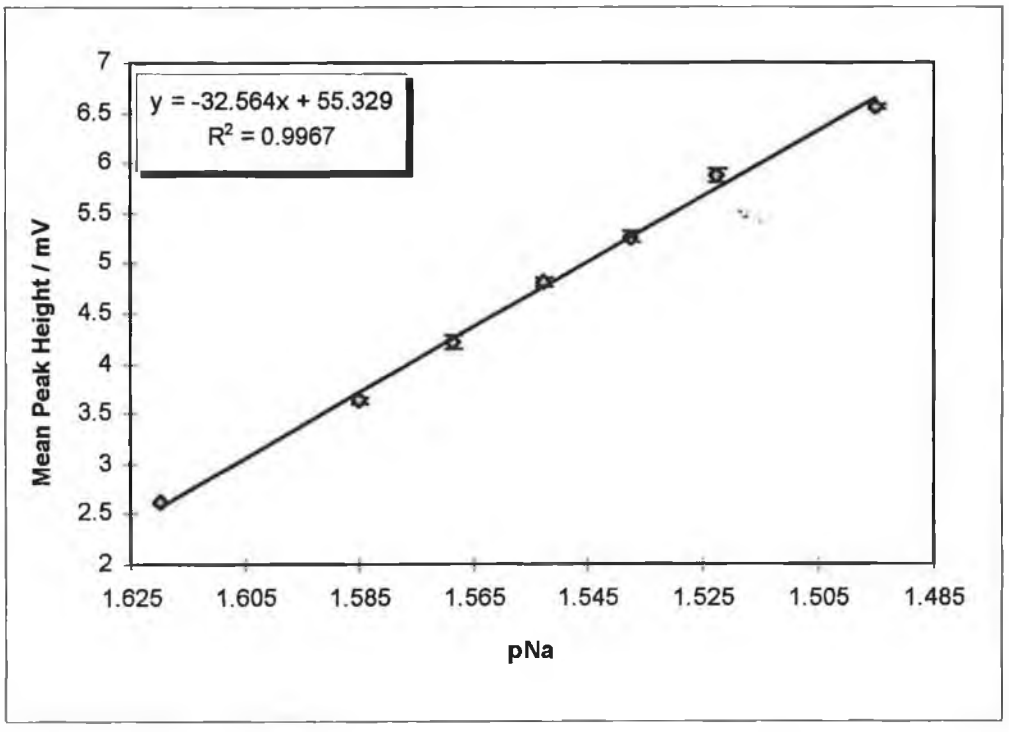

In order to observe accurately such a small range of concentrations, it is necessary to have a high background analyte concentration. In this case a background of 20 mM Na^+ (after a 5 fold buffer dilution) was used. From figure 3.4, it is clear that the slope of the calibration curve is sub-Nernstian (32.56 mV $decade^{-1}$), with each peak being about 50% of that predicted for steady-state measurements using the Nernst equation. This results from the non steady-state nature of FIA measurements and also the high sodium background used in the carrier solution. In previous studies[2], the use of a high background of sodium in the carrier solution was observed to suppress the electrode slope. However, the chemical offset effect obtained in this case means that high gains can be used to amplify the signal, leading to good precision over the

calibration range. Table 3.2 shows a comparison of the sodium concentrations obtained using flow injection analysis and those quoted by the hospital. A clear correlation exists between the estimated and the true values, suggesting that the mV responses follow closely the slight changes in sodium concentration in the blood samples. The relative % error is about ± 2% or less [mean squared error (n = 8) is 1.769], and is probably caused by a slight bias in the calibration plot. The relationship between the relative percentage error obtained and the matrix composition was studied by calculating the variance (R^2) values between the sodium error and the matrix components for which analytical data were available. These values are shown, together with the matrix composition in Table 3.2.

Table 3.2; Composition of blood samples and results of sodium analysis. The mean squared error (MSE) for n = 8 is also shown. All concentrations are in moles L^{-1}.

Sample	K^+	Urea	Creatinine	Hydrogencarbonate	Na^+ (Hospital)	Na^+ (FIA)	Relative error (%)
1	0.0027	0.0028	0.000049	0.027	0.126	0.1234	-2.15
2	0.0026	0.0163	0.000704	0.018	0.132	0.1303	-1.32
3	0.005	0.0181	0.000178	0.025	0.138	0.1349	-2.22
4	0.0046	0.0029	0.000079	0.03	0.139	0.1378	-0.88
5	0.004	0.0044	N/A	N/A	0.141	0.1418	0.60
6	0.0049	0.0047	0.000073	0.027	0.141	0.1400	-1.00
7	0.0051	0.004	N/A	N/A	0.142	0.1429	0.60
8	0.0038	0.0041	0.000087	0.029	0.142	0.1429	0.61
MSE							1.77
R^2	0.0599*	0.2496*	0.0155*	0.1281*	0.5135*	0.9967$	

* Variance (R^2) of hospital quoted values with relative % error of sodium.

$ Variance of estimated sodium values and hospital quoted values.

There is no correlation between the sodium relative percentage error and the sample matrix (potassium, urea, creatinine and hydrogencarbonate). Some correlation is observed for the relative percentage error and the sodium content ($R^2 = 0.5135$), supporting the view that calibration bias is an important factor in the error. Throughout these experiments there was no correction whatsoever for any kind of possible interference in the matrix. Therefore, this electrode has excellent potential for use in clinical analysis where the matrix is complex and there are several possible interferents. Protein deposition on the membrane surface is minimal owing to the flow rate of 1.0 ml min^{-1} and also because the sample loop was flushed both as the carrier pushed the sample towards the electrode and afterwards by repeated injection of carrier into the loop.

In conclusion, a novel highly selective sodium ionophore has been synthesised which shows excellent potential as a means of sodium analysis in blood, with only very limited sample preparation. It combines the advantages of flow injection analysis and potentiometric detection with those of computer control to produce a blood analyser with the potential to be both user friendly, analytically reliable, portable and applicable to continuous monitoring.

3.4 Bibliography.

[1] R. Henry, D. Cannon, W. Winkleman; *Clinical Chemistry*, Harper and Row, Hagerstown, Maryland, USA, 1974.

[2] M. Telting-Diaz, D. Diamond, M.R. Smyth; Anal. Chim. Acta., 251 (1991) 149.

[3] K. Cunningham, G. Svehla, S.J. Harris, M.A. McKervey; Anal. Proc., 28 (1991) 294.

[4] A. Cadogan, D. Diamond, M.R. Smyth, M. Deasy, M.A. McKervey, S.J. Harris; Analyst, 114 (1989) 1551.

[5] H. Yamamoto, S. Shinkai; Chem. Letters, (1994) 1115.

[6] **S. Walsh**, F. J. Sáez de Viteri, D. Diamond; Anal. Proc. Inc. Anal. Comm., 32 (1995) 365.

[7] F. J. Sáez de Viteri, D. Diamond; Anal. Proc., 31 (1994) 229.

[8] Sigma Chemical Catalogue; Sigma-Aldrich Co. Ltd., Dorset, UK, 1994.

Solid-State Sodium Selective Sensors based on Screen Printed Ag/AgCl Reference Electrodes

4.1 Introduction.

This Chapter follows the progress in development of a solid-state sodium selective sensor. It is based on a combination of planar screen printed Ag/AgCl electrodes and an ion-selective PVC membrane.

The preliminary aim of this research is to optimise the design and construction of the solid-state ion-selective electrode. With this in mind, two basic solid-state designs will be investigated and compared to a conventional ion-selective electrode with internal filling solution. A perspex cell will be designed to house the electrodes during the study and the electrochemical cell will be completed by use of a miniature Ag/AgCl reference electrode with internal filling solution. The solid-state electrodes will be compared in terms of their potentiometric response and charge transfer characteristics. In the first solid-state electrode (Electrode A), a sodium-selective PVC membrane is deposited directly on top of a screen printed Ag/AgCl electrode. The second solid-state design (Electrode B), involves the use of a NaCl doped hydrogel layer, between the Ag/AgCl electrode and the PVC membrane. This is intended to provide a mechanism to relieve any blockage to charge transfer which is known to occur when PVC membranes of this type are used directly on top of Ag/AgCl electrodes. In addition, it is thought that the adhesive properties of the hydrogel might improve the physical contact between the PVC/hydrogel and hydrogel/AgCl interfaces[1,2]. The more intimate contact at the boundaries of these films should facilitate charge transfer, leading to less probability of a blocked interface arising during deposition of the PVC film.

When these experiments are completed it should be possible to identify which solid-state design warrants further investigation. This electrode will then be characterised with respect to the effect of membrane components on the potentiometric and charge transfer characteristics. Once this has been achieved, our aim is to replace the miniature Ag/AgCl reference electrode with a screen printed Ag/AgCl electrode. This screen printed Ag/AgCl electrode will respond to changes in chloride concentration and so is expected to increase the potentiometric response according to equation 4.1.

$$E_{cell} = E_{ISE} - E_{ref.} \quad \textbf{(4.1)}$$

This is of course assuming that the sodium electrode will show an increase in potential as the NaCl concentration increases and that the chloride electrode will show a corresponding decrease in potential for the same change in NaCl concentration. In effect there will be no true reference electrode at this point but the electrodes will be referenced to their own baseline potential.

Finally the electrode design will be optimised and a study of reproducibility carried out. Conclusions will be drawn from the research to date and some proposals for further work made.

4.2 Equipment and Reagents.

Reagents **:**

2-Nitrophenyl-octylether (2-NPOE), tetrahydrofuran (THF), high molecular weight poly(vinyl)chloride and potassium tetrakis 4-chlorophenyl borate (KTpClPB) were selectophore® grade purchased from Fluka. The NaCl was reagent grade (99.8% pure) purchased from Riedel-de Haën.

Ionophore **:**

The sodium ionophore used was tetra-methoxyethyl p-t-butyl calix(4)arene tetracetate obtained from Professor M. Anthony McKervey of Queen's University, Belfast, Northern Ireland, and was used as received. This ligand (see Chapter 1, figure 1.4a), like other tetraester calix(4)arenes, is known to produce very stable sodium-selective electrodes with excellent characteristics[3,4].

***Hydrogel* :**

A hydrogel is defined as a polymeric material which has the ability to swell in water without dissolving and to retain water within its structure[1]. They can be of either natural or synthetic origin.

The hydrogel used in this study was a 5% carbopol gel (ETD2050) containing 0.2% NaCl[2]. The gel was prepared as follows:

5 g of Carbopol ETD 2050 was slowly dissolved in 90 g of a water:ethanol mixture (70:30) under mechanical mixing at 1500 rpm (Carbopol gels are more tolerant of salt addition when dissolved in a water:alcohol mixture[5]). During the mixing process 0.2 g of sodium chloride was added as 2 g of a 10% W/W solution in water. After complete dissolution of the polymer, the final gel weight was adjusted to 100 g with further addition of the water:ethanol mixture. As the mixing process caused entrapment of air within the gel, centrifugation (3000 rpm for 10 min.) was used to clarify the gel. Gels were then stored at 4°C until required.

***Membrane Composition* :**

A sodium-selective membrane (M1 in Table 4.1) was prepared as follows:

10 mg of the ionophore, together with 2 mg of ion exchanger (KTpClPB) was dissolved in 1 g of plasticiser (2-NPOE). 0.5 g of high molecular weight poly(vinyl)chloride was added to give a slurry. THF was added dropwise while stirring until a clear solution was obtained. This solution was poured into a 10 cm diameter glass petri dish and left covered with a loosely fitting lid. Evaporation of the THF (over approximately 3 days) left clear PVC membranes from which the sensing films were cut.

Three other membranes were also prepared for later use. These membranes (M2, M3 and M4) had compositions as described in Table 4.1, and were made up in a similar manner to membrane M1.

Table 4.1: Relative amounts of membrane components in each of the four different membranes involved in this study.

Component	Ionophore	KTpClPB	2-NPOE	PVC
Membrane M1	10 mg	2 mg	1 g	0.5 g
Membrane M2	None	2 mg	1 g	0.5 g
Membrane M3	10 mg	None	1 g	0.5 g
Membrane M4	None	None	1 g	0.5 g

***Screen Printing* :**

The silver and silver chloride inks used were Electrodag 477ss RFU and B4 458, respectively, obtained from Acheson Colloids Ltd., Plymouth , UK. The inks consisted of very finely divided particles in carbitol acetate solvent with a polyester resin binder. The silver and silver chloride layers were printed onto a polyester sheet through a polyester screen of mesh size T90 using an Avgon semi-automatic screen printer. The printed inks were cured in an oven at 120°C for 20 minutes. After curing the electrodes were cut to size (20 mm X 40mm) and the appropriate sensing films were deposited manually.

***Cell design* :**

The experimental cell is shown in figure 4.1. It consisted of two perspex sections (A and B) held together by 6 metal screws. Two central wells (ca. 1cm diameter), were machined in the upper portion of the cell. The electrodes were sandwiched between the two halves of the cell such that the sensing surfaces were positioned beneath the wells. This design enabled two planar screen printed electrodes to be mounted at the same time. The electrochemical circuit was completed by the use of a miniature (od ca. 2 mm) Ag/AgCl reference electrode (Sentek Ltd., Braintree, Essex, UK).

Leakage of sample was prevented by the inclusion of two rubber gaskets surrounding the wells. The cell has a capacity of approximately 30 mL.

Figure 4.1: (Not to scale), Side view of experimental cell showing an ion-selective electrode in place and the miniature Ag/AgCl reference electrode.

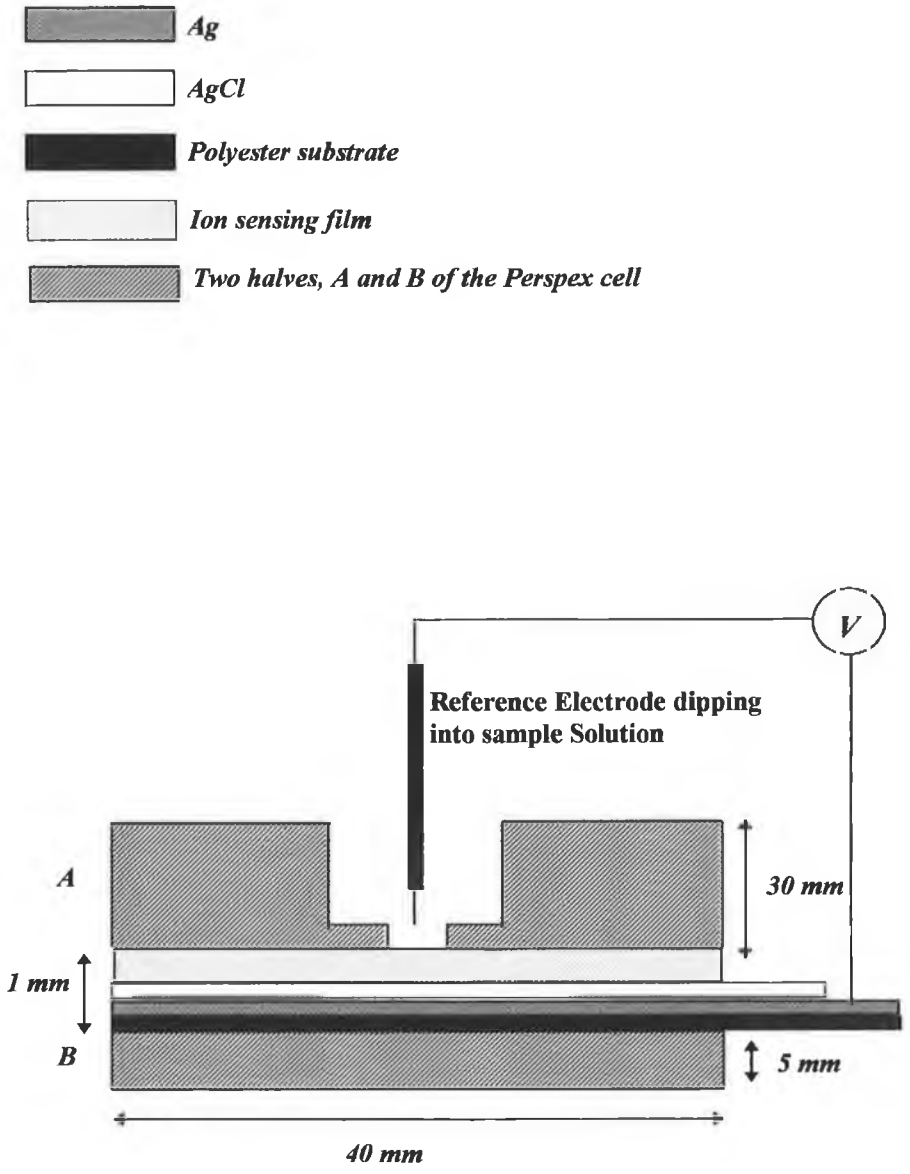

4.3 Electrode design.

Three sodium selective electrode designs were compared during this research. These ISEs have been given the identifiers A, B and C, are described below and are shown schematically in figure 4.2.

Electrode A:

The sodium selective PVC film (Na-PVC) was cut to size (2 cm x 2 cm) and placed directly on top of the AgCl layer.

Electrode B:

Approximately 150 uL of the 0.2% NaCl hydrogel was placed on top of a screen printed Ag/AgCl electrode using a spatula and was then smoothed out, using a glass slide to form a thin layer (approximately 100 μM in thickness). This was allowed to dry for approximately 1 minute, before a sodium selective PVC membrane was placed on top.

Electrode C:

This was a conventional ion-selective electrode[6]. An Ag/AgCl wire was placed inside a teflon (poly methyl methacrylate) electrode body and sealed in position using epoxy resin. A sodium selective PVC membrane was clipped into the electrode tip. The electrode body was then filled with a 1mol dm^{-3} NaCl solution.

Figure 4.2 : Electrodes used in the study. Electrode A consists of a sodium selective PVC membrane directly deposited onto the screen printed AgCl substrate. Electrode B includes a hydrogel layer between the AgCl and the PVC membrane. Electrode C represents a conventional ion-selective electrode with internal filling solution.

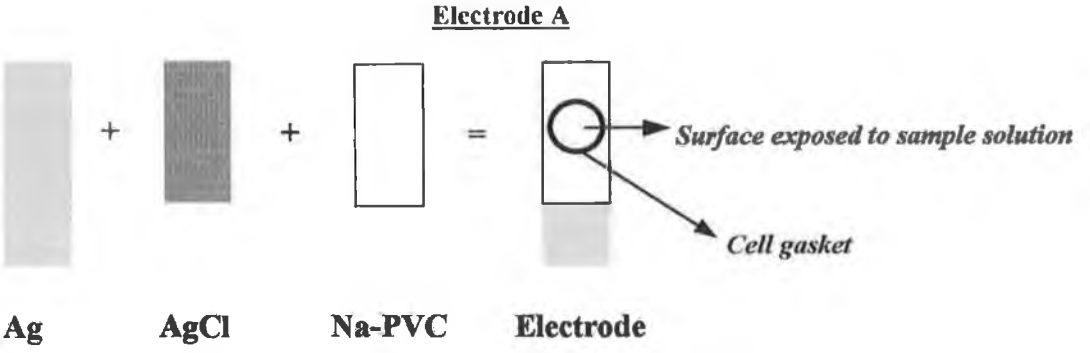

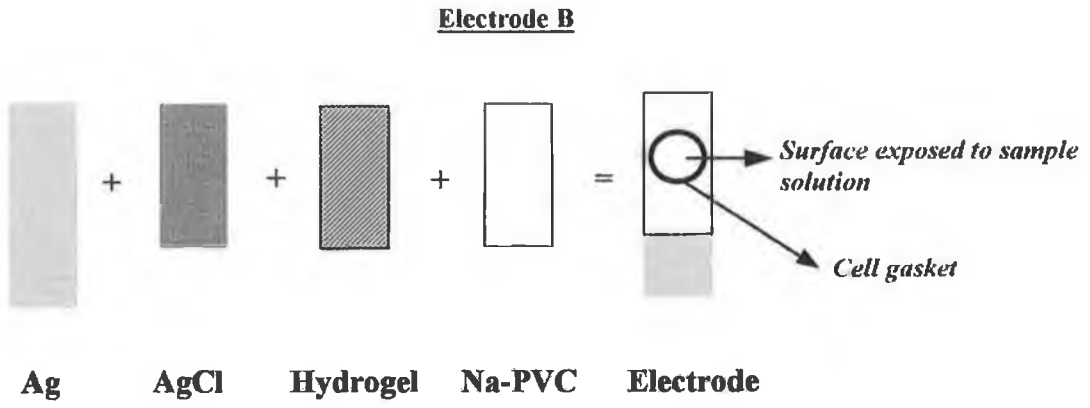

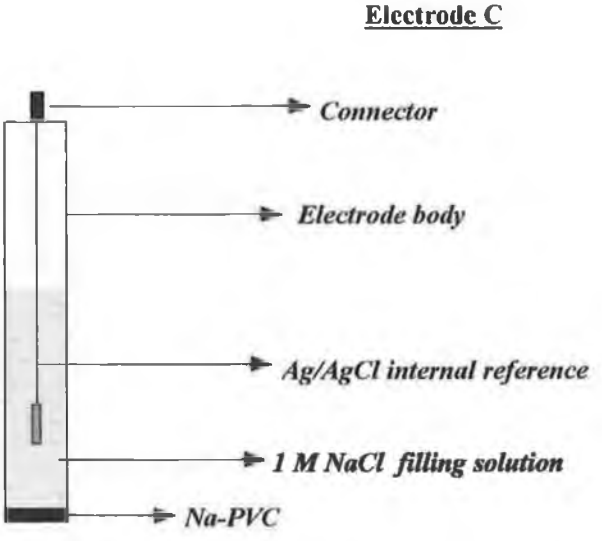

4.4 Experimental Procedures.

4.4.1 A : Characterisation of Solid-State ISEs

Potentiometric experiments.

During the potentiometric experiments, the electrodes were interfaced with a PC-486DX by means of an input/output (I/O) AT-MIO-16DL card (National Instruments, Austin, Texas, USA). The software used was written in-house using LabVIEW 4.0, which is a graphical programming environment specifically designed for applications involving laboratory data acquisition and analysis within the WINDOWS environment[7].

The general characteristics of the electrodes were established by a series of injection experiments in the following manner.
10 mL of 20 mM NaCl solution was placed in the cell. Electrical contact was made with the Ag portion of the screen printed electrode and the miniature Ag/AgCl reference electrode was dipped into the solution to complete the circuit. The electrochemical cells may be described as follows;

- **Electrode A**
  Ag | AgCl | Na-PVC | Test Solution || Sat'd KCl | AgCl | Ag

- **Electrode B**
  Ag | AgCl | 0.2% NaCl Hydrogel | Na-PVC | Test Solution || Sat'd KCl | AgCl | Ag

- **Electrode C**
  Ag | AgCl | 1M NaCl | Na-PVC | Test Solution || Sat'd KCl | AgCl | Ag

Each electrode was calibrated according to the following method:

After a stabilisation period of approximately 3 minutes in 20 mM NaCl, a 500 uL injection of NaCl was introduced such that the Na^+ concentration in the cell reached 30 mM. The solution was stirred moderately throughout, using a magnetic flea. A further three minutes stabilisation time was allowed and a second 500 uL injection of NaCl was performed so that the Na^+ concentration reached 40 mM. This procedure was repeated, with each injection designed to produce a 10 mM increase in NaCl concentration, until a final concentration of 60 mM NaCl was reached in the cell. All injections were introduced as far away from the electrodes as possible to prevent potential spikes occurring due to incomplete mixing. Having allowed time for the signal to stabilise at 60 mM the cell and electrodes were then rinsed with deionised water. A new 10 mL aliquot of 20 mM NaCl was placed in the cell and the above procedure was repeated until three calibrations were obtained for each electrode. The conventional Electrode C was calibrated in a similar manner but the perspex cell was not required.

A second set of potentiometric experiments involved the use of Electrode B and Electrode C, with different ion-selective membrane compositions. These membranes have been given the identifiers M2, M3 and M4 and are described in Table 4.1.

When these membranes were used, three calibration runs were collected as before using the miniature conventional Ag/AgCl reference electrode with internal filling solution.

The response of Electrode B to injections of KCl was also investigated. This was done in order to demonstrate that the potentiometric response was due to the selectivity of the ligand for sodium.
These experiments were carried out as follows:
10 mL of 20 mM NaCl solution was placed in the cell. Electrical contact was made with the Ag portion of the screen printed ion-selective electrode. The miniature conventional Ag/AgCl reference electrode was dipped into the solution to complete the circuit. After a stabilisation period of approximately three minutes, a 500 uL injection of 1 M KCl in 20 mM NaCl was introduced and the steady state potential recorded. The solution was stirred continuously using a magnetic flea. This was

repeated three times and the responses compared to those obtained for injections of NaCl.

AC Impedance Experiments.

Impedance data were obtained using a Solartron impedance measurement system, i.e. an SI 1260 frequency response analyser and an SI 1286 electrochemical interface (Schlumberger Instruments, Farnborough, Hampshire, U.K.). The entire system was interfaced to a 486-DX PC and controlled using ZPLOT software. All Impedance spectra were recorded using a 10 mV sinusoidal exciting voltage and a frequency range from 100 kHz to 1Hz. The test electrode (solid-state ISE) was mounted in the experimental cell (figure 4.1) and a conventional Ag/AgCl reference electrode and a platinum counter electrode were dipped into a 1 M NaCl solution. When recording data for the conventional ISE (Electrode C), it was dipped into the NaCl solution together with the reference and counter electrodes.

For each electrode in turn, the following series of experiments were carried out. Firstly, using a freshly prepared electrode, a spectrum was recorded in 20 mL of 1 M NaCl. Following this, the cell was rinsed several times with deionised water. 20 mL of deionised water was then placed in the cell. The reference and counter electrodes were removed, the cell was covered with parafilm to prevent evaporation and the electrodes were allowed to soak in the water overnight. After this, the water was emptied from the cell and was replaced with 20 mL 1 M NaCl. A spectrum was recorded immediately in this solution. The electrodes remained in this 1 M NaCl solution and the impedance was recorded after 24 hours. As before, the cell was covered with parafilm overnight to prevent evaporation.

4.4.2 **B** : Introduction of a Solid-State Ag/AgCl Electrode.

Potentiometric experiments.

In this series of experiments the miniature Ag/AgCl reference electrode was replaced by a screen printed Ag/AgCl electrode. The screen printed electrode will respond to changes in chloride ion concentration as was described in equation 4.1.

The complete electrochemical cells may be described as follows;

- **Electrode A**
  Ag | AgCl | Na-PVC | Test Solution | AgCl | Ag

- **Electrode B**
  Ag | AgCl | 0.2% NaCl Hydrogel | Na-PVC | Test Solution | AgCl | Ag

- **Electrode C**
  Ag | AgCl | 0.1M NaCl | Na-PVC | Test Solution | AgCl | Ag

During these experiments, both the solid-state ion-selective electrode (Electrode A or B in turn, as in figure 4.2) and the screen printed Ag/AgCl electrode were placed in the experimental cell, such that their sensing surfaces were exposed to the sample solution via the sample wells. For Electrode C, the solid-state chloride electrode was placed in the experimental cell and the ion-selective electrode was dipped into the sample solution.

For each electrode (A, B and C) in turn, 10 mL of 20 mM NaCl solution was placed in the cell. Electrical contact was made with the Ag portion of the screen printed electrodes. The calibration procedure was followed as before (4.4.1 **A**), with the final concentration of NaCl in the cell being 60 mM. The procedure was repeated five times and the data captured by the same LabVIEW based system as before.

AC Impedance Experiments.

Impedance data were obtained using a CHI660 computerised electrochemical instrument. The system contains a fast digital function generator, high speed data acquisition circuitry, a potentiostat and a galvanostat. The instrument was controlled by an external PC-486DX within the Windows 3.1.1 environment using software provided by EG&G instruments Ltd.. All Impedance spectra were recorded in 20 mM NaCl. A 10 mV sinusoidal exciting voltage was used and the frequency range scanned was from 100 kHz to 1Hz.

The screen printed Ag/AgCl electrode and the test electrode (solid-state ISE) were mounted in the experimental cell as before and a platinum counter electrode was dipped into 20 mL of a 20 mM NaCl solution. When Electrode C was tested, it was dipped into the sample solution together with the counter electrode and only the screen-printed Ag/AgCl electrode was placed in the experimental cell. This is shown schematically in figure 4.3 below.

Figure 4.3 : Schematic representation of the set-up used in the AC Impedance experiments.

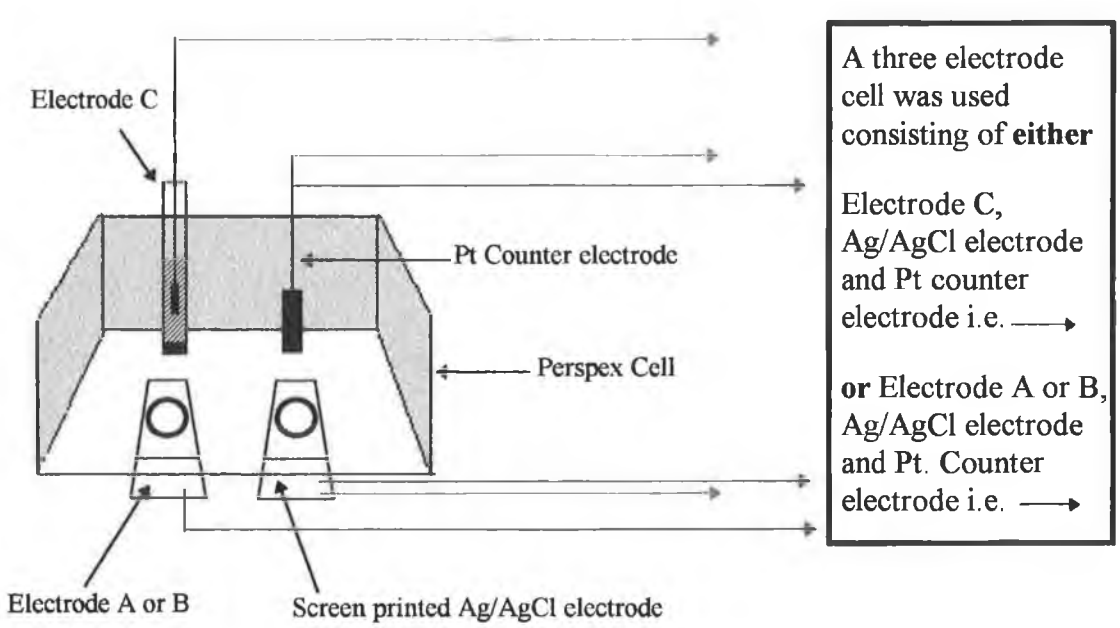

For each electrode in turn the following series of experiments were carried out. An AC impedance spectrum was recorded for each electrode just after preparation, i.e. the electrode was unconditioned. Following this, the electrode was conditioned overnight in 20 mM NaCl. Following the potentiometric calibrations already described, a second AC impedance spectrum was recorded on the conditioned electrode.

4.5 Discussion of Results.

4.5.1 : **A** : Characterisation of Solid-State ISEs.

Figure 4.4 shows the calibration data obtained using the ISEs and the miniature conventional Ag/AgCl reference electrode with sat'd KCl salt bridge. The data are the averages of three repeat experiments for each electrode, initially zeroed on the signal obtained for 20 mM NaCl. Clearly, all three electrode types exhibit similar dynamic behaviour and steady-state responses. Table 4.2 lists the steady-state potential values and in parenthesis, the associated noise value obtained from the standard deviation of 100 data points taken from the stabilised signal. The steady-state responses compare well with those predicted by the Nernst equation at 25°C. In general, Electrode type A displays a slightly higher noise level than either Electrodes B or C, averaging 0.15 mV over the entire concentration range investigated. This is not surprising, as Electrode type A was expected to have a blocked interface where the PVC membrane came into direct contact with the Ag/AgCl electrode (see figure 1.6, Chapter 1) which would lead to a larger overall electrode resistance and therefore a larger noise level. However, the noise values for electrode A are not significantly larger than those of the electrode types B and C, suggesting that the interface is not completely blocked, a fact which is supported by AC Impedance data. It was noticed throughout experiments, that the magnitude of the resistance of Electrode type A and corresponding noise level was very dependent on the quality of the physical contact achieved between the PVC and Ag/AgCl. This led to a much larger proportion of rejects with this design (only 1 in 3 were accepted for use in experiments). With Electrode type B, the noise level is reduced to an average of 0.05 mV over the concentration range investigated, due to the presence of the hydrogel layer. Electrode type C exhibits a noise level slightly less than that of Electrode A, averaging 0.12 mV over the concentration range investigated.

Standard deviations between calibration runs (n=3) were calculated at each concentration and averaged to give values of 0.86 mV, 0.57 mV and 1.17mV for

Electrode types A, B and C, respectively, suggesting that in potentiometric terms, each electrode type displays a similar degree of reproducibility.

Figure 4.4 : The mean of three potentiometric calibration runs performed on each of the three electrode designs. A miniature Ag/AgCl reference electrode with sat'd KCl internal filling solution was used and the sodium concentration was stepped up from 20 mM to 60 mM.

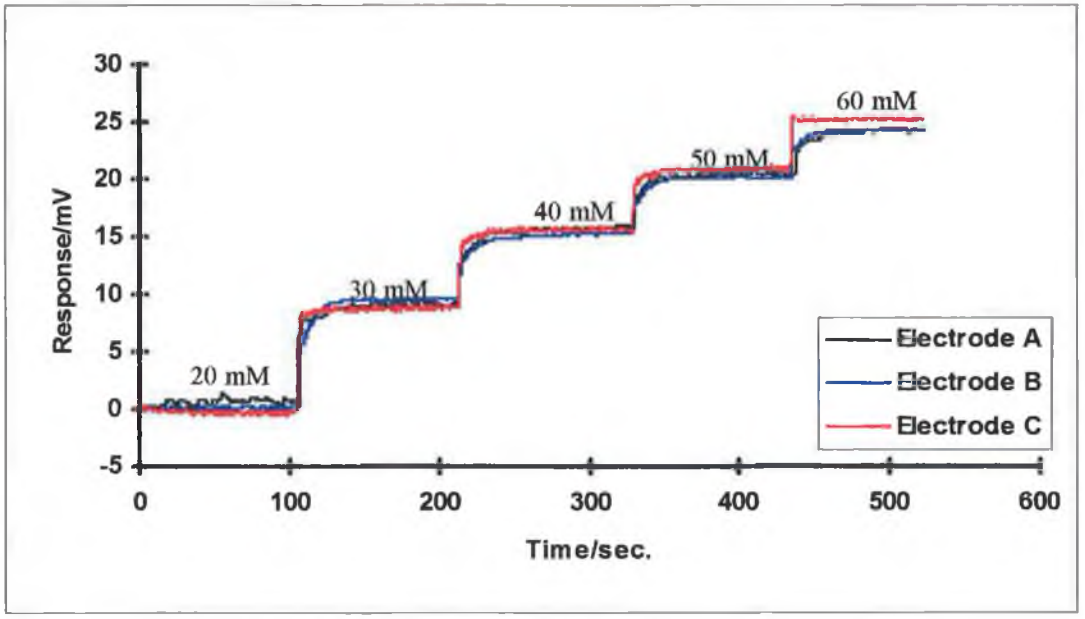

Table 4.2 : Steady state potentials obtained for each electrode type. Noise levels estimated from the standard deviation of the baseline after each addition are shown in parenthesis beside each value.

Membrane	M1			
Electrode Type	**A**	**B**	**C**	
$[Na^+]$ / mM	**Steady State Response /mV**			**Theoretical**
30 mM	8.73 (0.18)	9.58 (0.05)	9.46 (0.12)	9.77
40 mM	15.33 (0.11)	15.21 (0.07)	16.22 (0.11)	16.65
50 mM	20.22 (0.09)	20.00 (0.02)	21.63 (0.10)	21.96
60 mM	24.05 (0.09)	24.17 (0.04)	24.74 (0.11)	26.28
Slope mV/decade	54.98	53.81	56.60	59.20

Figures 4.5 and 4.6 show a comparison of the impedance spectra recorded for unconditioned and conditioned (following 24 hours in NaCl) Electrodes A, B and C respectively. In both figures, all electrodes display a high frequency semi-circle followed by a lower frequency region which is less clearly defined. In such studies, the high frequency semi-circle is attributed to a parallel resistance | capacitance combination thought to represent bulk electrode characteristics[8,9]. Bulk resistance (R_b) values are determined by the diameter of the high frequency semi-circle and bulk capacitance values (C_b) from the relationship[9]

$$C_b = \frac{1}{R_b \omega_0} \qquad \textbf{(4.2)}$$

Where ω_0 = Frequency at which the imaginary component of the impedance reaches a maximum.

Before conditioning (figure 4.5), Electrode B displays the lowest bulk resistance at $3.5x10^4$ Ω followed by Electrode C at $6x10^4$ Ω and Electrode A at $7.5x10^4$ Ω. It was also noted that the ω_0 value for Electrode A was smaller at16 kHz than those of Electrodes B or C, both of which were around 25 kHz. From equation 4.2, bulk capacitances before conditioning were estimated at approximately 10^{-10} $s\Omega^{-1}$ for Electrodes A and C, and slightly smaller at approximately 10^{-9} $s\Omega^{-1}$ for Electrode B.

Following conditioning (figure 4.6), the most obvious feature of the impedance spectra is that the diameter of the high frequency semi-circle is much larger for Electrode type A (ca. 10^5 Ω) than for either Electrode types B or C (both ca. $4x10^4$ Ω), which are of a similar magnitude (ca. 10^4 Ω) to those previously reported for PVC based ion-selective membranes[10]. In addition, the ω_0 value was found to change to 20 kHz for Electrode B and to 14 kHz for Electrode C, whereas for Electrode A it remained as before conditioning (16 kHz). This leads to little change in the magnitude of the bulk capacitance values, supporting the view that the PVC membrane is dominating the bulk capacitance. Bulk capacitance depends strongly on membrane dimensions and dielectric constant[9] all of which have remained fairly constant for Electrode types A,B and C as all membranes were taken from the same batch.

Figure 4.5: Comparison of the AC Impedance spectra recorded for unconditioned Electrodes A, B and C. A sinusoidal potential of 10 mV was used and a frequency range from 100 kHz to 1 Hz was scanned.

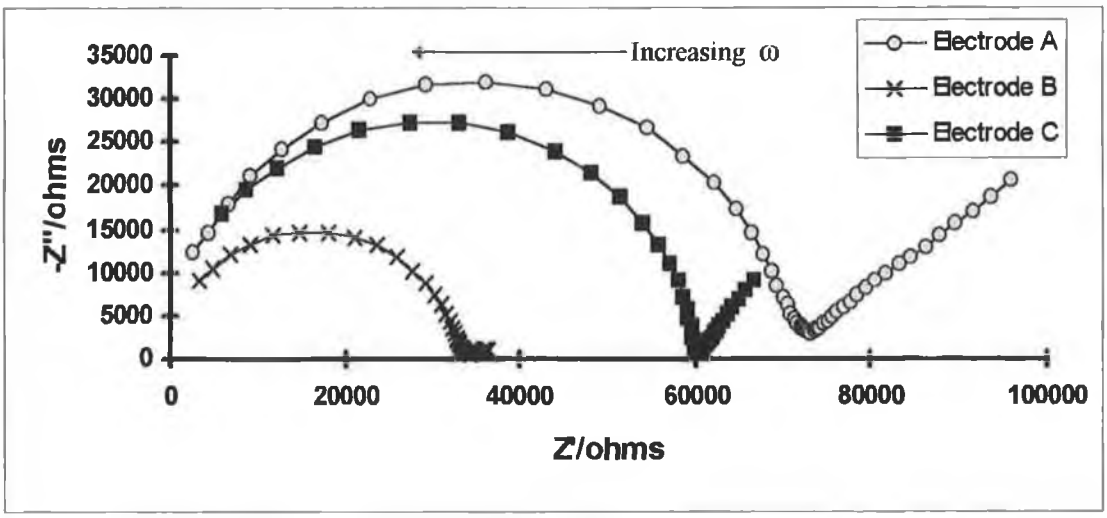

Figure 4.6: Comparison of the AC Impedance spectra recorded for Electrodes A, B and C, following conditioning as outlined in text. A sinusoidal potential of 10 mV was used and a frequency range from 100 kHz to 1 Hz was scanned.

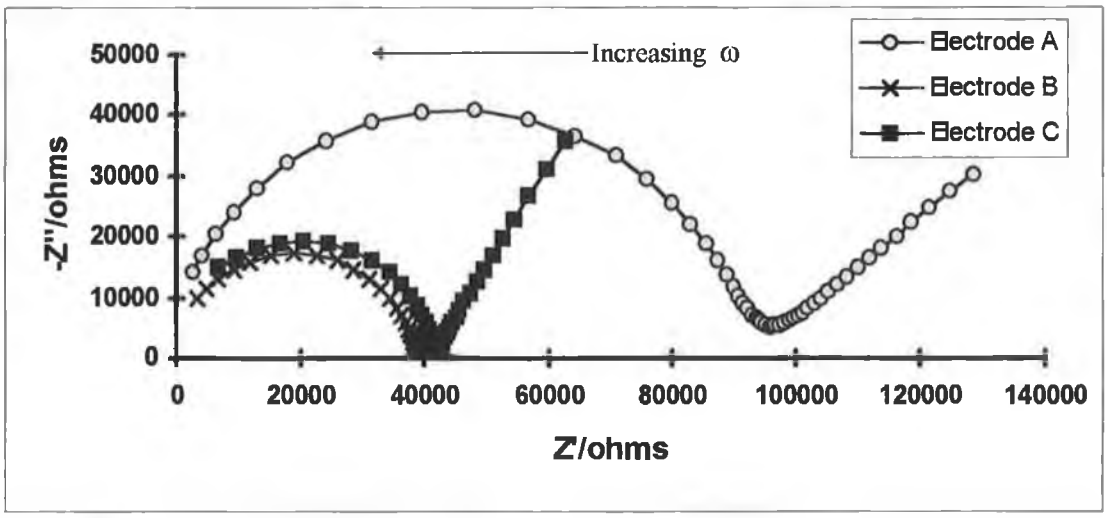

These impedance spectra also support the idea that the hydrogel helps decouple the interface between the PVC and Ag/AgCl, and also verify the potentiometric results which suggested that Electrode type A does not have a completely blocked interface. The bulk resistance value for Electrode type A is higher, but it nevertheless still exhibits reasonably satisfactory potentiometric behaviour.

Electrode type A was expected to behave rather like a coated wire electrode where the sensing element is in direct contact with the reference element[11]. Despite the lack of a formal mechanism for charge exchange at the internal AgCl/membrane boundary, the large number of reports detailing the successful construction and application of coated wire electrodes indicates that they can work satisfactorily[12,13]. It is generally agreed that some mechanism operates at the Ag/AgCl interface in coated wire electrodes and therefore screen-printed electrodes like Electrode A, to maintain a fairly constant internal reference potential[13]. In a paper by Cattrall et al[14], it was suggested that an oxygen electrode was set up at the interface. Schindler et al[15] observed the dependence of the potential of a Valinomycin electrode on oxygen partial pressure and showed how the potential shifted to more negative values when oxygen was replaced with hydrogen. However, others have claimed that the oxygen electrode is not very reversible and therefore is unlikely as such to provide the equilibrium needed to maintain a stable internal potential.

With reference to the screen-printed electrodes, it is possible that the binder used in the screen printed inks may be facilitating charge transfer by functioning in a similar manner to the ion-exchanger used in the membrane (KTpClPB). Also the presence of charged sites in the membrane (e.g. from the ion-exchanger and from the calixarene-sodium complex) and at the binder surface will tend to encourage the migration of water clusters to this region. The finite solubility of AgCl in water may provide enough of a population of free Cl^- ions to stabilise the potential. However, as the bulk resistance is larger in Electrode A, it may be implied that the charge transfer process is not as efficient for this electrode compared to Electrodes B or C, in which it is deliberately facilitated.

In addition to the high frequency semi-circle, electrode types A and B both show a lower frequency feature which may be the beginnings of a second semi-circle, or perhaps a Warburg impedance (the latter would appear to be the case in type C electrodes) although it is not possible to be certain of this at present. In ion-selective electrodes, a second semi-circle at this position is usually attributed to two main sources, a slow potential dependent transfer of ions across a membrane-solution interface or a slow potential dependent transfer of ions through a high resistance (relative to bulk) surface film. However, according to Buck et al.[16], the semi-circle should disappear as surface rates become fast when compared to bulk bathing electrolyte transport rates. Therefore the feature observed may not be reliably described as a second semi-circle.

During these experiments the effect that the different membrane components have on the electrode response was also studied. It is a well known fact that electrode performance depends strongly on the selectivity of the ionophore and also on the amount of ionic sites trapped in the membrane phase[17]. The dominant ionic sites are introduced via added salts in the form of ion-exchangers. Inclusion of such exchangers will guarantee the fast exchange of charge carriers between the electrode and aqueous phase needed to provide stable and reproducible potentiometric responses. Table 4.3 lists the potentiometric response to injections of NaCl obtained for Electrode types B and C with these different membrane compositions. In general some response was obtained in each case, except for the blank membrane. It was found that the signals produced with incomplete membranes are noisier, less reproducible, more prone to drift and in general, exhibit sub-Nernstian slopes. The noise levels were generally slightly higher for Electrode type B, averaging ±0.19 mV for M2 (no ionophore) and ±0.08 mV for M3 (no ion-exchanger) than for the conventional Electrode C averaging ±0.08 mV for both M2 and M3. Standard deviations between calibration runs (n=3) were calculated at each concentration and averaged to give values of 0.08 mV for both membranes M2 and M3 for Electrode C. Similarly, Electrode B displayed standard deviations (n=3) of 0.19 mV and 0.08 mV for membranes M2 and M3 respectively, suggesting that the electrodes still display a similar degree of reproducibility. It was not possible to measure the response obtained using the blank membrane for either electrodes as the response was too

unstable. Figure 4.6 compares schematically, the response of Electrode B with membranes M1, M2 and M3. Each bar represents the steady state potential achieved at each NaCl concentration. The % deviation of the experimental steady-state values from the theoretical values are shown as error bars. Finally, noise levels and electrode drift are quoted inside individual coloured boxes.

Figure 4.6 : Comparison of the steady-state responses obtained for Electrode B using different membrane compositions M1, M2 and M3 (see table 4.1). The % deviation of the individual potentials from the theoretical values are shown as error bars.

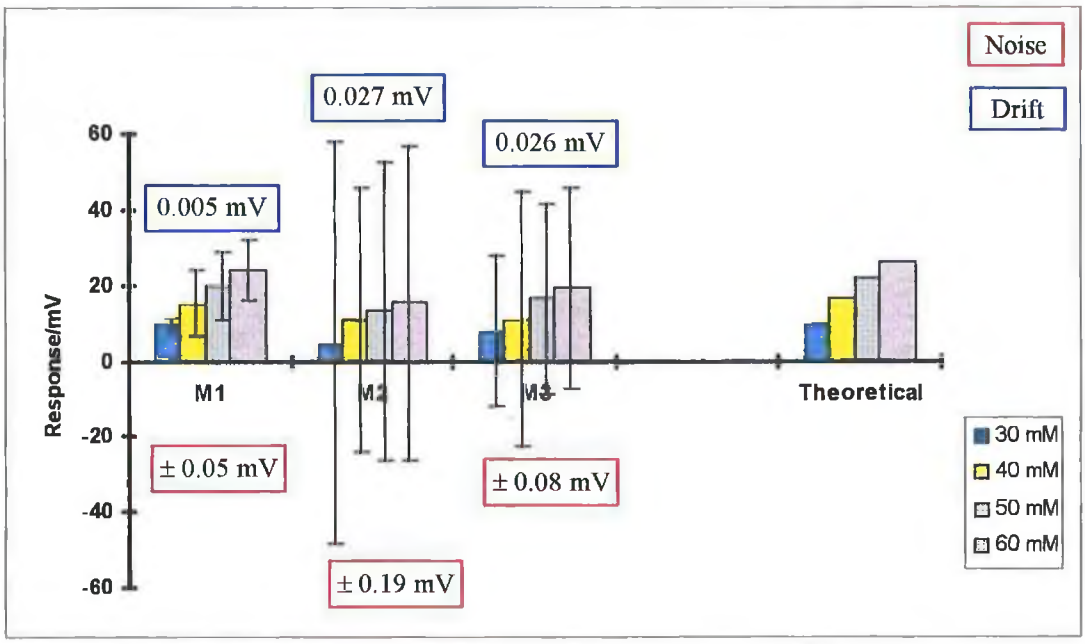

Table 4.3 also lists the steady state potentials obtained with Electrode type B, using membrane composition M1 (Table 4.1), when 10 mL of a 20 mM NaCl solution was spiked with 0.5 mL of 1M KCl (in 20 mM NaCl). The lack of response confirms that the sodium-selective ionophore[4] in this membrane is dominating the overall exchange characteristics of the membrane and not the ion-exchanger, which follows the Hoffmeister series in terms of selectivity and thus prefers K^+ to Na^+. Membrane M2

(Table 4.1) contains no ionophore and shows a much larger response to potassium (+190.97 mV). This is confirmed by the result obtained with membrane M3 (Table 4.1, no ion-exchanger) as the response falls dramatically to +2.66 mV upon addition of the same amount of potassium. This experiment shows that these solid-state sensors can be predicted to have similar potentiometric characteristics as the equivalent conventional liquid-filled electrodes.

Table 4.3 : Steady state potentials obtained for Electrodes A and B using different membrane compositions (see Table 4.1). Noise levels estimated from the standard deviation of the baseline after each addition are shown in parenthesis beside each value.

Membrane and Electrode Type[$]				
Membrane	**M2**	**M3**	**M2**	**M3**
	Electrode B		**Electrode C**	
$[Na^+]$ / mM	**Steady State Response /mV**			
30 mM	4.58 (0.35)	7.85 (0.09)	8.45 (0.08)	6.81 (0.08)
40 mM	10.83 (0.17)	11.06 (0.09)	14.31 (0.09)	12.29 (0.09)
50 mM	13.33 (0.18)	16.48 (0.08)	18.45 (0.05)	16.59 (0.07)
60 mM	15.41 (0.07)	19.34 (0.06)	22.24 (0.05)	20.00 (0.07)
Slope mV/decade	38.43	42.61	49.11	47.35
Experiments to Demonstrate Ligand Selectivity for Sodium				
Electrode B	**Steady-State Potential (mV) after introduction of KCl**			
M1	No Measurable Response			
M2	190.97 (0.57)			
M3	2.66 (0.57)			

[$] Membrane M4 produced no measurable response in any experiment.

4.5.2 : **B** : Introduction of a Solid-State Ag/AgCl Electrode.

In this section, the miniature Ag/AgCl reference electrode has been replaced by a screen-printed Ag/AgCl electrode. This electrode will respond to changes in chloride activity, as was described earlier in the introductory section and also in equation 4.1. Figure 4.8 shows a calibration performed to test the response of a screen printed Ag/AgCl electrode to changes in chloride activity. The chloride activity was stepped up from 20 mM to 60 mM as in all previous experiments. The only difference here is that the screen printed Ag/AgCl electrode was used as a chloride selective electrode and the signal obtained was referenced to that of a double junction electrode with a saturated $NaNO_3$ filling solution. From figure 4.8 it can be seen that a slope of 48.08 mV/decade was achieved which although sub-Nernstian, is quite acceptable given the nature of the experiment. In addition, a noise level of 0.23 mV was calculated from the standard deviation of the first 60 data points. This suggests that the bare electrode may be a source of noise in future experiments where this electrode will be used in place of a reference electrode.

Figure 4.8 : A calibration curve used to chart the response of a screen printed Ag/AgCl electrode to changes in chloride activity. A double junction electrode with saturated $NaNO_3$ filling solution (EDT Instruments Ltd., Dover, Kent, UK) was used as a reference and the chloride activity was stepped up from 20 mM NaCl to 60 mM NaCl.

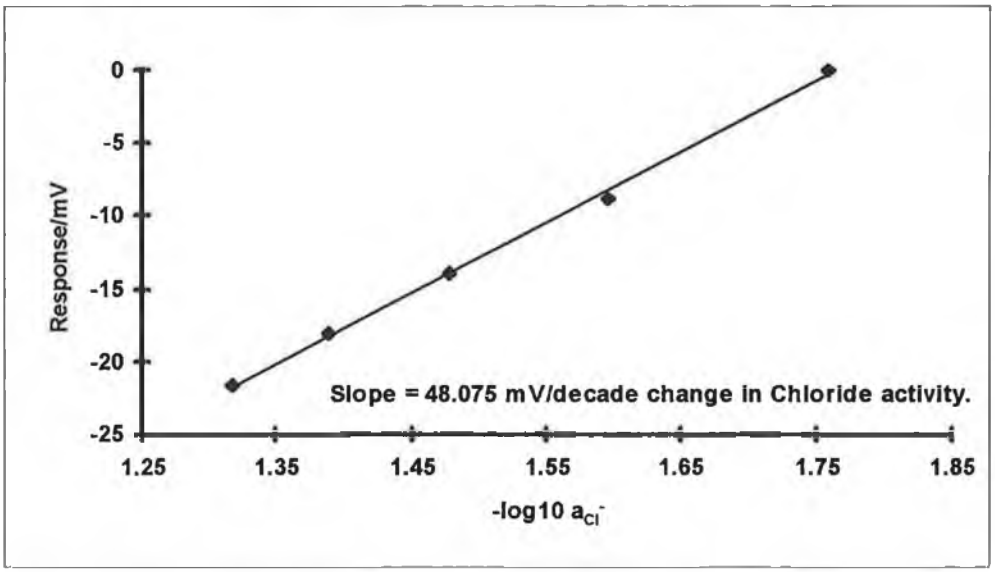

However, this result also shows that it is possible to use a bare screen-printed Ag/AgCl electrode as a chloride electrode and therefore that the idea to create a solid-state sodium selective ISE / screen-printed Ag/AgCl electrode combination is very feasible.

Figure 4.9 shows the mean calibration runs obtained using the ISEs (Electrodes A, B and C) and a screen-printed Ag/AgCl electrode. The data are the averages of five experimental runs and have been zeroed on the signal obtained for 20 mM NaCl. Electrode C displays the most stable dynamic response with a drift ranging from -0.04 mV/s at 20 mM to 0.001 mV/s at 60 mM, averaging -0.005 mV/s over the concentration range. This drift was calculated from the slope of the steady-state response over 60 points, after each injection. Electrodes A and B tend to drift slightly more at an average of +0.021 mV/sec. and +0.015 mV/sec. respectively. Drift for Electrode A ranged from 0.03 mV/s at 40mM to 0.014 mV/s at 20 mM to. Drift for Electrode B ranged from 0.034 mV/s at 40 mM to 0.002 mV/s at 60 mM.

Figure 4.9 : The mean of three potentiometric calibration runs performed on each of the three electrode designs. A solid-state sodium selective ISE and a solid-state chloride electrode were used and the NaCl concentration was stepped up from 20 mM to 60 mM.

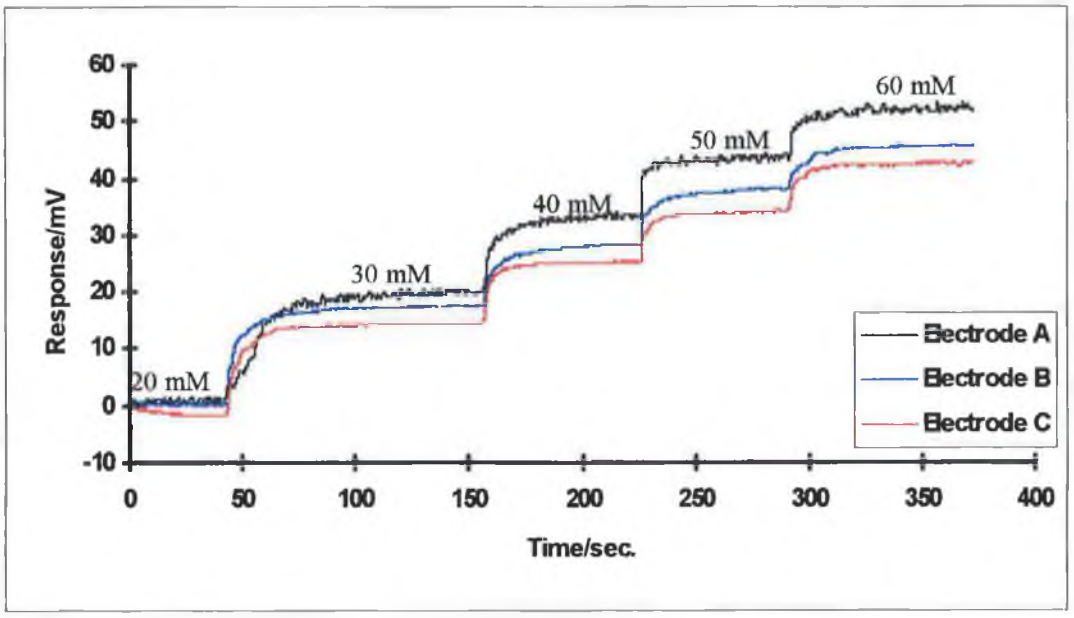

Steady-state potentials are shown in table 4.4 together with the standard deviation of 60 data points in parenthesis. Once again, the steady-state responses compare well with those predicted by the Nernst equation at 25°C. Noise levels are significantly higher for Electrode A than for either Electrodes B or C. It is possible that this particular Electrode A sample, had a higher resistance, due to a combination of a semi-blocked interface and poorer adhesion of the AgCl to the PVC membrane, as has already been discussed in Section **A**. In general, noise levels tend to be higher where the solid-state Ag/AgCl electrode is used in place of the conventional miniature Ag/AgCl reference (see table 4.2), which can only be expected as there is no stable reference potential. However it does perform extremely well in comparison to what could be expected. Standard deviations between experimental runs (n=5) were calculated at each steady-state potential and averaged to give values of 3.58 mV, 1.64 mV and 2.75 mV for Electrodes A, B and C respectively which indicates that all three electrodes still display a similar degree of reproducibility between calibrations. These values are higher than those calculated where the miniature Ag/AgCl reference electrode was used (i.e. 0.86, 0.57 and 1.17 for Electrodes A, B and C) but this is to be expected as two ISEs are now involved in producing the steady-state potential.

Table 4.4 : Steady state potentials obtained for each electrode type using a screen printed Ag/AgCl reference electrode. Noise levels estimated from the standard deviation of the baseline after each addition are shown in parenthesis beside each value.

Membrane	**M1**			
Electrode Type	**A**	**B**	**C**	
$[Na^+]$ / mM	**Steady State Response /mV**			**Theoretical**
30 mM	17.67 (0.48)	17.43 (0.14)	17.71 (0.09)	19.54
40 mM	31.34 (0.43)	28.57 (0.31)	28.85 (0.09)	33.33
50 mM	41.67 (0.43)	38.00 (0.25)	37.14 (0.10)	43.92
60 mM	50.00 (0.43)	46.00 (0.19)	44.85 (0.15)	52.56
Slope mV/decade	115.88	102.32	96.62	118.40

Figure 4.10 shows a comparison of the potentiometric response obtained for Electrode B using firstly the miniature Ag/AgCl reference electrode and then the screen printed Ag/AgCl electrode. As expected, when the solid-state Ag/AgCl electrode is introduced the potential steps are seen to increase according to equation 4.1. resulting in a much more sensitive response.

Figure 4.10 : Comparison of the response of Electrode B to changes in NaCl concentration using firstly a miniature Ag/AgCl reference electrode and then a screen printed Ag/AgCl electrode.

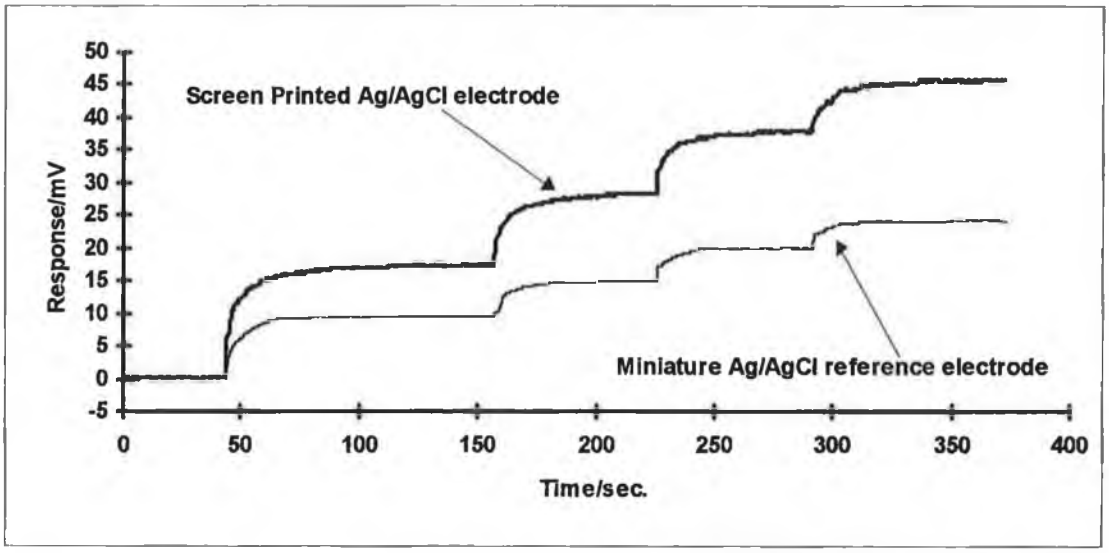

Figures 4.11 and 4.12 show a comparison of the impedance spectra recorded for unconditioned and conditioned Electrodes A, B and C respectively. It must be noted that these spectra were recorded using a different instrument (see experimental section B) to those previously and are not of the same quality. The higher noise observed in these traces is thought to be related to the sensitivity of this instrument and is not experimental in origin. All previous conditions have been maintained in these experiments with the exception of the reference electrode used. As for previous spectra recorded (shown in figures 4.5 and 4.6), all electrodes display a high frequency semi-circle followed by a lower frequency region which is less clearly

defined. The high frequency semi-circle is once again attributed to a parallel resistance | capacitance combination thought to represent bulk electrode characteristics[8,9].

Before conditioning (figure 4.11), Electrode B displays the lowest bulk resistance at $4.7x10^4$ Ω followed by Electrodes A at $7x10^4$ Ω and Electrode C at $7.6x10^4$ Ω. As in previous experiments (section **A**) the ω_0 value for Electrode A was smaller at14.7 kHz than those of Electrodes B or C, both of which were around 22 kHz. From equation 4.2, bulk capacitances before conditioning were estimated at approximately 10^{-10} $s\Omega^{-1}$ for all electrodes.

Following conditioning (figure 4.12), the diameter of the high frequency semi-circle decreased in size slightly for both Electrodes A and C to values of $6.2x10^4\Omega$ and $6.5x10^4\Omega$ respectively but remained at approximately $4.7x10^4$ Ω for Electrode B. During these experiments, the ω_0 value was not found to change following conditioning leading to little change in the magnitude of the bulk capacitance values, (all ca. 10^{-10} $s\Omega^{-1}$).

Figure 4.11 : Comparison of the AC Impedance spectra recorded for unconditioned Electrodes A, B and C. A sinusoidal potential of 10 mV was used and a frequency range from 100 kHz to 1 Hz was scanned.

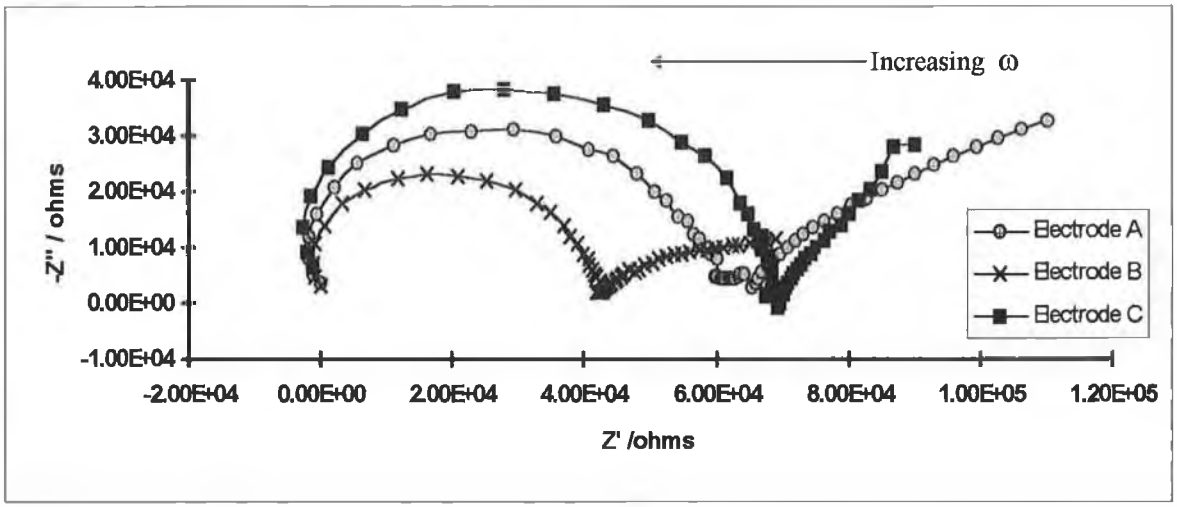

Figure 4.12 : Comparison of the AC Impedance spectra recorded for conditioned Electrodes A, B and C. A sinusoidal potential of 10 mV was used and a frequency range from 100 kHz to 1 Hz was scanned.

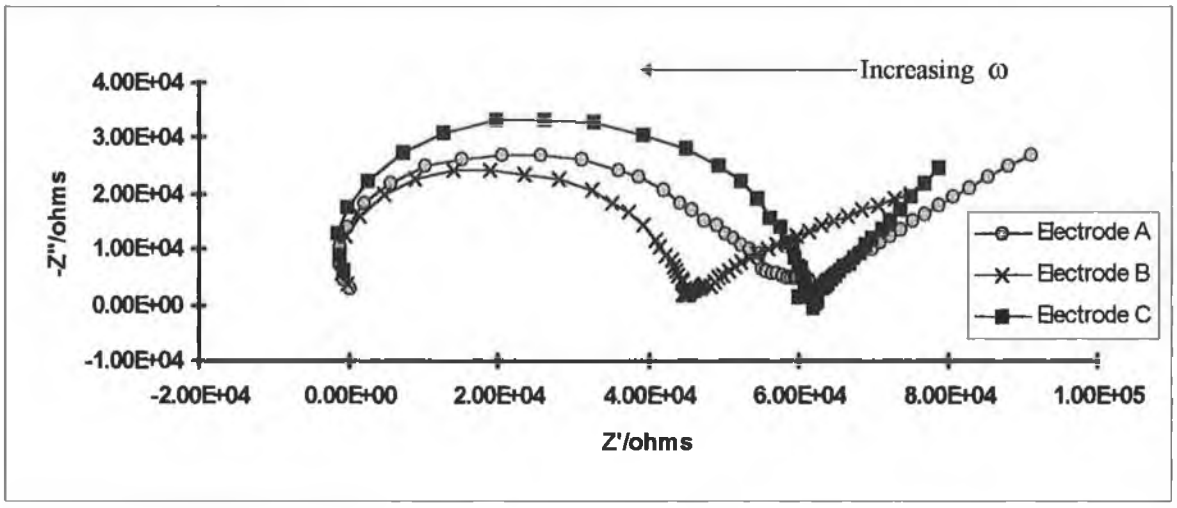

From the data presented it is clear that development of solid-state sensors based on screen printing technology is certainly possible. Most of the problems encountered with Electrode type A were mechanical and serve to highlight the need for some kind of contact layer between the membrane and the AgCl surface, although it did perform very well in comparison to what was initially expected. Electrode B appears to be the most likely candidate for further study, based mainly on the much lower number of rejects. This is probably due to the improved physical contact between the membrane and AgCl surface, which may be due to the well-known adhesive properties of hydrogels.

4.6 Reproducibility Study.

Based on the previous experiments, Electrode B was chosen as the most suitable electrode for further study. In this section the electrode design was further optimised and experiments were carried out to investigate the reproducibility observed within a batch of five solid state devices. Results of these experiments should give some indication of the spread of baseline potentials and therefore of the type of calibration which will be needed before the electrodes can be used. Each electrode may have to be individually calibrated before use. Alternately, poising the electrodes at a particular sodium concentration may be sufficient to bring the baseline potentials close enough to allow immediate use of the electrodes.

4.6.1 Optimised Electrode Design.

The screen printed electrodes were prepared using the equipment and reagents already discussed in section 4.2. However, a new electrode design was introduced consisting of a pair of screen printed electrodes, one of which was used as an internal reference for the ISE and the other used as a solid-state chloride selective electrode. A pair of these electrodes are shown in figure 4.13 below and were of the dimensions indicated.

Figure 4.13 : A screen printed Ag/AgCl electrode used to construct a solid-state sensor (i.e. a solid-state ISE | chloride electrode combination).

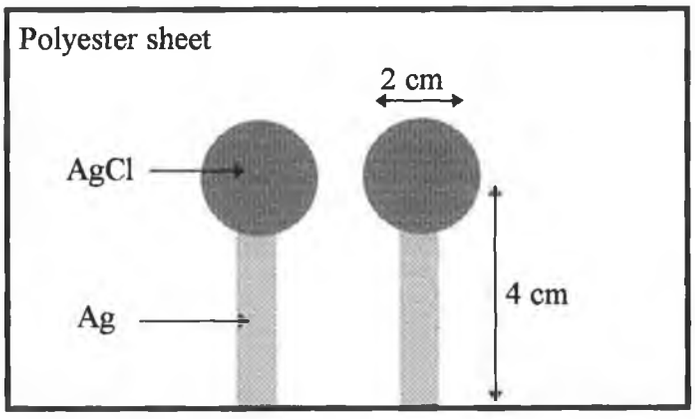

The five ion-selective electrodes were prepared in the following manner and were given the identifiers EB1, EB2, EB3, EB4 and EB5♠ .

A layer of 0.2% NaCl hydrogel was placed over one AgCl electrode portion. The hydrogel was smoothed into a thin layer using a glass slide and left to dry for approximately 2 minutes.
The edges around the AgCl were wiped clean of any hydrogel residue and a layer of primer was painted on the polyester just surrounding the AgCl layer. The primer (Loctite® 770 polyolefin primer from Loctite, Dublin , Ireland) was used to facilitate bonding of the polyester sheet to the subsequent PVC membrane. The primer dried immediately at room temperature and so a thin layer of a cyanoacrylate adhesive (Loctite® product 406) was placed on top. A 2.5 cm diameter sodium selective PVC membrane was immediately placed over the hydrogel and allowed to bond with the adhesive layer. The electrode was left to bond for approximately 1 minute before using it in any experiments (fixture time quoted in product brochure was from 2 to 10 seconds for PVC to Polyester).

4.6.2 Experimental Procedures.

The following series of experiments were carried out on each of electrodes EB1, EB2, EB3, EB4 and EB5 in turn.

AC Impedance Experiments.

AC Impedance spectra were recorded using the CHI660 potentiostat and CHI software provided by EG&G instruments Ltd. already described. A three electrode design was used again, consisting of an Ag/AgCl screen printed electrode, a sodium

---

♠ Note: this identifier refers to both the ISE and its corresponding screen printed Ag/AgCl electrode.

selective solid-state ISE (test electrode) and a platinum counter electrode. A sinusoidal exciting voltage of 10 mV was used and a frequency range from 100 kHz to 1 Hz was scanned. All Impedance spectra were recorded in 20 mL of 20 mM NaCl. Firstly, an AC Impedance spectrum was recorded on each freshly prepared electrode i.e. before conditioning. Following conditioning for 24 hours in 20 mM NaCl, a second AC Impedance spectrum was recorded for each electrode.

Potentiometric Experiments.

During potentiometric experiments the electrodes were contained in the experimental cell already described, and were interfaced to an Elonex PC-5100/I via a national instruments AT-MIO-16DL data acquisition card. As in previous experiments, data was recorded using a LabVIEW 4.0 program (National instruments Ltd., Austin, Texas, USA) which was written in house.

After conditioning for 24 hours in 20 mM NaCl, the following series of experiments was carried out.
10 mL of 20 mM NaCl was placed in the experimental cell. The solution was stirred continuously using a magnetic flea. Following a stabilisation time of approximately three minutes, a 100uL injection was made onto the 20 mM background such that the overall sodium concentration was stepped up to 70 mM. The resulting potential was monitored for a further 4 -5 minutes. The cell and electrodes were then rinsed thoroughly with deionised water. A further 10 mL of 20 mM NaCl was placed in the cell and the above repeated until data for five injections were obtained for each of the five electrodes (i.e. EB1, EB2, EB3, EB4 or EB5).

4.7 Discussion of Reproducibility Study.

Figure 4.14 shows the AC Impedance spectra recorded for unconditioned electrodes EB1-EB5. All five electrodes show a high frequency semi-circle which varies in diameter from $2.24x10^4$ ohms for EB4 to $6.08x10^4$ ohms for EB2. This semi-circular portion defines the bulk resistance and capacitance of each electrode. Table 4.5 lists the bulk capacitance (C_b), bulk resistance (R_b) and ω_0 values for each electrode, calculated from the high frequency semi-circle and the relationship defined in Equation 4.2.

Figure 4.14 : AC Impedance spectra recorded for each electrode EB1-EB5 before conditioning. A 10 mV sinusoidal exciting voltage was used and a frequency range from 100 kHz to 1Hz was scanned.

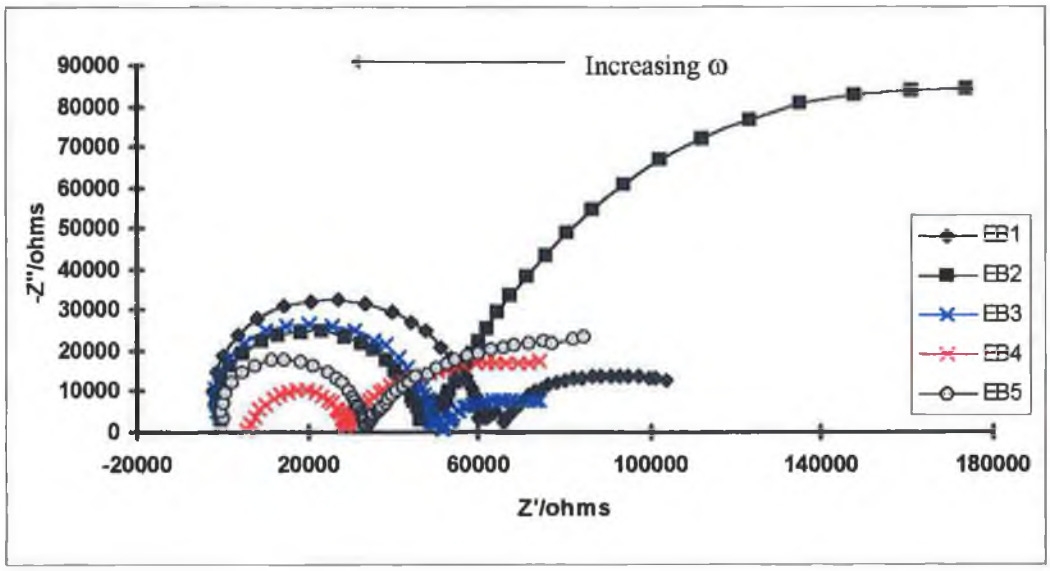

Figure 4.15 shows the AC Impedance data recorded for each electrode following conditioning for 24 hours in 20 mM NaCl. Once again a high frequency semi-circle is observed ranging in diameter from $3.1x10^4$ ohms for EB5 to $6.4x10^4$ ohms for EB1. Table 4.5 lists the bulk capacitance (C_b), bulk resistance (R_b) and ω_0 values for each conditioned electrode, which were calculated as before from the high frequency semi-circle.

Figure 4.15 : AC Impedance spectra recorded for each conditioned electrode (EB1-EB5). A 10 mV sinusoidal exciting voltage was used and a frequency range from 100 kHz to 1Hz was scanned.

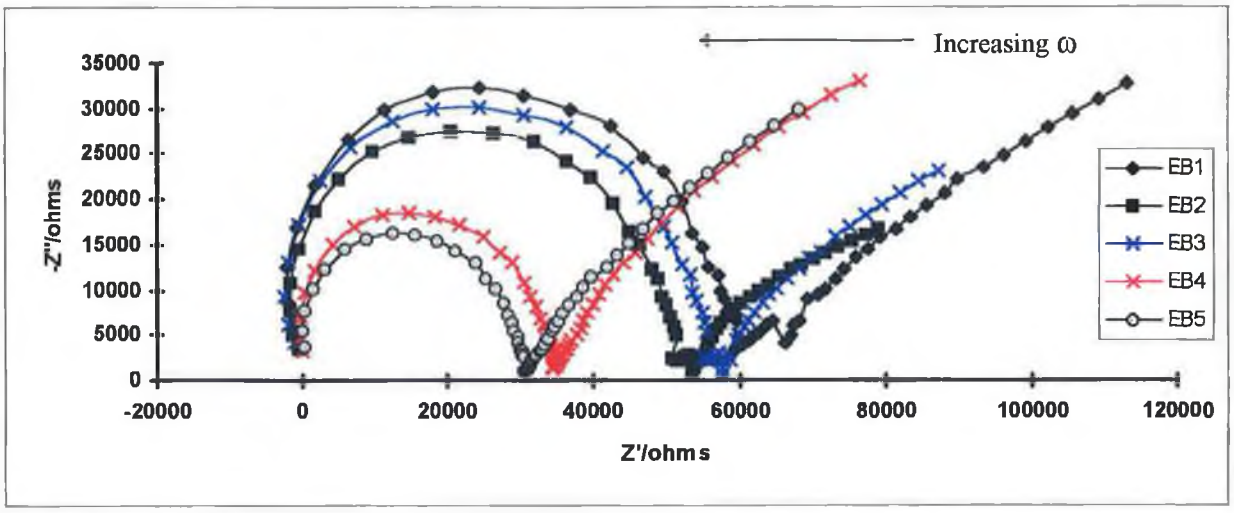

In addition to the high frequency semi-circle, spectra for both the unconditioned and conditioned electrodes show a low frequency effect. In the unconditioned electrodes (figure 4.14) this appears to be the start of a second semi-circle. In particular EB2 shows a very large second feature. It is quite common to see a second semi-circle in unconditioned ion-selective electrodes[16]. This effect is caused by a slow exchange of ionic species at the membrane solution interface and is expected to disappear as surface rates become fast in comparison to bulk bathing electrolyte transport rates. Looking at the spectra for the conditioned electrodes (figure 4.15) it is clear that this second semi-circle is becoming far less obvious and more difficult to interpret. However the low frequency feature is still clearly curved.

Table 4.5 : A list of bulk capacitance (C_b), bulk resistance (R_b) and ω_0 values for each electrode before and after conditioning.

Unconditioned Electrodes			
Electrode Identifier ↓	**ω_0 / Hz**	**R_b / ohms**	**C_b / $s\Omega^{-1}$**
EB1	$1.76x10^4$	$6.08x10^4$	$9.35x10^{-10}$
EB2	$1.76x10^4$	$4.88x10^4$	$1.16x10^{-9}$
EB3	$1.76x10^4$	$5.20x10^4$	$1.09x10^{-9}$
EB4	$1.76x10^4$	$2.24x10^4$	$2.54x10^{-9}$
EB5	$2.15x10^4$	$3.44x10^4$	$1.35x10^{-9}$
Conditioned Electrodes			
	ω_0 / Hz	**R_b / ohms**	**C_b / $s\Omega^{-1}$**
EB1	$2.15x10^4$	$6.49x10^4$	$7.16x10^{-10}$
EB2	$1.76x10^4$	$5.71x10^4$	$9.94x10^{-10}$
EB3	$1.76x10^4$	$5.97x10^4$	$9.51x10^{-10}$
EB4	$2.15x10^4$	$3.53x10^4$	$1.32x10^{-9}$
EB5	$2.54x10^4$	$3.12x10^4$	$1.26x10^{-9}$

Figure 4.16 shows potentiometric data recorded for each conditioned electrode. The data are the mean of five experimental runs for each electrode and have been zeroed on the signal obtained for 20 mM NaCl. All electrodes display similar dynamic profiles and display steady state potentials which are in agreement with those predicted by the Nernst equation at 25°C. Table 4.6 lists the steady-state potentials obtained for each electrode and in parenthesis the noise levels calculated from the standard deviation of the first 60 data points.

Figure 4.16 : Potentiometric data recorded for each electrode as the NaCl concentration was stepped up from 20 mM to 70 mM.

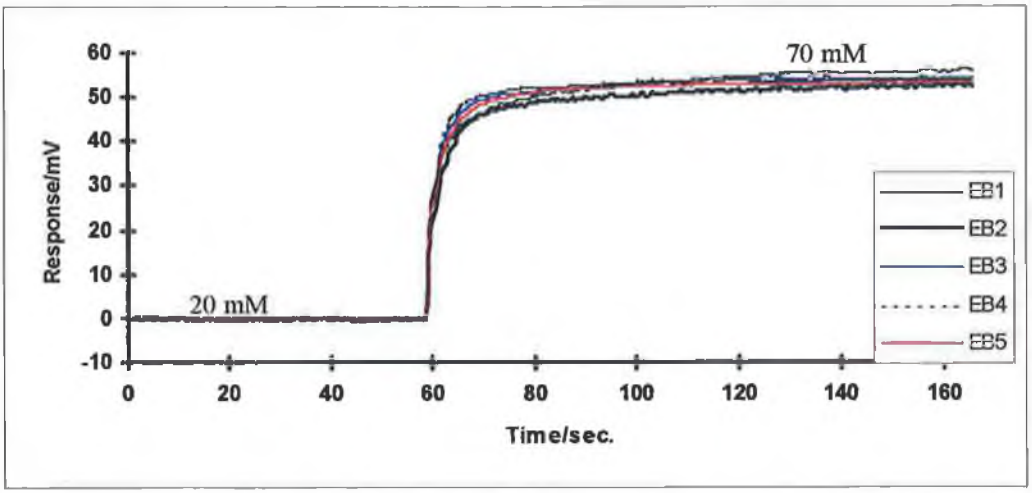

Table 4.6 : The steady state potentials recorded for each electrode as the NaCl concentration was stepped up from 20 mM to 70 mM. Signal noise levels are shown in parenthesis beside each value.

Electrode	**Steady-state Potential (mV)**	**Slope mV/decade**	**Standard deviation (mV) (n=5)**
EB1	55.70 (0.21)	110.19	3.77
EB2	52.33 (0.19)	103.53	3.03
EB3	53.63 (0.05)	106.10	1.22
Eb4	54.15 (0.06)	107.12	1.72
EB5	52.87 (0.04)	104.59	1.85
Theoretical*	59.85	118.40	

* Assuming Nernstian slopes for both the sodium selective ISE and the screen-printed Ag/AgCl electrode.

All electrodes display a similar response time reaching 80% of their steady-state potential between 5 and 9 seconds after injection. Standard deviations between experimental runs (n=5) were calculated for each electrode and are shown in table 4.6. Although EB1 and EB2 show slightly higher values than the others, they are still only approximately 6% of the theoretical steady-state potential and cannot be directly correlated to higher bulk resistance values in the AC impedance spectra. Overall, the electrodes show a similar degree of reproducibility. The slight differences in the bulk resistance of the electrodes (see table 4.5) have proved insignificant at this time and do not affect the potentiometric data recorded.

During experiments it was noted, that although each electrode does produce a similar potential step as the NaCl concentration is increased, differences do occur in their absolute baseline potentials varying from -6.20 mV to -39.05 mV for unconditioned electrodes and from -21.06 mV to -31.92 mV for the conditioned electrodes. This suggests that a baseline potential will have to be established for each electrode before use. Differences in absolute potentials may be attributed to two main areas. Firstly, inaccuracies involving stirring, injection methods and fluctuations in ground potentials. Secondly, there are likely to be contributions from the way in which electrodes are prepared. Small differences in the thickness of the hydrogel layer may effect the absolute potential and so a more reproducible method of deposition should be considered, for example a template or screen printing. The PVC membrane composition and thickness are also likely to be crucial. The current membranes were cast in petri dishes. This leads to variations in thickness of the samples cut, although this was kept to a minimum by careful preparation.

4.8 Bibliography.

[1] K. Park, S. L. Cooper, J. R. Robinson, Bioadhesive Hydrogels, Chapter 8 in: N. A. Peppas, (ed.), *Hydrogels in Medicine and Pharmacy*, CRC Press, Boca Raton, Florida, (1986).

[2] A.D. Woolfson, D.F. McCafferty, C.R. McCallion, E.T. McAdams and J.MCC. Anderson; J. App. Polymer Science, 56 (1995) 1151.

[3] D. Diamond; J. Inc. Phenomen. mol. recog. Chem., 19 (1994) 149.

[4] A. Cadogan, D. Diamond, M.R. Smyth, M. Deasy, M.A. McKervey, S.J. Harris; Analyst, 114 (1989) 1551.

[5] D. Jones, M. Bonner, A.D. Woolfson; *Proc. 16th Pharmaceutical Technology Conference*, Athens, Greece, 1997.

[6] A. Evans; *Potentiometry and Ion Selective Electrodes,* Ed. M. James, J. Wiley & Sons Ltd., Chichester, U.K., (1987) p170.

[7] F. J. Sáez de Viteri and D. Diamond; Anal. Proc., 31 (1994) 229.

[8] A.K. Covington, D. Zhou; Electrochimica Acta., 37 (1992) 2691.

[9] G. Horvai, E. Gráf, K. Tóth, E. Pungor, R.P. Buck; Anal. Chem., 58 (1986) 2735.

[10] R.D. Armstrong, A.K. Covington, G. Evans; J. Electroanal. Chem., 159 (1983) 33.

[11] R. Cattrall and H. Freiser; Anal. Chem., 43 (1971) 1905.

[12] L. Cunningham and H. Freiser; Anal. Chim. Acta, 180 (1986) 271.

[13] R. Cattrall and I. Hamilton; Ion-selective electrode reviews, 6 (1984) 125.

[14] R. Cattrall, D. Drew, I. Hamilton; Anal. Chim. Acta, 76 (1975) 269.

[15] J. Schindler, G. Stork, H. Struh, W. Schmid, K. Karaschinski, Z. Fresenius; Anal. Chem., 295 (1979) 248.

[16] R.P. Buck, K. Tóth, E. Gráf, G. Horvai, E. Pungor; Anal. Chem., 58 (1986) 2741.

[17] G. Horvai, V. Horvath, A. Farkas, E. Pungor; Analytical letters, 21 (1988) 2165.

Development of a Screening Test for Cystic Fibrosis based on Solid-State Ion-Selective Electrodes

5.1 Introduction.

This chapter details experiments involved in the development of a screening test for Cystic Fibrosis (CF). Our test will be based on the use of solid-state ion-selective electrodes, such as those already discussed in Chapter 4, to monitor levels of Na^+ and Cl^- ions in sweat. Abnormally high levels of such electrolytes is diagnostic of CF and will be discussed in more detail later.

Our initial aim is to further optimise the design and construction of the electrodes. This will involve reducing their size, improvements in packaging and the introduction of some means by which the electrodes may be easily connected to our data collection system. Following this, a batch of electrodes will be calibrated in a series of potentiometric experiments. This is intended to establish that the electrodes are functioning as expected on the bench. The ultimate aim of this research is to obtain some indication that it is possible to monitor electrolyte levels in the sweat whilst an electrode is in contact with the skin. Following these experiments and data analysis some conclusions will be drawn on the research to date and some suggestions will be made concerning future work.

5.2 Cystic Fibrosis.

Cystic Fibrosis is the commonest lethal hereditary disease amongst Caucasians[1]. In CF, abnormal exocrine secretions contain too little water relative to protein and electrolyte concentrations and lead to a raised sodium level in sweat. Cystic Fibrosis is due to a genetically determined defect in the chloride channel, which regulates the flow of chloride ions and osmotically associated water across the cell membrane. An affected cell is able to absorb sodium ions and an osmotic equivalent volume of water but the excretion of chloride ions is impaired. The observation by Darling and co-workers in 1953 that the concentrations of sodium and chloride in sweat are elevated in patients with CF, led to the development of the diagnostic sweat test[2]. The test

was further refined and developed by Gibson and Cooke in 1959, to become the standard diagnostic test for Cystic Fibrosis[3].

5.3 Current Techniques[4].

A sweat test generally has three parts, sweat stimulation by pilocarpine iontophoresis, collection of the sweat and analysis for sodium concentration and/or chloride concentration.

5.3.1 : Procedure for Pilocarpine Iontophoresis and electrolyte analysis.

Pilocarpine iontophoresis involves activating the sweat glands on a localised area of skin, typically a 2" x 2" square[5] by the introduction of pilocarpine. Pilocarpine occurs naturally in the leaflets of South American shrubs, Pilocarpus Jaborandi and Pilocarpus Microphyllus. It is among the three major cholinomimetic alkaloids and has a structure as shown in figure 5.1. Its major action is to stimulate autonomic effector cells in a fashion analogous to cholinergic post-ganglionic nerve impulses.

Figure 5.1 : Pilocarpine.

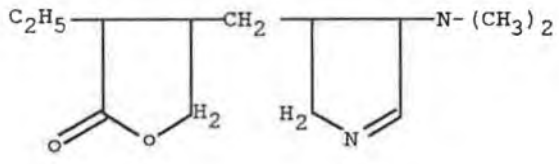

Using copper electrodes and a power supply, an electrical potential is established so that the pharmacologically active ions (pilocarpine ions) carry a current and are therefore introduced into the skin. The arm is the most common area for iontophoresis, as the current must not cross the heart. The current source must provide a 20 volt potential and have a milliampere meter to determine the current flow through the electrodes accurately from zero to four milliamps. Suitable electrodes are made from pliable copper and are approximately 1.6" x 1.6" square. For comfort and the delivery of sufficient pilocarpine the DC current density should be in the order of 0.16 mA cm^{-2}.

Initially the area is washed with distilled water and dried with salt-free gauze. A 2" x 2" gauze square is placed on the flexor surface of the forearm. It is well moistened with pilocarpine and the positive electrode is placed over the gauze. A rubber strap is used to secure the electrode. Another 2" x 2" gauze is placed elsewhere on the arm, moistened with saline or dilute H_2SO_4 and the negative electrode attached and secured.

When the electrodes are in place the current is slowly raised over 10 seconds to 4 mA. Upon application of current, the pilocarpine ions become positively charged, move away from the electrode and penetrate the skin such that the drug becomes locally concentrated in the dermis and subcutaneous tissues and stimulates the sweat glands without producing general systemic effects. Iontophoresis is continued for five minutes. A photograph of iontophoresis in progress is shown in figure 5.2.

Once completed, the electrodes are removed and the skin is cleansed with distilled water and carefully dried with gauze. A 2" x 2" filter paper square is taken with forceps from a previously weighed bottle and is placed over the exact area which was iontophoresed. A parafilm sheet is placed over the filter paper and the edges secured with strips of waterproof adhesive tape, such that there is an airtight seal between the skin and the plastic sheet. Sweat is collected for thirty minutes after which time the filter paper is returned to the weighing bottle and weighed again. When a 2" x 2" gauze is used, specimens weighing less than 100 mg should not be analysed. Generally the average sweat rate during the thirty minute collection should be at least 1 g m^{-2} min^{-1}.

The sweat samples are then sent for laboratory analysis by ion-selective electrode[6] flame photometry[7] or titration[5,8].

Figure 5.2 : Pilocarpine Iontophoresis in progress.

5.3.2 Problems encountered with current methods.

Unreliable methods, technical errors and errors in interpretation will all lead to incorrect sweat test results[9]. Methods that do not quantitate sweat collected or do not have an established minimum sample volume or weight are subject to false-negative results because an adequate sweat rate cannot be ensured. Other problems with sweat testing include technical errors of evaporation and contamination, errors in dilution, instrument calibration and the centralised analysis leading to delays in

diagnosis. Interpretation errors in sweat testing result from, a lack of knowledge about the laboratory method, failure to repeat tests with borderline or positive results, failure to repeat tests with a negative result when inconsistent with the clinical picture and failure to repeat testing in patients with a diagnosis of CF that does not follow the expected clinical course[10].

5.3.3 Sweat Sodium or Chloride.

Gleeson et al.[11] undertook a study to determine the ability of chloride and sodium measurements in sweat to discriminate between normal and CF subjects. Sweat electrolyte analysis was performed on samples from 233 children aged 2 weeks to 15 years. It was found that all children with CF had chloride > 80 mM and sodium > 50 mM. In the normal comparison population all children had chloride < 40 mM and sodium < 50 mM. The difference between results for normal and for CF subjects was much greater for chloride than for sodium. This led to the conclusion that the chloride concentration provides a greater discrimination between normal and CF positive results than does sodium and so chloride has become the electrolyte most often sought. Interpretation of the chloride concentration is made with regard to the patients clinical presentation, family history, age and the knowledge that certain rare mutations of the Cystic Fibrosis gene are associated with a borderline or negative sweat chloride concentration[12]. The reference values quoted for children are as follows; < 40 mM Negative, > 60 mM Positive and 40-60 mM Borderline[4]. Approximately 98% of CF positive patients will have sweat chloride levels greater than 60 mM.

5.4 The role of ISEs in the diagnosis of Cystic Fibrosis.

The 1975 Cystic Fibrosis Foundation GAP conference recommended that diagnosis of Cystic Fibrosis be based on a quantitative pilocarpine iontophoresis sweat test followed by the determination of chloride by titration[8] and sodium by flame photometry[13]. In 1976 a report was published from the US Committee for a study for evaluation of testing for Cystic Fibrosis[14]. This article included a critical analysis of the state of the art of CF testing and came again to the conclusion that the Gibson-Cooke sweat test should be the accepted method. In terms of the quantitative diagnosis of Cystic fibrosis little has changed since this time, however research into the development of diagnostic screening methods has always focused considerable interest on the scope of chloride and sodium ion-selective electrodes. The 1976 report also stated that there were no tests, at that time, to meet the established criteria for general screening for Cystic Fibrosis. Neonates produce insufficient sweat to permit screening by the sweat test before the age of about 4-6 weeks. Even after the neonatal period, the quantitative pilocarpine iontophoresis sweat test is too complex and expensive for screening large populations. Therefore, it was proposed that research to develop a reliable and safe neonatal screening test and a reliable and safe antenatal test for Cystic Fibrosis be essential[14].

Ion-selective electrodes had been proposed as a possible solution before and since then. Indeed, hydrogen ion-selective glass electrodes have been used successfully since 1939 for the determination of skin pH[15]. As ISEs have developed, attempts seemed warranted to use these electrodes to determine in addition to pH, sodium and chloride ion activities on the skin surface. Goldbloom and Sekelj described a procedure which consisted of placing a glass sodium electrode directly on a washed skin area and calculating sodium activity from the developed electrical potential observed on an expanded scale pH meter[16]. In 1965, Warwick and Hansen proposed the use of a chloride ion-selective electrode for the direct measurement of chloride in sweat while on the skin site[17]. One change which they made to Goldbloom and Sekelj's method was the stimulation of local sweating by placing small heated aluminium cylinders over pliofilm covered skin. In a paper by Kopito and

Schwachman[18] the work of Warwick and Hansen[17] was repeated using a more recently developed chloride glass electrode and using pilocarpine iontophoresis to stimulate sweating.

In all of the above cases it was found that the use of ISEs makes for simpler methodology but there is a greater chance of errors going undetected. A paper by Moody et al.[19] describes some factors which can limit the use of the combination chloride electrodes which were often used at the time. For example, any error through filling solution leakage will tend to increase the number of false negative sweat tests (although this was not thought to be a problem if the electrode was in contact with the skin for less than 15 seconds). With reference to temperature effects it was concluded that attention must be paid to the difference in temperature between the electrode and the skin surface. This point was also discussed in a paper by Green et al.[20] which described a standardised procedure for measuring in immediate succession, Na^+, Cl^- and H^+ activities on the skin surface. In agreement with Sekelj and Goldbloom[16], it was concluded that when determinations are made on the skin, the potential determining temperature is closer to that of the skin than that within the electrode itself. Therefore all calibrations were carried out with standard solutions within the range of skin temperature i.e. 32-35°C. The use of ion-selective electrodes has been criticised as the amount of sweat produced is not measured[21]. In a paper by Tocci et al.[7]it was suggested that the Gibson-Cooke test is more accurate because the sweat on the filter paper is weighed and the test discarded if it is not enough. A major source of error quoted for ISEs has been the rapid evaporation of sweat from the stimulated area. Indeed, evaporation from a collection matrix may produce up to a two fold increase in the concentration of sweat electrolytes in 30 seconds[22]. In general however skin surface measurements have been more reproducible and accurate than expected. The aforementioned problems are likely to be overcome in the future, with meticulous attention to details of device design and experimental procedure. Therefore ISEs may still be regarded as one of the most obvious candidates to revamp testing for Cystic Fibrosis.

5.5 Development of a screening test for CF based on Solid-State ISEs.

5.5.1 Electrode Design.

The screen printed electrodes were prepared using the equipment, reagents and materials already discussed in Chapter 4. However, it was necessary to modify their design to some extent for application as skin contact electrodes.

The new screen printed design is displayed in Figures 5.3a and 5.3b. Figure 5.3a shows the stages involved in producing the screen printed electrodes. Following printing and curing of the Ag portion, as detailed in Chapter 4, an insulator layer was placed over the silver leads and over a small portion of the silver disc at the top of the electrode. This was both to protect the leads and prevent fluctuating internal reference potentials at the "to be" ISE where the Ag lead could contact both the PVC layer and the AgCl. Each pair of Ag/AgCl electrodes were printed such that, one Ag/AgCl portion could function as a solid-state chloride electrode and the other when further modified, function as a solid-state sodium selective electrode.

Figure 5.3a : The stages involved in producing the screen printed Ag/AgCl electrodes.

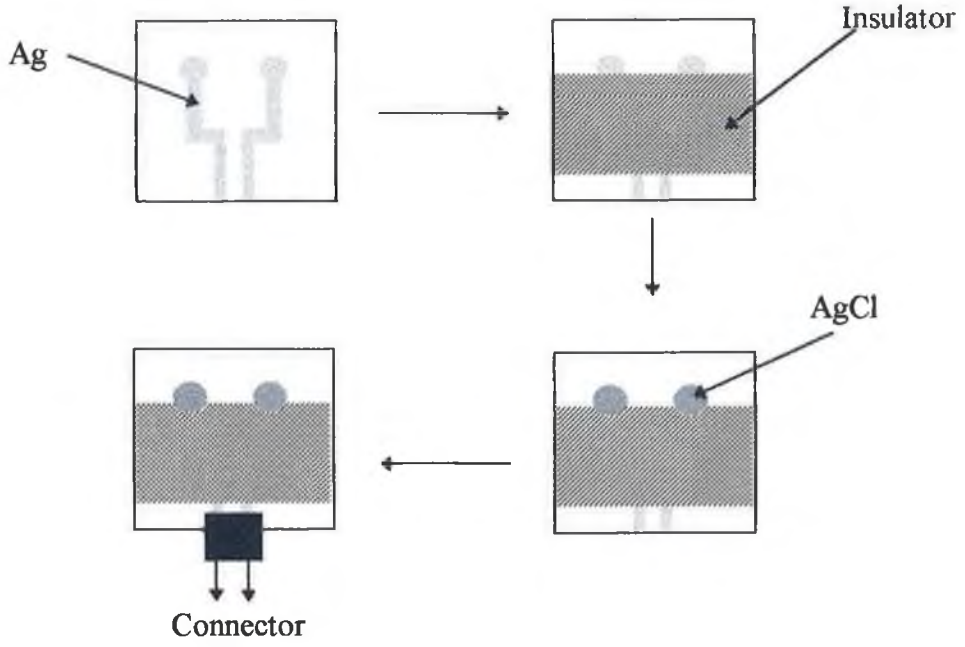

Figure 5.3b : Screen printed Ag/AgCl electrodes.

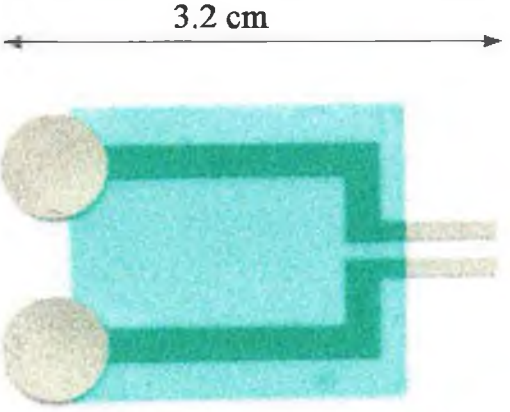

5.5.2 Preparation of a Solid-State Sensor.

A layer of 0.2% NaCl doped hydrogel was placed over one AgCl portion of the electrodes described in figure 5.3a. This was done using a polyester template cut to the exact dimensions of the AgCl disc. The polyester sheet used to construct the template was of the same type as that used as a backing sheet for the electrodes. The hydrogel was smoothed into a thin layer using a glass slide and left to dry for approximately 2 minutes. The edges around the AgCl were wiped clean of any hydrogel residue and a layer of cyanoacrylate adhesive (Loctite® product 406) was painted onto the polyester just surrounding the AgCl. A 0.5 cm diameter sodium selective PVC membrane,(Membrane M1 table 4.1) was placed over the hydrogel and allowed to bond with the adhesive layer. The electrode was left to bond for at least 1 minute (fixture time quoted in product brochure was from 2 to 10 seconds). The other AgCl portion of the electrode was left bare to function as a Chloride electrode. The entire electrode excluding the two sensing surfaces and the connectors was then covered with a layer of adhesive-backed clear plastic. Electrodes were generally left overnight before use in any experiments.

5.6 Experimental Design.

The above solid-state sensor is designed to respond to changes in sodium and chloride activity simultaneously. As explained previously in Chapter 4, the screen printed Ag/AgCl electrode will respond to changes in chloride concentration and the solid-state ISE will respond to changes in sodium activity. The overall potentiometric response (E_{cell}) will therefore be far more sensitive as shown in equation 5.1.

$$E_{cell} = E_{ISE} - E_{Chloride} \qquad \textbf{(5.1)}$$

As already mentioned there will be no true reference electrode at this point but the electrodes will be referenced to their own baseline potential.

5.6.1 Bench Experiments.

A batch of 10 electrodes was prepared according to the procedure outlined in section 5.5.2. These electrodes were given the identifiers E1-E10 and were calibrated in turn, as follows:

The electrode was placed on the bench and secured using adhesive tape. A 1.5x3 cm piece of sodium free filter paper (Whatman 541, Hardened Ashless) was placed over the sensing surface of the electrode. 100 ul of 20 mM NaCl was slowly deposited onto the filter paper using a micro-pipette. The filter paper was then covered with a glass slide and a 90g weight was placed on top. This was intended to prevent evaporation and to ensure that a good contact was maintained with the sensing surfaces. A schematic of this process excluding the weight, is shown in figure 5.4. As in previous experiments, the electrode potential was monitored using an AT-MIO-16DL data acquisition card (National Instruments, Austin, Texas, USA) in combination with LabVIEW 4.0 software. After approximately 10 minutes, the filter paper was removed and the electrode blotted dry. A fresh piece of filter paper was placed over the electrode and 100 ul of 40 mM NaCl was deposited as before. The electrode potential was then monitored for a further 10 minutes. The above procedure was repeated until the electrode had been exposed to all of the following concentrations of NaCl : 20 mM, 40 mM, 60 mM, 80 mM, 100 mM.

To demonstrate reproducibility, one electrode, E1, was calibrated a total of five times.

Figure 5.4 : Bench measurements.

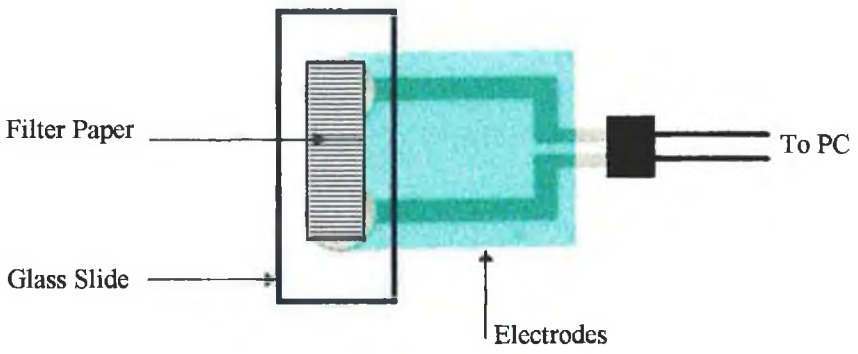

5.6.2 Skin Measurements.

Following calibration of the electrodes, two sets of skin measurements were collected. Each set of data was collected following pilocarpine iontophoresis which was carried out as outlined in section 5.3.1 with the following reagents;

0.4% (w/v) solution of Pilocarpine nitrate (1g/250 ml de-ionised H_2O).
0.35% (v/v) solution H_2SO_4 (0.7 ml in 200 ml de-ionised H_2O).

The above solutions were used to saturate 2" x 2" gauze squares which were then placed at the positive (pilocarpine nitrate) and negative (H_2SO_4) electrodes as described earlier.

Experimental Set 1 **:**

A calibrated and conditioned electrode was placed on the bench as before and a 1.5 x 3 cm piece of filter paper was placed over its sensing surface. This filter paper size was chosen as it just covered the sensing area without extending beyond the edges of the sensor. This was found to help maintain the adhesion between the polyester sheet and the plastic cover. 100 ul of 20 mM NaCl was deposited onto the filter paper using a micro-pipette. A glass slide and weight were placed over the electrodes as previously done and the electrode potential monitored until stabilised (approximately 10 minutes). During the latter five minutes, pilocarpine iontophoresis was carried out on a volunteer. Once iontophoresis was finished, the filter paper was removed from the electrode and a pre-weighed paper of the same size was placed over the area which had just been subjected to iontophoresis. The electrode was then attached to the patients arm as is shown in figure 5.5. The electrode potential was monitored for approximately 20 minutes after which time both filter paper and electrode were removed. Three volunteers were involved in this study and each was tested in turn. A flow diagram outlining this procedure is shown in figure 5.6.

Figure 5.5 : Electrodes in place.

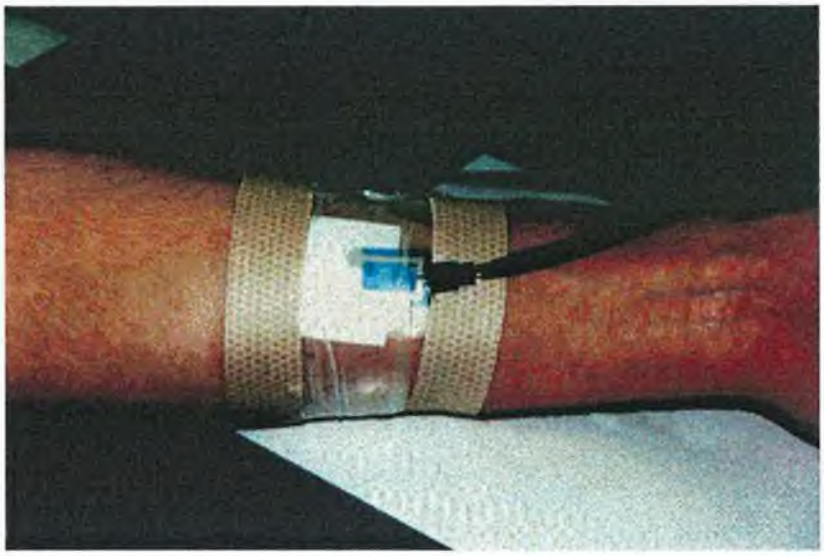

Figure 5.6 : Flow diagram outlining Experimental Set 1.

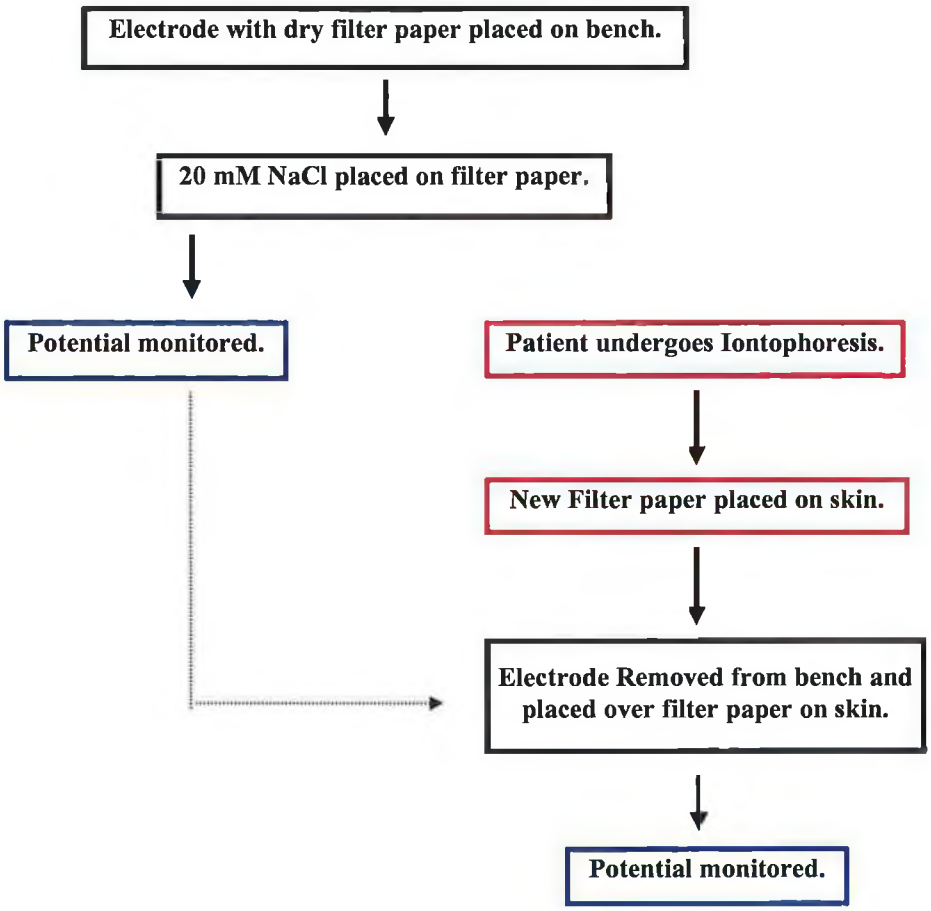

Experimental Set 2 :

A calibrated and conditioned electrode was placed on the bench as before and a 1.5x3 cm piece of filter paper was placed over its sensing surface. 100 ul of 10 mM NaCl was deposited onto the filter paper using a micro-pipette. This step was simply to ensure that the electrode was producing a stable signal. A glass slide and weight were placed over the electrodes as previously done and the electrode potential monitored until stabilised (approximately 10 minutes). The filter paper was then removed from the electrode and the surface dried. A pre-weighed piece of filter paper was then placed over the electrode and 100 ul of 5 mM NaCl was deposited onto the filter paper. The electrode was covered with a glass slide and weight and the potential monitored for approximately 10 minutes. During the latter five minutes, pilocarpine iontophoresis was carried out on a volunteer. Once iontophoresis was finished, a piece of parafilm was placed over the area which had just been iontophoresed. The patient was left for approximately 5 minutes until the area under the parafilm was wet. The glass slide and weight were then removed from the electrode and both filter paper and electrode were placed onto the skin as shown in figure 5.5. Care was taken to ensure that a waterproof shield was placed underneath the leads. The electrode potential was monitored for approximately 30 minutes after which time both filter paper and electrode were returned to the bench. They were covered as before with a glass slide and weight and the electrode potential was monitored for another short time (ca. 3 minutes) on the bench. The filter paper was then re-weighed, placed in a sterile container and 4 ml of de-ionised water added. Samples were then stored at 4°C until required. The above procedure was repeated on three volunteers. In a further three volunteers the baseline sodium concentration used was 20 mM not 5 mM. A flow diagram of the entire procedure is shown in figure 5.7. The same electrode was used in each case following careful washing in deionised water.

Figure 5.7 : Flow diagram outlining Experimental Set 2.

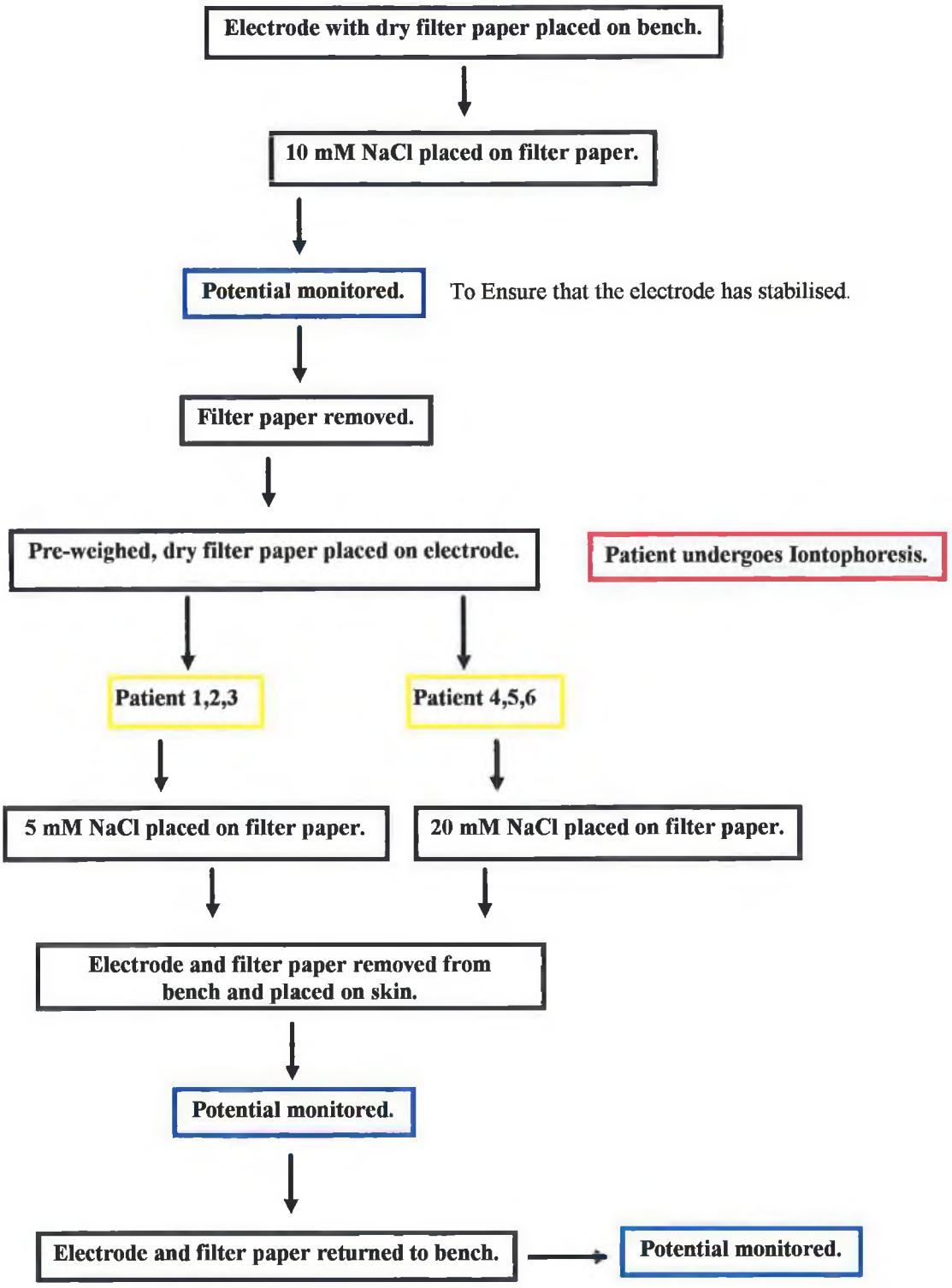

5.6.3 Analysis of sweat samples by conventional ISE.

The stored sweat samples were later analysed for sodium content using an ion-selective electrode and the method of standard additions.

Reagents: 2-Nitrophenyl-octylether (2-NPOE), tetrahydrofuran (THF), high molecular weight poly(vinyl)chloride and potassium tetrakis 4-chlorophenyl borate (KTpClPB) were selectophore® grade purchased from Fluka. NaCl was reagent grade and was purchased form Riedel-de-Haën. KCl was used to make a reference electrode filling solution, was reagent grade and was purchased from Fluka.

Ionophore: The sodium ionophore used was tetra-methoxyethyl p-t-butyl calix(4)arene tetracetate obtained from Professor M. Anthony McKervey of Queen's University, Belfast, Northern Ireland, and was used as received.

Membrane composition:

10 mg of the ionophore, together with 2 mg of ion exchanger (KTpClPB) was dissolved in 1 g of plasticiser (2-NPOE). 0.5 g of high molecular weight poly(vinyl)chloride was added to give a slurry. THF was added dropwise while stirring until a clear solution was obtained. This solution was poured into a 10 cm diameter glass petri dish and left covered with a loosely fitting lid. Evaporation of the THF (over approximately 3 days) left a clear PVC membrane from which the sensing films were cut.

Electrode Construction: An Ag/AgCl wire was placed inside a teflon electrode body and sealed in position using epoxy resin. A sodium selective PVC membrane was clipped into the electrode tip. The electrode body was then filled with 0.1M NaCl.

5.6.3.1 Sodium Analysis by Potentiometric Standard Additions.

A calibration curve was prepared for sodium as follows.

10 ml of 10^{-5} M NaCl was placed in a beaker. The sodium selective ISE and a miniature Ag/AgCl reference electrode (Sentek Ltd., Braintree, Essex, UK) were dipped into the sample solution. The electrode potential was monitored for approximately 5 minutes until a stable signal was obtained. The electrodes were then removed from the solution, rinsed with deionised water and dried gently with a tissue. 10 ml of the next standard solution was placed in the beaker and the electrodes placed in the solution as before. The signal was then monitored for a further 5 minutes. The above procedure was repeated for each standard in the following order; 10^{-5} , 10^{-4} , $5x10^{-4}$, 10^{-3}, 10^{-2} and 10^{-1} M NaCl.

***Sweat Samples*:** The sodium level in the sweat samples was analysed using the standard additions method. 2 ml of the sweat sample was placed in a beaker and the sodium selective ISE and Ag/AgCl reference were dipped into the solution. The electrode potential was monitored for 5 minutes after which time a 20 ul injection of 10^{-2} M NaCl was introduced via a micro-pipette. The beaker was swirled by hand to facilitate mixing. After monitoring the signal for a further 5 minutes a second injection was introduced consisting of 50ul 10^{-2} M NaCl. After monitoring the potential at this concentration, two more injections were introduced both consisting of 100ul 10^{-2} M NaCl. Data were analysed according to equation 5.2.

$$C_i = \frac{\frac{C_s V_s}{V_s + V_i}}{10^{\Delta E/S} - \left(\frac{V_i}{V_i + V_s}\right)} \qquad \textbf{(5.2)}$$

C_i = Concentration of sodium in 2 ml sample (unknown).

V_i = Volume of sweat sample (2 ml).

C_s = Concentration of sodium in standard addition.

V_s = Volume of standard addition.

ΔE = Potential step after addition.

S = Slope of the calibration curve.

5.7 Discussion of Results.

A set of 10 sensors, consisting of both a sodium and chloride electrode, was prepared and calibrated according to the method previously outlined in section 5.5.2. These sensors are identified as E1 to E10. The steady-state potentials recorded for each are shown in table 5.1. Also shown in parenthesis, are the standard deviations of the steady-state responses (over 30 points) at each concentration which is taken to represent signal noise. The potentiometric slope of the device is also included. An example of one calibration (E8) is shown in figure 5.8. The steady-state responses for E8 are obviously very stable at every concentration of NaCl. In addition this device displays a drift ranging from $4x10^{-3}$ mV/min. at 100 mM to 0.19 mV/min at 40 mM. Drift was calculated from the slope of the mV response over 240 points, at each NaCl concentration.

Figure 5.8: Calibration for electrode E8.

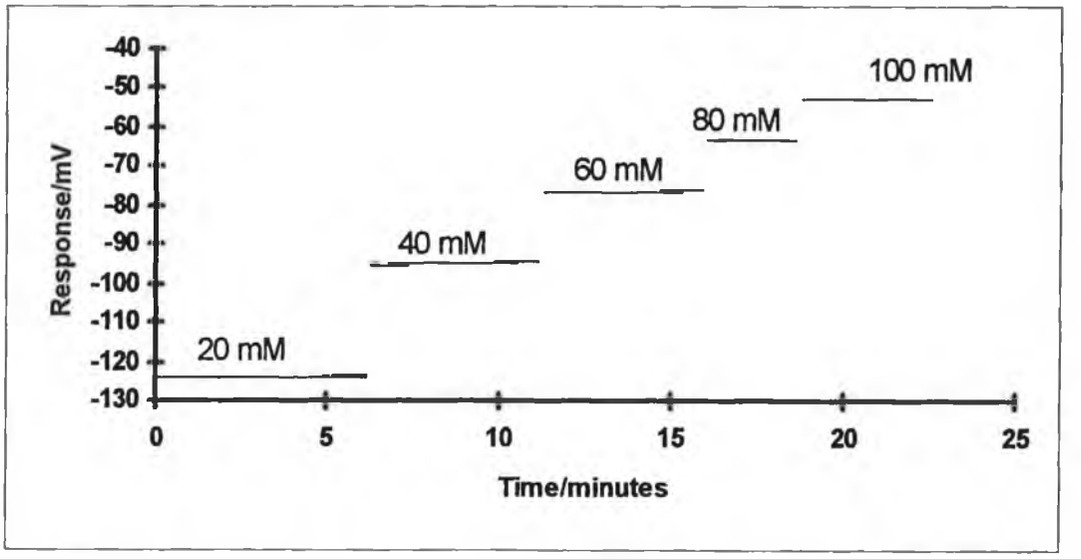

Although the steady-state response of device E8 may be very stable, it is in fact sub-Nernstian with a slope of the slope of only 97.31 mV/decade (see table 5.1). The sub-Nernstian slope is possibly a function of the bare Ag/AgCl electrode as discussed in

Chapter 4, section 4.5.2 **B**, and was noted to varying degrees in most of the devices studied. With reference to the data in table 5.1, it may be implied that a major weakness of these devices is in the reproducibility of absolute potentials and slopes. E5 displays a slope of 163.45 mV which is significantly larger than the theoretical value of 118.40 mV expected for combined sodium and chloride electrodes, responding to decade changes in NaCl at 25°C.

Table 5.1 : Steady state potentials recorded for the calibration of ten solid-state sensors.

[NaCl] / mM →	40	60	80	100	
Electrode ↓	*Steady-State Response / mV*				*Slope*
E1	27.12 (0.29)	46.78 (0.41)	58.98 (0.13)	69.15 (0.29)	107.36
E2	33.94 (0.25)	52.12 (0.14)	64.24 (0.09)	75.14 (0.12)	115.25
E3	30.00 (0.07)	48.13 (0.10)	60.63 (0.02)	68.13 (0.04)	106.57
E4	29.47 (0.11)	45.26 (0.10)	57.37 (0.32)	66.32 (0.14)	102.19
E5	45.71 (0.12)	72.38 (0.17)	91.43 (0.08)	105.72 (0.41)	163.45
E6	25.83 (0.16)	42.50 (0.37)	52.08 (0.61)	60.41 (0.37)	93.66
E7	26.35 (0.28)	43.91 (0.37)	57.08 (0.30)	66.84 (0.41)	105.48
E8	21.00 (0.17)	40.51 (0.36)	52.51 (0.24)	62.28 (0.44)	97.31
E9	30.00 (0.20)	47.00 (0.21)	60.00 (0.23)	71.00 (0.22)	108.77
E10	30.48 (0.23)	47.62 (0.43)	60.00 (0.18)	71.43 (0.53)	109.14
Theoretical	33.29	52.55	66.14	76.66	118.40

Figure 5.9 shows the mean of five calibration runs performed on device E1. Once again the steady-state response is very stable with a drift ranging from 0.06 mV at 40

mM to 0.79 mV at 60 mM. Drift was calculated from the slope of the mV response over 120 points, at each NaCl concentration. Table 5.2 lists the steady state potentials obtained for electrode E1 and in parenthesis beside each value the standard deviation of 100 data points representing signal noise. The data have been zeroed on the signal obtained for 20 mM NaCl as some variation in baseline potential was observed leading to a standard deviation between injections of approximately 16 mV at 20 mM NaCl. Once the data were zeroed on the baseline signal, the standard deviation between injections fell to an average of 4.17 mV over the entire concentration range. This is shown in table 5.2, where the mean of five calibration runs is listed, ± the standard deviation between runs at each concentration. This demonstrates that the device is responding in a reproducible fashion to changes in NaCl activity but also that reproducibility of absolute baseline potentials is proving difficult.

Figure 5.9 : Mean of 5 calibration runs performed on electrode E1.

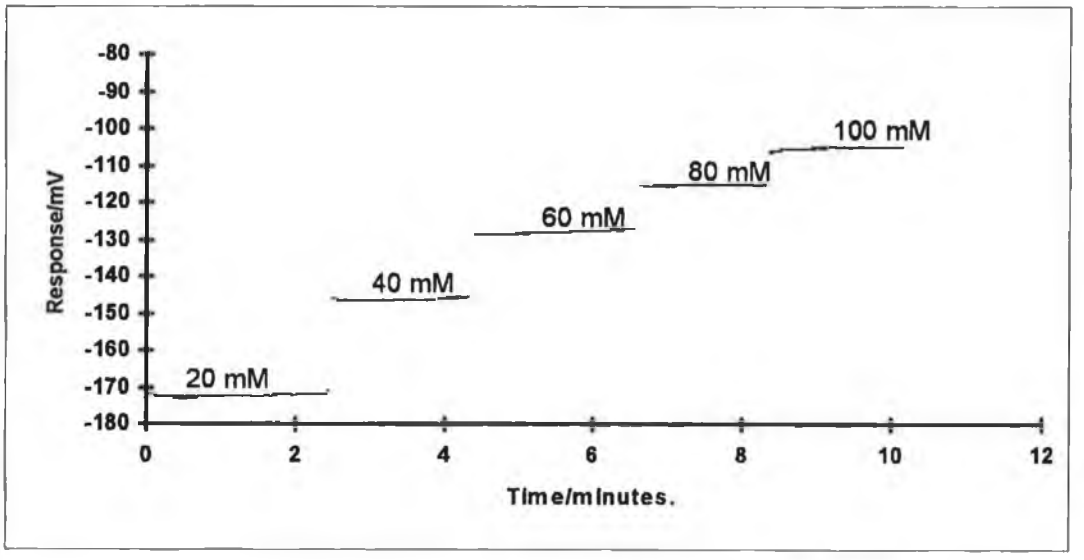

Table 5.2 : Steady-State potentials obtained for five calibration runs involving electrode E1. The signal noise at each concentration is shown in parenthesis. The mean steady-state potential is listed, ± the standard deviation between runs at each concentration. Data has been zeroed on the signal obtained for 20 mM NaCl. Figure 5.9 shows the mean of these five calibrations.

Steady-State Potential / mV							
Run	**1**	**2**	**3**	**4**	**5**	**Mean**	**Theoretical**
[NaCl] ↓							
40 mM	20.93 (0.75)	31.06 (0.63)	26.31 (0.19)	23.94 (0.13)	25.36 (0.78)	25.52 ± 3.35	33.29
60 mM	38.59 (0.13)	52.60 (0.24)	40.37 (0.10)	42.24 (0.37)	45.30 (0.44)	43.82 ± 5.76	52.55
80 mM	50.37 (0.67)	65.31 (0.20)	56.26 (0.68)	53.24 (0.13)	57.53 (0.24)	56.54 ± 5.83	66.14
100 mM	59.33 (0.19)	72.63 (0.16)	67.33 (0.09)	65.40 (0.23)	68.58 (0.20)	66.65 ± 4.82	76.66
Slope	101.04	114.66	112.96	111.09	117.00	111.35	118.40

Calibration 1 above suggests a sub-Nernstian response from the electrode whereas calibration 2 is significantly closer to the theoretical. Calibrations 3,4 and 5 are less accurate than calibration 2 but are very similar. This suggests that problems may occur with reproducibility in real situations if the electrode is not carefully conditioned before use. However, it also suggests that improvements in reproducibility between runs may be achieved over time, leading to the conclusion that a longer conditioning time may be needed, perhaps overnight.

Following calibration of the sensors, two sets of skin measurements were collected by two slightly different techniques. Three volunteers were involved in the first study which is described in section 5.6.2, ***Experimental Set 1.*** In brief, the electrode was first allowed to stabilise on the bench using a piece of filter paper saturated in 20 mM NaCl, see figure 5.6. Following iontophoresis, this filter paper was removed from the electrode and a dry paper placed over the treated area of skin. The electrode was

then placed over the filter paper and secured as shown in figure 5.5. The electrode potential was monitored for approximately 20 minutes. The results of these experiments are shown in figures 5.10, 5.11 and 5.12.

Figure 5.10 : Data for skin measurements for Volunteer 1, ***(Experimental Set 1).*** *Also shows the upper limit beyond which a CF positive result is expected.*

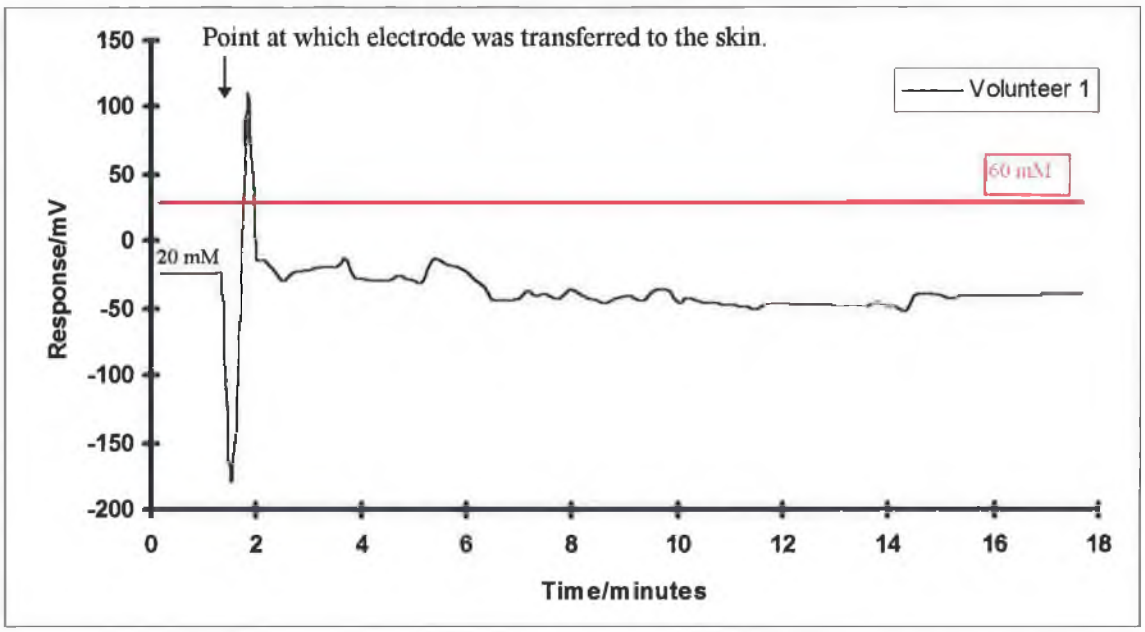

The signal obtained for Volunteer 1 is very stable and suggests that the electrode is functioning extremely well. The signal was not expected to stray too far from the established baseline, as all volunteers were known not to have Cystic Fibrosis. Figure 2.11 shows data obtained for volunteer 2. Here the signal is extremely unstable and does not tend to follow any particular direction. As the device (E1) has already been shown to respond very well to changes in NaCl activity, it was concluded that these

stabilisation problems were a result of poor contact between the skin and the device. During the experiment, it was noted that a very small quantity of sweat was obtained from this volunteer. Once removed, the filter paper was only slightly damp with very little excess moisture. It is likely that a good contact was never obtained between the electrode and the sweat in this experiment. It must be remembered that the sweat had to first permeate the dry filter paper before it reached the sensing surface to produce a stable signal.

Figure 5.11 : Data for skin measurements for Volunteer 2, ***(Experimental Set 1).*** *Also shows the upper limit beyond which a CF positive result is expected.*

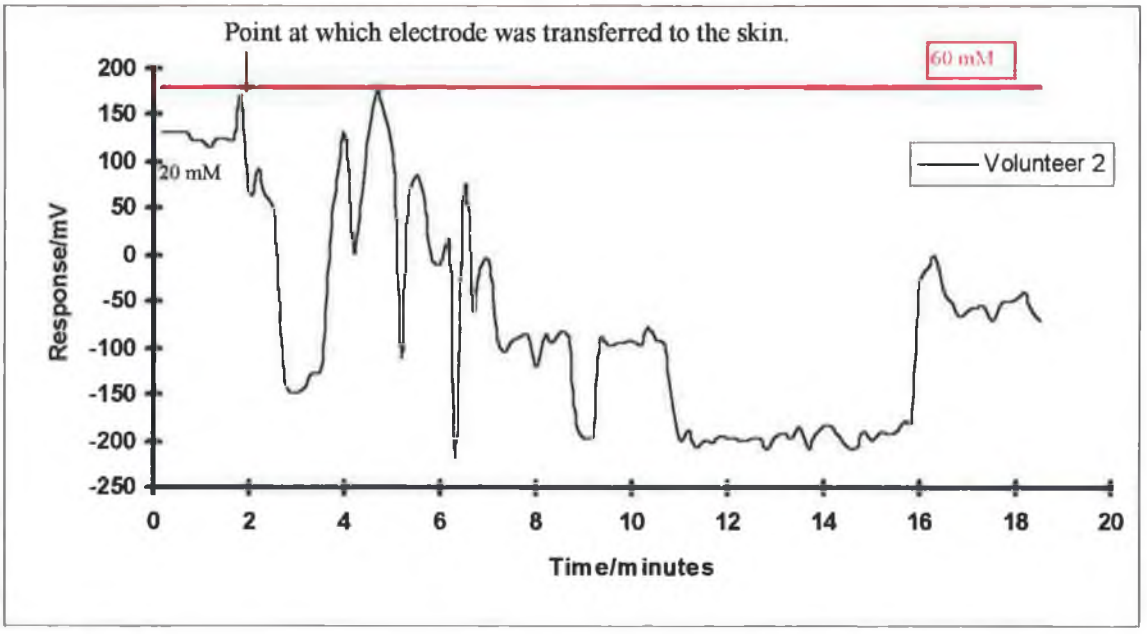

Figure 5.12 shows data obtained for volunteer 3. For the first 10 minutes the response is reasonably stable and suggests a level of NaCl below 20 mM which is quite acceptable for a CF negative patient. However, after this time a substantial increase in potential occurs with the signal remaining unstable for the remainder of

this experiment. This volunteer produced a higher volume of sweat than either of the other two. As the electrodes were removed from the skin, it was noticed that the leads and connector were quite wet. This may explain the stabilisation problems encountered with this experiment. This artefact has appeared after 10 minutes and so is likely to be due to this build up of sweat. From this point on, care was taken to isolate the leads and connectors from the skin in all experiments, by wrapping them in waterproof adhesive plaster and placing a layer of waterproof plaster over parts of the skin surface with which they might make contact.

Figure 5.12 : Data for skin measurements for Volunteer 3, ***(Experimental Set 1)****. Also shows the upper limit beyond which a CF positive result is expected.*

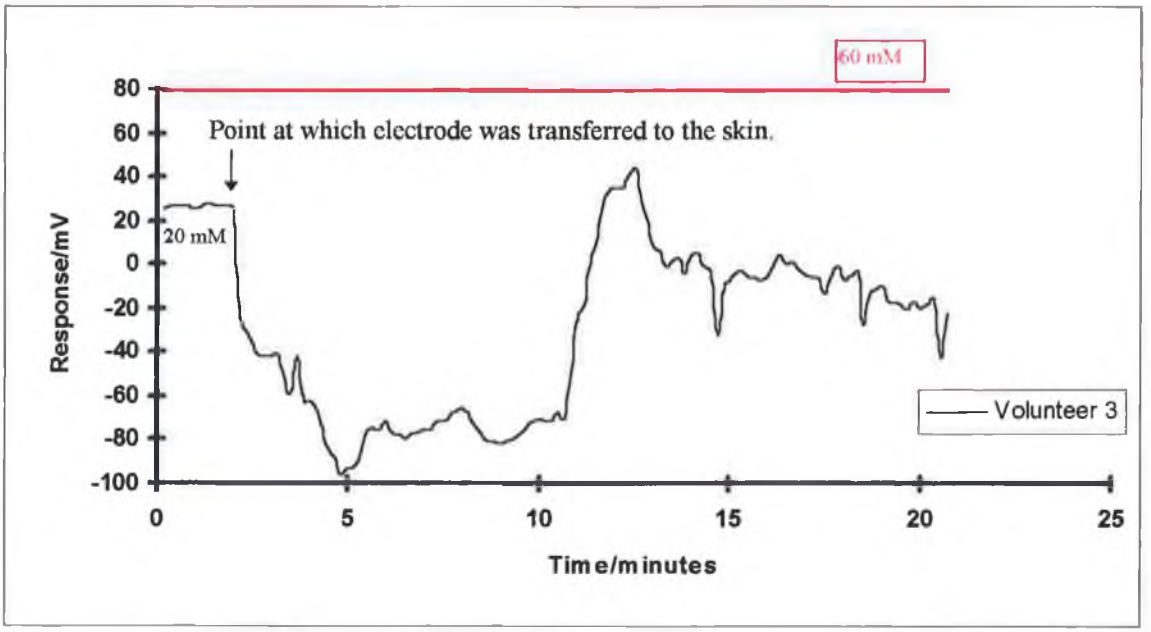

In addition, an open circuit exists from the time the electrode is removed from the bench until the filter paper becomes saturated with sweat.

With this, and the previous experimental observations in mind, a second series of skin experiments (***Experimental Set 2***) was recorded involving six volunteers. In this case the electrode was conditioned in 10 mM NaCl and a baseline potential was then

established at either 5 mM NaCl (Volunteers 1-3) or at 20 mM NaCl (Volunteers 4-6). When the electrode was then transferred to the skin the filter paper was not removed but was placed on the skin as well (see section 5.6.2). This prevents the open circuit previously obtained and it was hoped that this would facilitate electrode stabilisation. Figures 5.13, 5.14 and 5.15 show the data recorded for Volunteers 1 to 3 respectively. Clearly, stability is still a problem. In figure 5.13 the general trend suggests that the NaCl concentration is higher than 5 mM. Transferring the electrodes back to the bench causes a large increase in potential which rapidly returns to a value close to that obtained on the skin. This artefact may be due in part to temperature fluctuations as well as sample evaporation. Figures 5.13, 5.14 and 5.15 also include two coloured lines indicating the theoretical potentials expected for 5 mM and 60 mM NaCl. The potential at 5 mM corresponds to that expected when the NaCl concentration changes from 10 mM to 5 mM. In figure 5.13, this theoretical potential agrees closely with the experimental trace. Therefore, it may be concluded that the electrode is functioning correctly. The instability observed is therefore likely to be a result of contact problems which obviously have not been solved to date.

Figure 5.13 : Data recorded for skin measurements for volunteer 1, ***(Experimental Set 2)*** *using a baseline of 5 mM NaCl.*

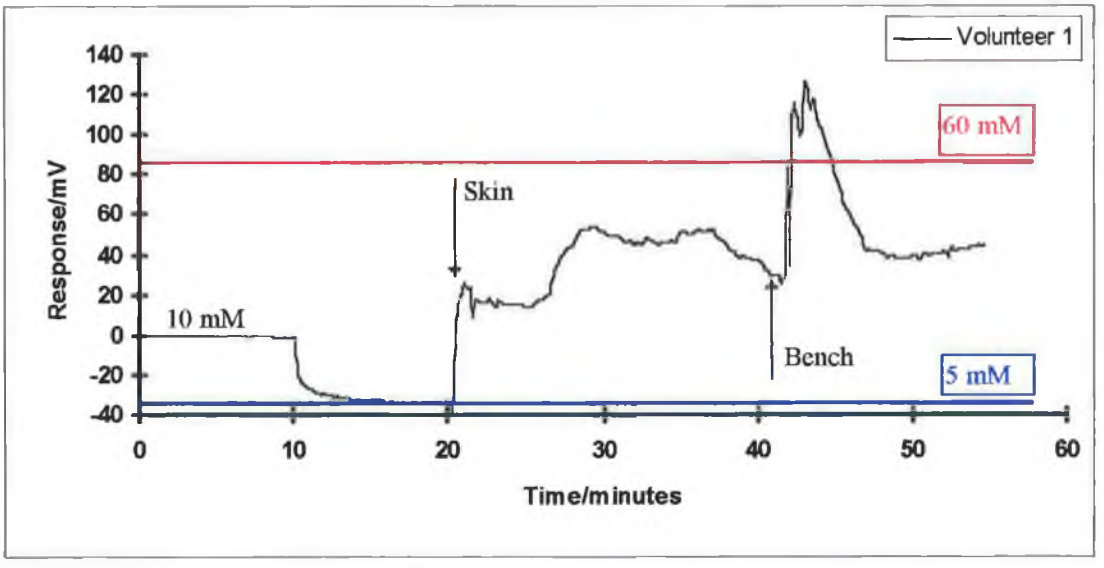

Figure 5.14 shows the result of a similar experiment for volunteer 2. The general trend is upwards suggesting a concentration of NaCl greater than 5 mM. This trace begins to stabilise after approximately 15 minutes of skin contact. Once the electrode is transferred to the bench, the response becomes far more stable but the potential increases significantly becoming very close to the 60 mM upper limit for a CF negative result.

Figure 5.14 : Data recorded for skin measurements for volunteer 2, ***(Experimental Set 2)*** *using a baseline of 5 mM NaCl.*

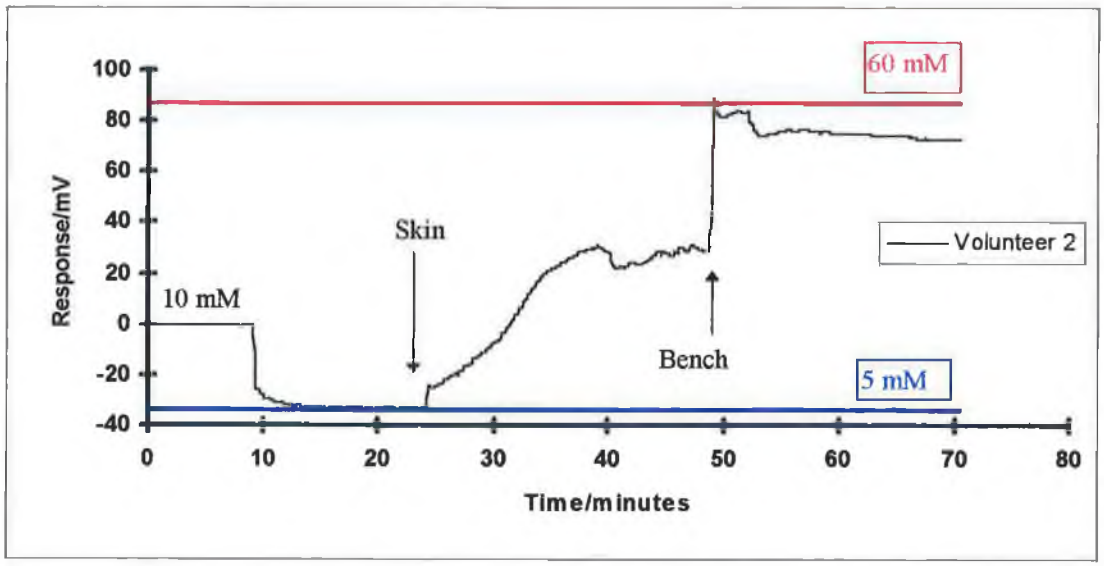

Figure 5.15 contains data recorded for volunteer 3. In this case the 10 mM to 5 mM potential step is not as large as that theoretically predicted (blue line). Therefore, the electrode may not have been stabilised sufficiently before starting the experiment. It may also be displaying some carryover from a previous experiment having been used on the two previous volunteers. Despite this discrepancy between theoretical and experimental potentials the trace is generally unstable but suggests a NaCl concentration in the region of 5 mM.

Figure 5.15 : Data recorded for skin measurements for volunteer 3, ***(Experimental Set 2)*** *using a baseline of 5 mM NaCl.*

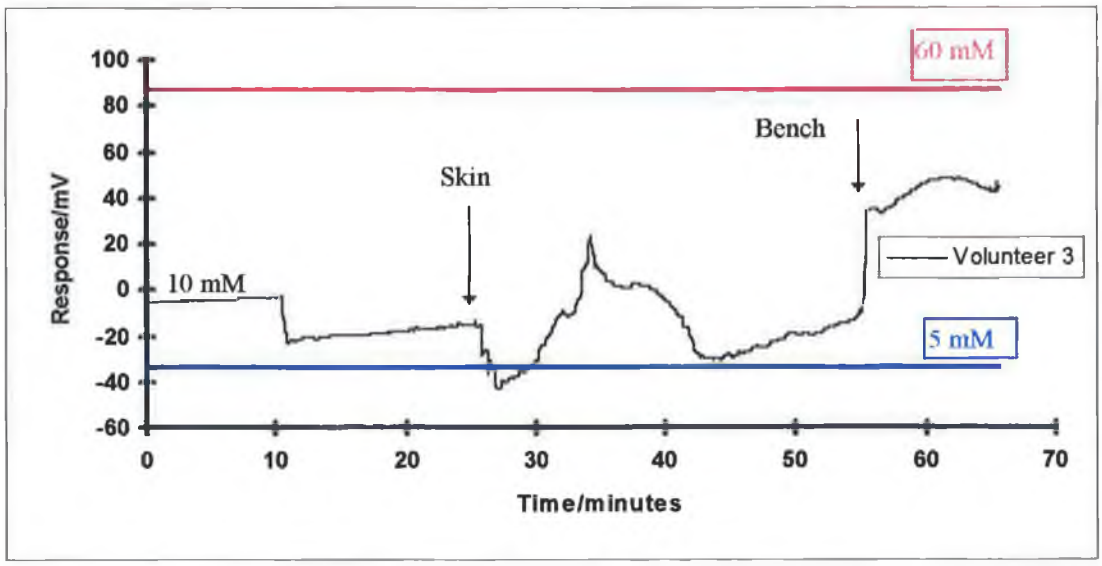

Figures 5.16, 5.17 and 5.18 show data recorded using a baseline of 20 mM NaCl. These figures also include indicators of the theoretical potential expected for 60 mM NaCl and that expected when the concentration is stepped up from 10 mM to 20 mM NaCl. Figure 5.16 represents volunteer 4. Here the trend suggests a concentration of NaCl greater than 20 mM. This trace is very stable, increasing gradually over approximately 15 minutes to a stable potential of around 60 mV i.e. approximately 35 mM NaCl. This type of trace corresponds to that theoretically expected. The experimental procedure is such that sweat has to saturate the filter paper and change the existing concentration of NaCl i.e. 20 mM. Once again, the potential increases when the electrode is returned to the bench which may be a reaction to different pressure. On the bench, the electrode is covered with a glass slide and 90g weight. Electrodes were noted throughout experiments to be pressure sensitive as the potential changed easily if the electrode was touched, either when in contact with the skin or on the bench.

Figure 5.16 : Data recorded for skin measurements on volunteer 4, ***(Experimental Set 2)*** *using a baseline of 20 mM NaCl.*

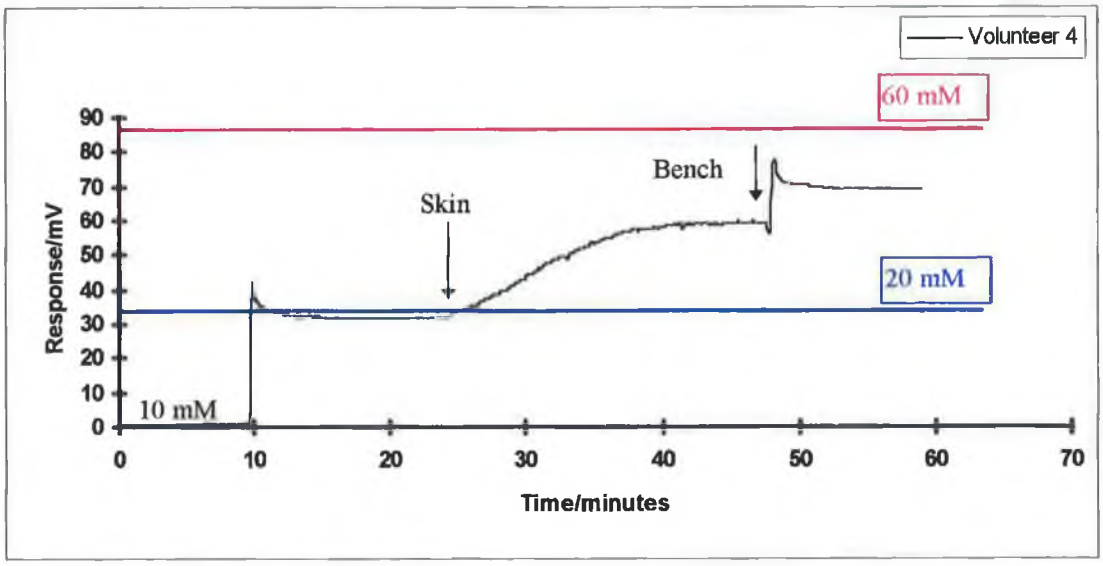

Figure 5.17 shows a similar experiment for volunteer 5. In this case, the potential step obtained when the concentration of NaCl increases from 10 mM to 20 mM falls slightly short of that theoretically expected. This electrode should have been stabilised for a longer period of time before proceeding. That aside, the general trend is downwards, suggesting a concentration less than 20 mM NaCl. Indeed the concentration seems to lie close to the 10 mM level. When the experiment is transferred back to the bench a large increase in potential is observed exceeding the 60 mM upper limit for a CF negative result. As the volunteer is known to be CF negative, this result is of little significance.

Figure 5.18 shows the final set of experimental data i.e. volunteer 6. Following application of the electrode to the skin, the potential initially falls but then increases slightly after approximately 10 minutes. Following this increase the trace is reasonably stable, although it does drift slightly downwards, suggesting a NaCl concentration between 10 mM and 20 mM. When returned to the bench a large increase in potential is observed but this is likely to be an experimental artefact as the potential rapidly falls back to a level less than 60 mM.

Figure 5.17 : Data recorded for skin measurements on volunteer 5, ***(Experimental Set 2)*** *using a baseline of 20 mM NaCl.*

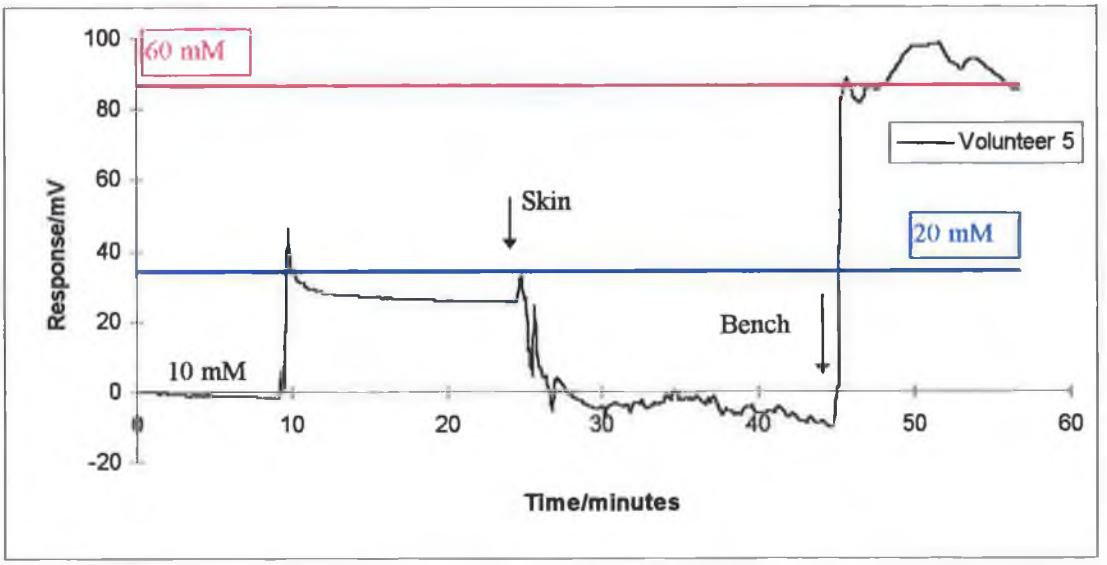

Figure 5.18 : Data recorded for skin measurements on volunteer 6, ***(Experimental Set 2)*** *using a baseline of 20 mM NaCl.*

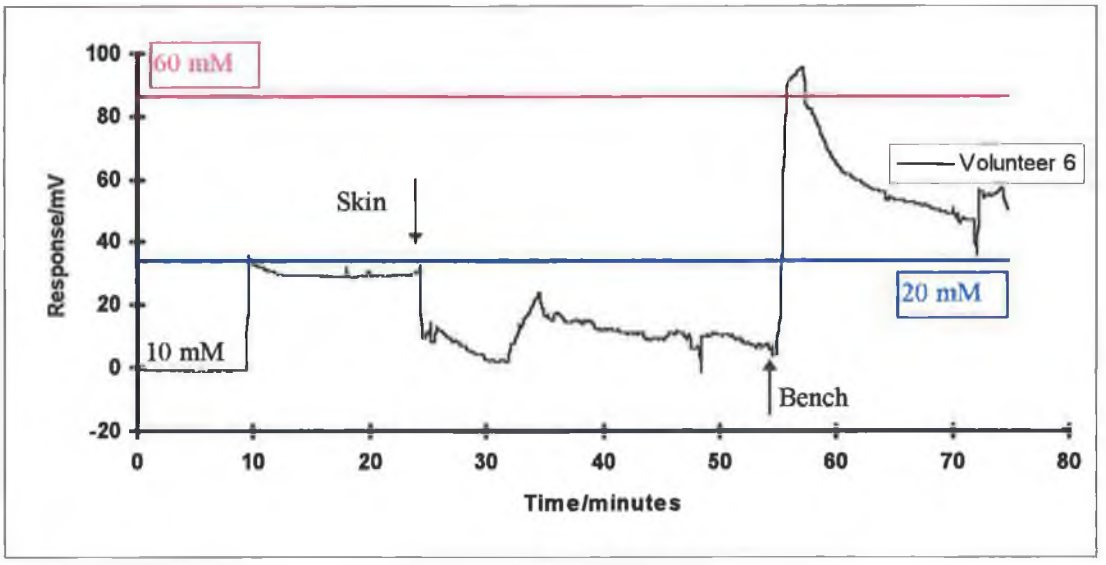

The samples collected for these six volunteers were all stored and analysed for sodium concentration by conventional ion-selective electrode using the method of standard additions. Table 5.4 lists the individual additions made to a 2 ml diluted sweat sample.

Table 5.4 ; Series of standard additions involved in the determination of sodium in sweat samples by conventional ion-selective electrode.

Addition Number	Addition Concentration (M)	Addition Volume (ul)
1	$1x10^{-2}$	20
2	$1x10^{-2}$	50
3	$1x10^{-2}$	100
4	$1x10^{-2}$	100

Table 5.5 lists the potential steps and the corresponding sodium concentrations calculated in the sweat sample following each of four standard additions. These values were calculated using equation 5.2, the standard addition volumes and concentrations listed in table 5.4, a sample volume of 2 ml and a slope of 25 mV/ decade relating to the calibration slope between 10^{-5} M and 10^{-4} M NaCl (see section 5.6.3.1).

As expected, the sodium concentrations calculated following each addition are all quite similar. Therefore, these values were averaged as shown in table 5.5 and these average values used to determine the concentration of sodium in each individual sweat sample prior to dilution. As mentioned in section 5.6.2 ***Experimental Set 2***, the sweat sample collected on filter paper was diluted in 4 ml of deionised water. However only 2 ml of this diluted sample was involved in this standard addition experiment. A sample calculation of sodium concentration is shown overleaf;

Sample calculation for Volunteer 1

Average $[Na^+]$ determined using equation 5.2 = $2.53x10^{-4}$ M

Moles of Na^+ in 4 ml sample = $\frac{2.53x10^{-4}}{1000}x4$

= $1.01x10^{-6}$ moles

Sample collected = 0.0486 g (0.0486 ml)

Adjusting concentration for volume collected = $\frac{1.01x10^{-6}}{0.0486}x1000$

= 0.0208 M

= 20.80 mM

Table 5.5 ; the potential steps and the corresponding sodium concentrations calculated in the sweat sample following each of the four standard additions.

Steady State Potential / mV						
Volunteer Number	**1**	**2**	**3**	**4**	**5**	**6**
Addition 1	3.33	2.78	5.17	4.14	7.92	6.07
Addition 2	8.81	7.45	12.76	11.28	20.42	16.07
Addition 3	15.48	13.56	22.76	21.56	32.50	26.78
Addition 4	20.24	18.00	28.62	27.56	40.00	33.92
Sodium Concentration in sweat sample / M						
Volunteer Number	**1**	**2**	**3**	**4**	**5**	**6**
Addition 1	$2.76x10^{-4}$	$3.39x10^{-4}$	$1.62x10^{-4}$	$2.13x10^{-4}$	$9.22x10^{-5}$	$1.32x10^{-4}$
Addition 2	$2.70x10^{-4}$	$3.43x10^{-4}$	$1.51x10^{-4}$	$1.85x10^{-4}$	$6.08x10^{-5}$	$9.97x10^{-5}$
Addition 3	$2.48x10^{-4}$	$3.15x10^{-4}$	$1.10x10^{-4}$	$1.25x10^{-4}$	$4.13x10^{-5}$	$7.27x10^{-5}$
Addition 4	$2.18x10^{-4}$	$2.80x10^{-4}$	$9.18x10^{-5}$	$1.02x10^{-4}$	$3.07x10^{-5}$	$5.47x10^{-5}$
Average	$2.53x10^{-4}$	$3.19x10^{-4}$	$1.29x10^{-4}$	$1.56x10^{-4}$	$5.63x10^{-5}$	$8.98x10^{-5}$

The results of the potentiometric standard additions, together with the trends observed in figures 5.13 to 5.18 are shown in table 5.6. As already mentioned, the ion-selective electrode results have all been adjusted according to the quantity of sweat collected in each sample. Results generally follow the trends observed in figures 5.13 to 5.18 with the exception of Volunteer 4. As the trace for this sample is very stable and clear (figure 5.16), it is difficult to know why this discrepancy has occurred.

Table 5.6 : Data form both skin measurements and ion-selective electrode determinations for each of six volunteers.

Volunteer	Sample / g	Skin Measurement $[Na^+]$ / mM	Ion-selective electrode Measurement $[Na^+]$ / mM
1	4.86×10^{-2}	> 5	20.80
2	1.69×10^{-1}	> 5	25.27
3	5.79×10^{-2}	≈ 5	3.05
4	5.05×10^{-2}	> 20	4.32
5	1.44×10^{-1}	< 20	3.88
6	5.57×10^{-2}	< 20	6.45

Overall the results are promising, but it is clear that the problems encountered with skin contact have not been solved to date. In conclusion, there are several areas which need to be addressed before these devices can be directly applied to cystic fibrosis detection. Some suggestions will be made in the following section as to how these problems may be solved. It must be remembered however, that bench experiments discussed earlier indicate strongly that such an application is possible. It

only remains to address the fine details of electrode and experimental design which will form the basis of future project work in this area.

5.8 Proposals for Future Work.

There are two main areas which need attention. The first is the bare Ag/AgCl electrode and the second the contact problems arising when electrodes are placed on the skin. A bare Ag/AgCl electrode has been shown to respond to changes in chloride activity, but it produces nosier and less stable responses than a traditional ISE, which also tend to be sub-Nernstian. These problems arise as there is no internal reference element in this electrode and therefore no stable internal reference potential. This problem may be addressed in two ways. Either the Ag/AgCl electrode should be further modified to function as a stable Ag/AgCl reference electrode or it should be modified to perform as a true chloride ISE. If the first option is chosen, the Ag/AgCl electrode needs to be covered with a solid or semi-solid layer, such that the AgCl layer is preserved and the electrode can function as a reference. Possible coatings include salt doped polymers or hydrogels. In this way, the electrode will retain the ability to exchange electrolyte but at a rate slow enough not to register as a change in potential over the time period of the experiment. Preliminary experiments suggest that a salt doped hydrogel layer will function as a reasonable diffusional barrier for approximately 30 minutes. Poly (vinyl) acetates are another possibility, but curing conditions, suitable initiators and accelerators need to be carefully chosen. In figure 5.19 the response of a bare Ag/AgCl electrode to changes in chloride concentration is compared to that of an Ag/AgCl electrode covered by a NaCl doped hydrogel layer. Clearly the hydrogel layer serves to slow down the diffusion of chloride to the electrode surface resulting in an logarithmic based response profile.

Figure 5.19 : Comparison of the response to changes in chloride activity of an Ag/AgCl electrode and Ag/AgCl electrode with hydrogel layer

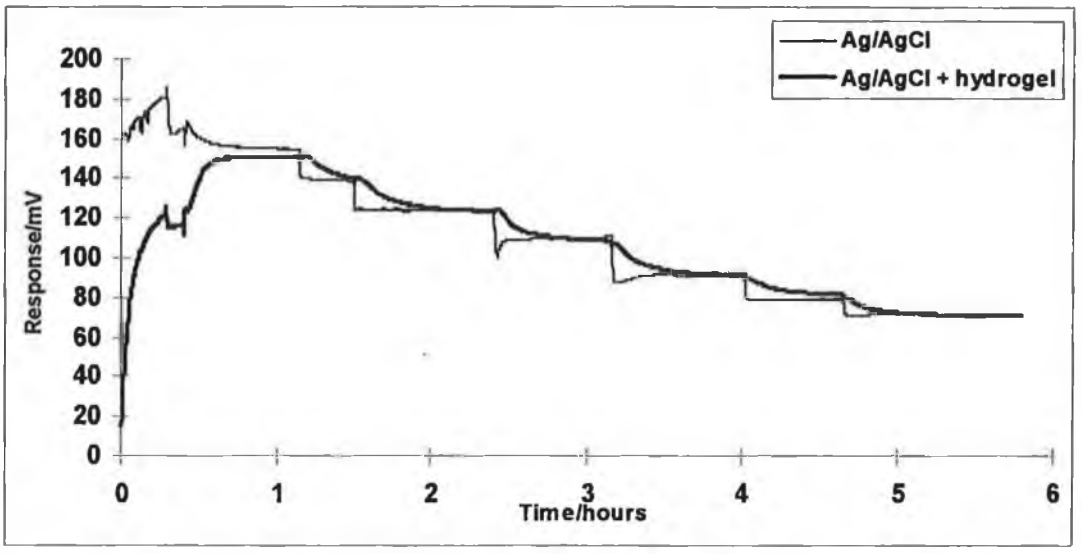

This response has been modelled using Microsoft EXCEL *solver*, an analysis tool incorporated into EXCEL which will be described in detail in Chapter 6. Basically, *solver* is used to model non-linear relationships by comparing an array of data predicted by a model with a set of experimental data[23]. The solver model consists of an equation containing several variables, which can be adjusted by the module until the difference between the modelled and experimental data sets is minimised. In this way, an equation concerning the diffusion of ions across a membrane[24] was used to model one of the logarithmic steps seen in figure 5.19. Equation 5.5 is based on Ficks laws of diffusion. Ficks laws are differential equations describing the flux or movement of a substance and its concentration under diffusion control as functions of time and position. Ficks first law states that the flux or net movement of molecules per unit time, is proportional to the concentration gradient.

$$\text{Flux per unit area} = -D\left(\frac{dC}{dx}\right) \qquad \textbf{(5.3)}$$

D = Diffusion Coefficient.

$\frac{dC}{dx}$ = Concentration gradient.

Ficks second law pertains to the change in the concentration gradient as a function of time. It is derived from the first law by noting that the change in concentration at a location is given by the differences in the flux into and the flux out of an element of width dx.

$$\left(\frac{dC}{dt}\right) = D\left[\frac{d^2C}{(dx)^2}\right] \qquad \textbf{(5.4)}$$

for $\left(\frac{dC}{dt}\right)$ = change in concentration per unit time (t).

Solver equation:

$$X_t = \left[k\left(1-\frac{4}{\pi}\right)\right]\left[\sum_{n=0}^{\infty}\left(\frac{-1^n}{2n+1}\right)e^{\left(-(2n+1)^2(\pi)^2\left(\frac{t-t_0}{4}\right)\left(\frac{D}{d^2}\right)\right)}\right] \qquad \textbf{(5.5)}$$

for

t = time.

t_0 = Response start time.

D = Diffusion coefficient.

d = Hydrogel thickness.

k = Constant, relating to the particular step size.

n = Number from zero to infinity.

X_t = Data point at time t.

Equation 5.5 modelled the experimental data in figure 5.19 and calculated a diffusion coefficient of approximately 10^{-14} which is in the region of that expected for PVC

based membranes. Therefore the rate of diffusion has been slowed considerably by incorporating the hydrogel layer.

Following this result, it was decided to place a layer of dialysis tubing over the hydrogel to act as a further diffusional barrier. The dialysis tubing used consisted of a transparent, seamless viscose cellulose containing glycerine, water and approximately 0.1% sulphur. It had an average pore radius of 24Å. The Ag/AgCl, hydrogel, dialysis tubing combination was then tested for response to chloride and the result of this experiment is shown in figure 5.20. The covered electrode shows very little response to chloride, producing a reasonably stable potential over a period of approximately 5 hours. It remains a possibility therefore, that with a suitable diffusional barrier in place, the potential of the Ag/AgCl electrode may be kept constant for long enough to use the electrode as a reference.

Figure 5.20 : Comparison of the response to changes in chloride activity of an Ag/AgCl electrode and Ag/AgCl electrode with hydrogel layer which is covered with dialysis tubing.

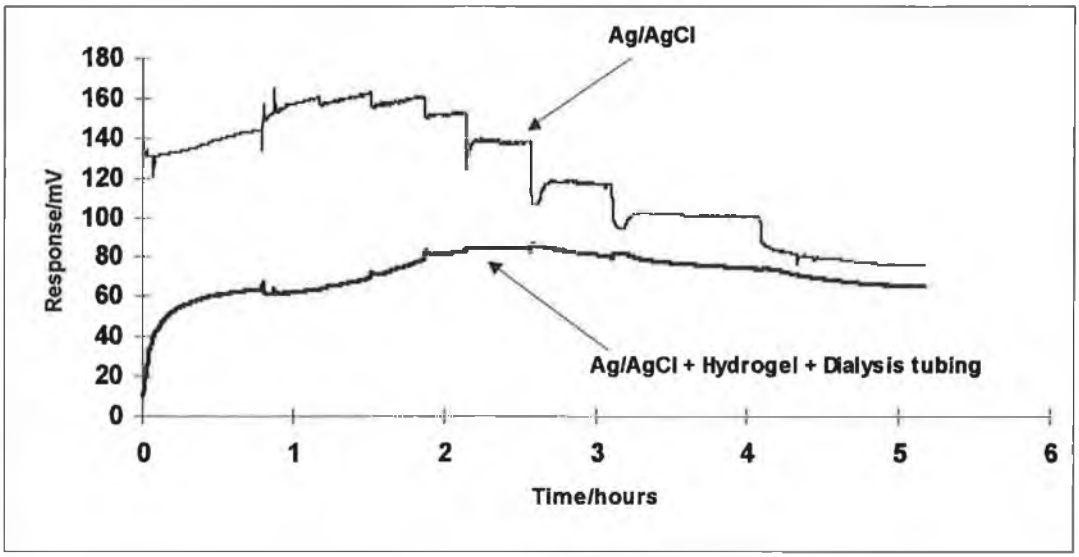

The second option available i.e. to improve the performance of the electrode as a chloride ISE may be achieved by incorporating a chloride selective PVC membrane into the device. Several chloride ligands are available such as Tri-dodecyl-methyl ammonium chloride which can be purchased from Fluka.

The contact problems can be approached in several different ways. They probably result from the fact that, at present, the sensing portions of the electrode are slightly recessed. Ideally they should come into contact with the skin before the rest of the electrode. This may be achieved using a polyester substrate with slightly raised portions where the Ag and AgCl layers may be printed. It may also be possible to thicken the ink layers to have the same effect. However this may have adverse effects on the electrical properties of the electrode as AgCl is a poor conductor.

Another approach to the contact problems would be to somehow increase the volume of sweat collected in the region of the sensing surfaces. In other words, the electrode may be incorporated into some kind of sweat collecting device, thus ensuring that a suitable volume of sample comes into contact with the electrodes in all experiments. One such device is available from Wescor Ltd. (Logan, Utah, USA) and is shown in figure 5.21. This device forms part of a CF testing unit which is based on conductivity measurement. The device shown in figure 5.21 is attached to the skin following pilocarpine iontophoresis and draws the sweat through a circular capillary tube into an absorbent disc sealed inside the device.

Figure 5.21 ; Capillary sweat collecting device.

Reducing the size and layout of the electrode, perhaps curving the reference around the ISE, will also improve contact. Some improvements also need to be made with respect to the packaging of the entire device. The seal around the sensing portion is still not ideal although a great deal better than initial attempts. Encapsulating the entire device in a suitable polymeric material will improve this. At present these devices are quite difficult to manufacture reproducibly. Screen printing of the hydrogel and PVC layers should be considered. Experiments suggest that it should be possible to screen print these layers if a screen with a suitable mesh size is chosen.

Finally a data collection system needs to be developed. A hand held monitor which would perform initial calculations and could report results as positive or negative is one possibility.

Although targeted at Cystic Fibrosis detection in this instance, there should be a wide range of applications for this technology, once optimised. Possibilities include analysis of sweat for illegal drugs and their metabolites. Incorporating several ligands onto one device opens up the possibility of multi-sensor arrays. These devices may also be incorporated in flow systems and perhaps targeted at electrolyte analysis in blood or plasma samples. Other sensing systems should also be considered, for example the immobilisation of enzymes to form bio-chemical devices.

5.9 Bibliography

[1] R. Talamo, B. Rosenstein and R. Beringer; in *The metabolic basis of inherited disease, chapter 87, ed. 5,* McGraw-Hill book company, New York.

[2] R.C. Darling, P.A. Di Sant'Agnese, G.A. Perera, et al.; Am. J. Med. Sci., 225 (1953) 67.

[3] L.E. Gibson and R.E. Cooke; Pediatrics, 23 (1959) 545.

[4] V.A. LeGrys; J. Pediatrics, 129 (1996) 892.

[5] L.E. Gibson, P.A. Di Sant'Agnese, H. Shwachman; *Procedure for the quantitative iontophoretic sweat test for cystic fibrosis,* Cystic Fibrosis Foundation, Atlanta, Georgia, USA.

[6] G.J. Moody and J.D.R. Thomas; Ion selective electrode reviews, 2 (1980) 73.

[7] P.M. Tocci and R.M. McKey; Clinical chemistry, 22 (1976) 1841.

[8] O. Schales, S. Schales; J. Biol. Chem., 140 (1941) 879.

[9] B.J. Rosenstein, T.S. Langbaum, E. Gordes, S.W. Brusilow; JAMA, 240 (1978) 1987.

[10] B.J. Rosenstein; J. Respir. Dis., 11 (1990) 519.

[11] M. Gleeson, R. Henry; Clin. Chem., 37 (1991) 112.

[12] W. Highsmith, L. Burch, Z. Zhou; N. Engl. J. Med., 331 (1994) 974.

[13] Frankel; G.A.P. Conference on problems in sweat testing, Hilton Head, S. Carolina, Feb. 6-7, 1975.

[14] Committee for a study for evaluation of testing for Cystic Fibrosis; Pediatrics, 88 (1976) 711.

[15] I. Blanc; J. Invest. Dermatol., 2 (1939) 67.

[16] R.P. Goldbloom, P. Sekelj; N. Engl. J. Med., 269 (1963) 1349.

[17] W. Warwick, L. Hansen; Pediatrics, 36 (1965) 261.

[18] L. Kopito and H. Schwachman; Pediatrics, 43 (1969) 794.

[19] G.J. Moody, P. Bray, G. Clark, J. Thomas; Clin. Chim. Acta, 77 (1977) 69.

[20] M. Green, H. Behrendt, G. Libien; Clin. Chem., 18 (1972) 427.

[21] L.E. Gibson; J. Pediatrics, 81 (1972) 193.

[22] V. Schwarz, C. Sutcliffe, P. Style; Archs. Dis. Childhood, 43 (1968) 695.

[23] **S. Walsh**, D. Diamond; Talanta, 42 (1995) 561.

[24] U. Spichiger, D. Citterio, M. Bott; in a lecture to the European Symposium on optics for Environmental and Public Safety, Munich, June 1995.

Computational Methods

6.1 Introduction.

In the recent past there has been a complete revolution in laboratory personal computing and this is likely to be ongoing as PC prices continue to fall rapidly. The capture and analysis of instrumental data via a computer interface is now becoming the norm in most analytical laboratories. Microsoft is one of the largest software houses in the world and Windows based applications are routinely used. Windows provides an object oriented operating system which can be easily used by people unfamiliar with the intricacies of computer programming i.e. most chemists[1].

6.2 Computer Controlled Data Acquisition.

A transducer may be defined as a device which converts a non-electrical signal into an electrical one. Most phenomena of interest to chemists are not inherently electrical and therefore transducers are commonly used to convert the product of a chemical reaction into some sort of electrical signal which can be easily manipulated. Ion-selective electrodes produce a voltage which can be easily monitored using a conventional high input impedance voltmeter. However, if one could arrange to continuously monitor and save the experimental data, one then opens up the possibilities for the continuous monitoring of analytical processes.

The first problem to be overcome is to convert the analog voltage into a digital form. Data acquisition cards, which are readily available, include an analog to digital converter which converts the analog signal and presents it to the computer via a digital interface.

In order to get these data acquisition cards to function, one also needs appropriate software. Until recently, this required a comprehensive knowledge of high level languages such as C or Quick Basic. Other problems arose when one tried to develop windows based software, as windows compatible drivers were not readily available for data acquisition cards. Therefore, it was only possible to function in a DOS based environment[2]. One new programming approach is to produce an integrated data

acquisition, analysis and presentation package. This problem was addressed by National Instruments Inc., Austin, Texas, USA in their development LabVIEW[3].

6.3 LabVIEW.

LabVIEW is a graphical programming environment specifically designed for applications involving laboratory data acquisition and analysis within the Windows environment. Extensive post run data analysis libraries are available for filtering, transforms and other data processing operations. Dynamic data exchange can be implemented with Windows packages such as EXCEL and therefore post run data analysis may be carried out by spreadsheet.

LabVIEW programs have been used extensively throughout this research. The Flow Injection Analysis system used in the experiments described in Chapter 3 was controlled using a data acquisition card and a virtual instrument* . The front panel of this instrument is shown in figure 6.1. Control of the pump (Minipulse 3, Gilson Medical Electronics Inc., Middleton, USA) was achieved through its built-in computer port. Features such as on/off, forward/reverse and pump speed were controlled by the use of two TTL digital channels and one analog out channel (0-5V) respectively. The panel also contains a switch to trigger the auto injector using another digital control line.

Another virtual instrument was used to determine the peak heights which were used to determine analytical data. This software was used to automatically locate flow injection peaks from a set of saved data and display the peak height in mV.

Finally, in Chapters 4 and 5, a series of experiments relating to solid-state electrodes was described. LabVIEW was once again used to record and save the data produced.

---

* All virtual instruments used in this research were designed by Dr. F. J. Sáez de Viteri at Dublin City University.

Figure 6.1; Front panel of flow injection analysis system used in the experiments described in Chapter 3.

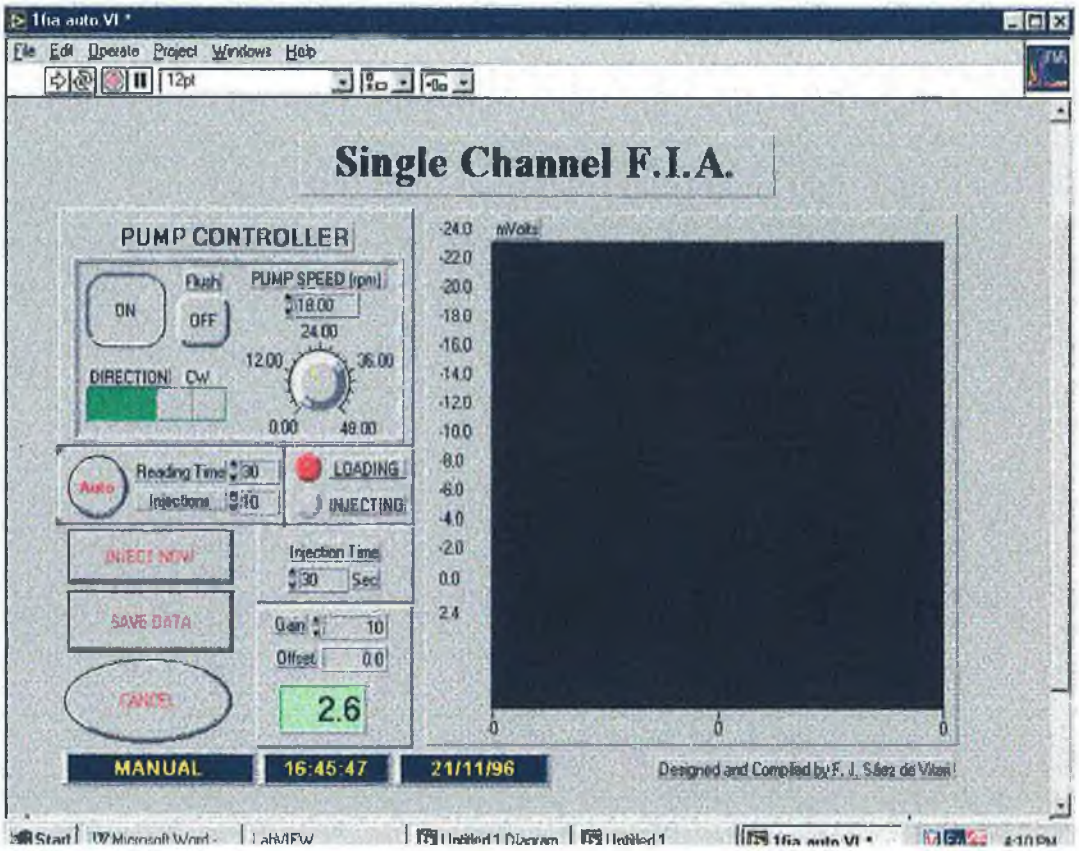

6.4 Data Processing.

Recent trends in data generation, due in part to the computerisation of instrumentation, have led to larger and more complex data sets. Traditional approaches to experimental data processing are largely based on linearisation and/or graphical methods. However, this can lead to problems where the model describing the data is inherently non-linear, or where the linearisation process introduces data distortion (e.g. in standard deviations of data which are logarithmically related to the analyte concentration as with ion-selective electrodes). Hence, with the ready availability of PCs in laboratories, there is increasing interest in applying non-linear curve fitting techniques to experimental data.

Although statistical programs have been available for large main-frame computers for many years, these were often cumbersome to use and the computers were not readily available. Many of these statistical packages have now been converted for PCs, but their application to solving analytical data processing problems is still relatively rare as, although scientifically correct and effective, these packages tend to be engineer-orientated, not especially user-friendly and expensive.

In contrast, many analysts are very familiar with spreadsheets such as Microsoft EXCEL and LOTUS 1-2-3, and several books have appeared recently describing their use as sophisticated calculators for processing, displaying and interpreting scientific data, and as tools for teaching calculations in chemistry[4,5]. The familiar WINDOWS user interface, ready availability (often bundled free with new machines or on site-wide licence) and access to desk-top publishing for integrating text and graphics were the main attractions for Microsoft EXCEL. However, like Lotus 1-2-3, EXCEL was primarily targeted at the business market, and was frustratingly under-developed for scientific applications, particularly in terms of display and data processing tools (e.g. non-linear regression). The balance has been somewhat addressed in recent years, and the appearance of powerful analysis tools such as *solver* makes EXCEL an important addition to the analyst's armoury for processing experimental data[6].

6.4.1 Solver.

Central to the successful application of *solver* is the users depth of understanding of the problem, in contrast to many analytical data processing packages, in particular those bundled with instruments, which often employ a 'black-box' approach. With *solver*, the user must present the raw data in a spreadsheet, enter the model and model parameters correctly, and finally initiate the model building process. Graphical windows enable the dynamics of the model building process to be observed, a feature which can be used to great effect in teaching the principles of data modelling.

The following steps describe the general principles of using *solver* which were used in all of the theoretical and practical examples described later. The data set to be modelled must first be obtained. In the case of theoretical studies, the data are generated by means of the equation of interest. A suitable range of values can be quickly obtained by means of the **edit-fill-down** command. Figures 6.2 and 6.3 show the various procedures involved in finding the solution to a Gaussian peak generated using the well-known equation;

$$f(X) = \mathrm{H}\exp\left[\frac{-(X-\bar{x})^2}{\sigma^2}\right] + \mathrm{B} \qquad \textbf{(6.1)}$$

where;

H = Peak Height above baseline.

X = Point on x-axis.

$\bar{x}$ = Distance along X-axis to peak maximum.

σ = Standard deviation of the peak.

B = Baseline offset from zero.

Figure 6.2 shows the layout of a typical EXCEL spreadsheet prior to using *Solver* using data generated with equation 6.1. Column A contains the x-axis data, and column C Gaussian data generated via equation 6.1 using column A data and known values for the parameters H, $\bar{x}$, σ and B, which have to be found by *Solver*. Column B shows data generated using equation B with the initial starting values of H, $\bar{x}$, σ and B shown in cells G3 to G6. For convenience, these parameters should be entered as named variables in EXCEL using the '***insert-name***' command.

In order to find the solution to the best-fit values of the Gaussian parameters, the user must present a target cell which contains the sum of squared residuals (SSR) between the known data (column C) and the estimated data (column B). The residuals are listed in column D and are obtained by subtracting equivalent cells in columns B and C. Column E contains the squared residuals, and cell G9 the sum of the squared residuals (i.e. the sum of cells E2 to E200). This is the quantity which will be minimised by *Solver*.

Figure 6.2; Typical layout of a solver problem in EXCEL. The data in column C are for the gaussian peak (generated via equation 6.1), and the model is entered in column B. Residual errors are in Column D and their squares are in column E. The named variables used in solver are in cells G3-G6 and the sum of squared residuals (SSR) is in cell G9. Note that $\bar{x}$ is represented by z and σ by S in the named variables list.

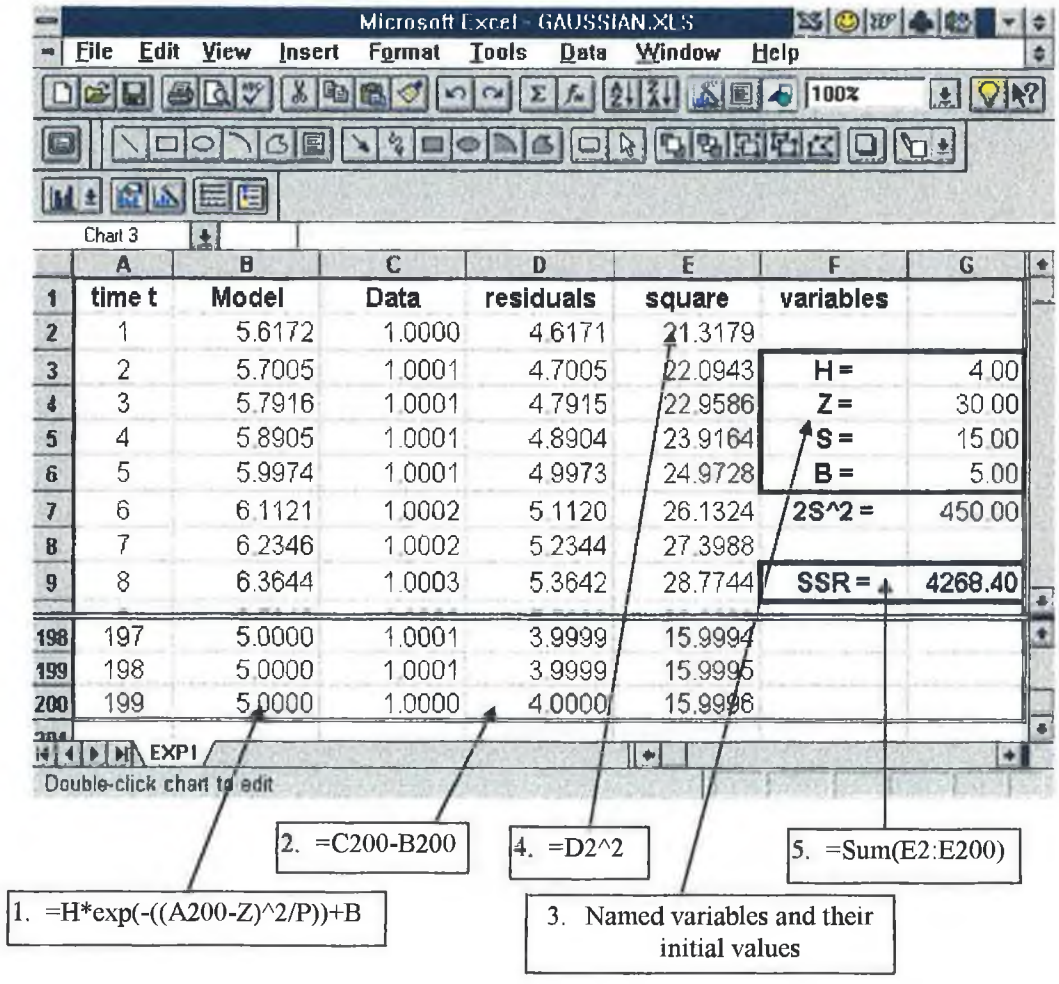

Solver is activated via the ***tools*** menu. On activation, the user is presented with the panel shown in figure 6.3a, which in this case, is set up to solve the Gaussian problem described previously. The user options available are;

A) *Set target cell* specifies the target cell which can be maximised, minimised or set to a certain value. In this case the target cell is ***G9*** and it is set to be minimised.

B) *By changing cells* specifies the cells which will be varied by the search algorithm in order to minimise the number in cell ***G9***, i.e. cells **G3** to **G6** in this example.

C) *Subject to the constraints* : Constraints can be applied by the user to limit the search space explored by the optimisation algorithm. As is usual in iterative search procedures based on gradient-type algorithms, efficiency is best if the search is initiated as near the global solution of the problem, and the unknown variables are restricted in value to realistic ranges. This of course implies that the user has considerable knowledge of the problem prior to initiating the search.

D) *Options* displays the solver options dialog box (figure 6.3b) in which the user can vary more features of the solution process. These are;

E) *Max. time*: limits the time allowed for the search process.

F) *Iterations* limits the number of iterations during the search process.

G) *Precision* : sets the precision of the search process. This will determine the minimum change in the target cell which will cause the search process to stop. The best value for precision varies according to how far from the global optimum the initial search position is, and how smooth the error surface is.

H) *Tolerance*: represents a percentage of error allowed in the optimal solution. A higher tolerance would tend to speed up the solution process but at the expense of accuracy in the final solution.

I) *Assume linear model* will speed up the solution process but obviously should be used only if the relationship is linear.

J) *Estimates* : This specifies the approach used to obtain initial estimates of the variables. Briefly, these are;

- **Tangent -** This uses linear extrapolation from a tangent vector. That is from a tangent, *solver* extrapolates in different directions to identify which gives a minimum for the target cell. This identifies the next direction of the search process.

- **Quadratic -** uses quadratic (i.e. non-linear) extrapolation which can greatly improve results in very non-linear problems at the expense of speed at arriving at an answer.

K) *Derivatives* : Forward and central differencing options exist for estimates of partial derivatives which give the gradient of the search at that point.

L) *Search* : This determines which search algorithm (Newton and Conjugate) is used at each iteration. Both methods are dependent on the calculation of gradient values in the error surface at each stage in the iteration [7,8].

The Newton method typically requires more memory than the conjugate search but requires fewer iterations. The conjugate search is useful if you have a complex problem (multiple model parameters, large data sets) and memory usage is a concern. We have found little difference in using either algorithm to date.

M) *Load/save model* is used when more than one solver model is to be used with the worksheet.

N) *Show Iteration Results* gives the user a complete update of all data after each complete iteration. If the estimated and known data are graphed, the user can observe then a dynamic display of the search process as it proceeds though each iteration. This is very useful in observing visually the progress of the algorithm, but can obviously greatly slow down the process where a large number of iterations are involved. If this option is not exercised, the search process

proceeds automatically, reporting only the value of the target cell after each iteration.

O) *Use Automatic Scaling* This option is useful in situations where data may be distorted through gross differences in the magnitude of various parameters in the search algorithm.

Figure 6.3; (a) initial panel presented to the user when solver is activated via the "tools" menu. (b) the "options" dialog box which opens when activated by the user.

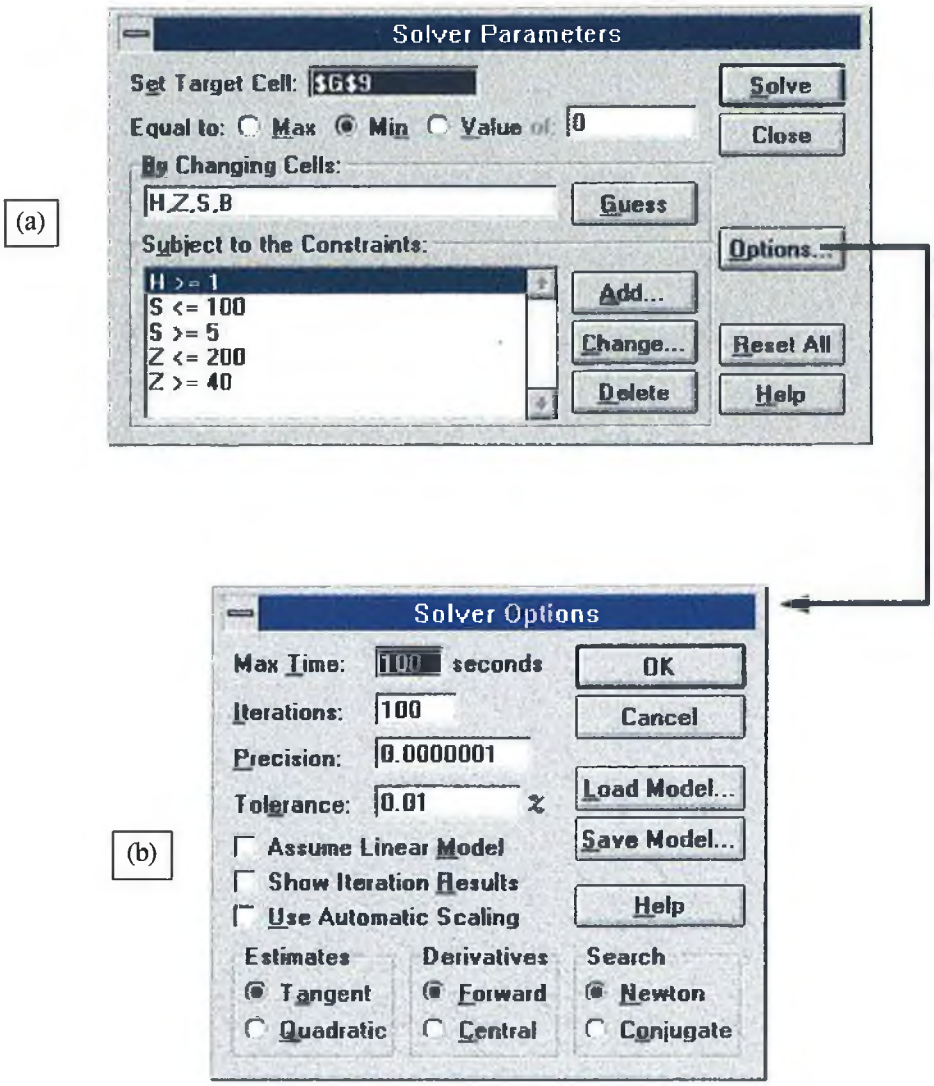

Figure 6.4 shows the results obtained with Solver for the Gaussian problem. Figure 6.4a shows the initial position of the search, with the estimated data being well displaced from the required Gaussian curve. Figure 6.4b shows the final positions of the known and estimated data, illustrating the excellent fit obtained. The values returned by solver for the model parameters (H=10, $\bar{x}$=20, σ =100 and B=1) are equal to the values used to generate the test Gaussian curve.

Figure 6.4; Results returned by solver for the fit to the Gaussian data shown in figure 6.3. (a) The initial positions of the solver data and the Gaussian peak. (b) The final fit to the Gaussian peak obtained using solver.

(a)

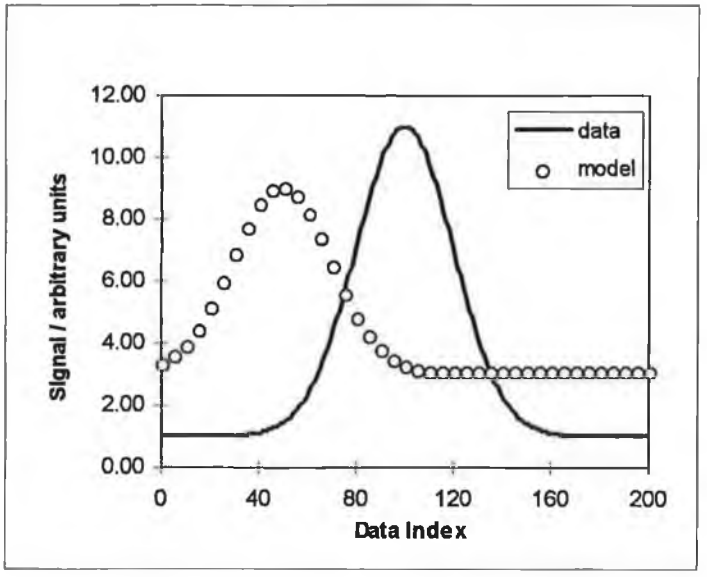

(b)

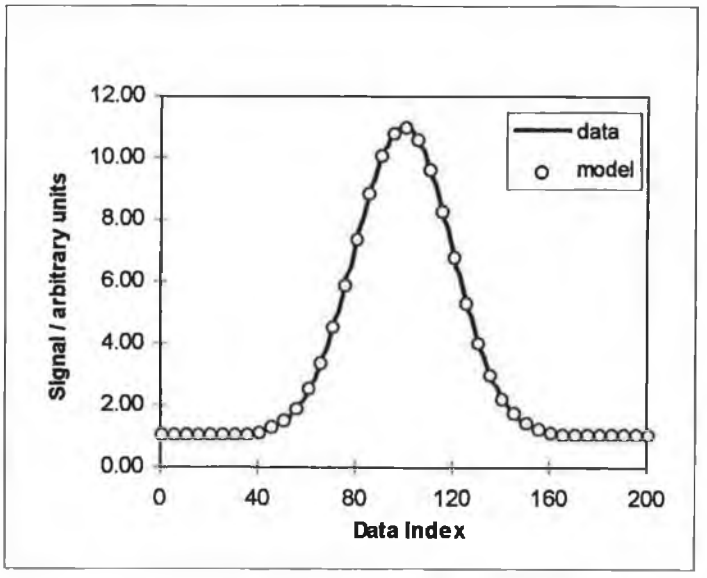

6.4.2 Modelling Experimental Data.

Solver may also be applied to the modelling of experimental data sets which, unlike the theoretical test discussed, will not have exact solutions. However, the validity of the results can be inferred by comparison with results obtained with other optimisation algorithms, through knowledge of the system being studied or through examination of the error of the fit.

Example 1: Modelling of Ion-Selective Electrode Characteristics.

ISEs can be characterised in terms of the Nikolskii-Eisenmann equation below (6.2), in terms of the standard cell potential (E^0), the slope (S), and selectivity coefficients (K_{ij}^{pot}) which describe the effect of various interfering ions (j) on the response of the electrode to the primary ion (i).

$$E = E^0 + S\log(a_i + \sum K_{ij}^{pot} a_j^{z_i/z_j}) \qquad \textbf{(6.2)}$$

where a_i and a_j are the activity of the primary and interfering ions respectively and z_i and z_j are their charges. Approaches such as simplex optimisation and genetic algorithms have been investigated for estimating the electrode characteristics (selectivity coefficients, slopes, cell constants) but these involved extensive program development[9,10]. In this section, *solver* is used to estimate electrode characteristics and the results compared to those produced by both simplex optimisation and genetic algorithm.

In table 6.2 a matrix of ion activities is listed which have been set according to a fractional factorial calibration design[9]. In these experiments four ion-selective electrodes were used, contained within a flow injection detector array, thus making it impossible to use a single ion calibration. Each ion present in each calibration solution will effect the response of all four electrodes in the array. Therefore the calibration procedure must explore these interactions and explain the effect of the

primary ion and interferents. For this reason, a factorial calibration design was chosen. In a factorial design, such as this, the number of factors corresponds to the number of electrodes in the array i.e. 4. In an *f*-factor system, where the interactions are studied at *l* different levels, the number of calibration experiments needed is l^f. Therefore, a high number of experiments are needed to explain all of the occurring interactions. A fractional factorial design studies only the lower order interactions i.e. l^{f-n} where n represents the disregarded higher interactions, but is still able to explain the analytical system with great accuracy. In the calibration set listed in table 6.2, a fractional factorial design was used with ion activities being either high or low (+ or -) in each calibration solution as described in table 6.1. Thus for a four electrode array, 32 solutions were required, 8 of which were targeted at each electrode. Solutions 1-8, table 6.2 are for an ammonium electrode, solutions 9-16 for a sodium electrode, solutions 17-24 for a potassium electrode and solutions 25-32 for a calcium electrode. It can be seen in table 6.2 that the activities were varied slightly within these high and low limits to obtain more information.

Table 6.1 ; Fractional factorial design for a 2^{4-1} system[9].

Experiment Number	Factor 1 level	Factor 2 level	Factor 3 level	Factor 4 level
1	+	+	+	+
2	+	+	-	-
3	+	-	+	-
4	+	-	-	+
5	-	+	+	-
6	-	+	-	+
7	-	-	+	+
8	-	-	-	-

A matrix of electrode responses to this series of calibration solutions is shown in table 6.3.

The Nikolskii-Eisenman parameters for the potassium and sodium electrodes were modelled using the matrix of potentials obtained from the electrode array with the 8 calibration solutions for each electrode Then the validity of the model was evaluated by examining the residuals between the predicted array potentials (calculated via the model parameters and the known activities in table 6.2) and the observed array potentials (table 6.3).

This was done by three different researchers using three different methods; *Genetic algorithm with simplex optimisation*[10] (uses a genetic algorithm to locate the approximate position of the minimum of the error surface, and then switches to a simplex to fine-tune the position of the minimum), *Simplex*[9] (uses the simplex only) and *Solver* - results obtained with *solver*.

A simplex algorithm will search for the minimum (or maximum) of a function by moving along an n-dimensional surface until it reaches a minimum[11,12] (or maximum). A simplex is a geometric figure with the same number of dimensions as the surface it searches. The function is a surface which exists in an n+1 dimensional space, which can be searched by a simplex algorithm to find a local minimum (or maximum), the co-ordinates of which indicate the optimum set of system parameters. In the experiments defined in tables 6.2. and 6.3, the function can be defined as the sum of the square relative difference between the real response of the ISEs obtained from experimental results and the response simulated with a suggested set of parameters.

Genetic algorithms are based on the principles that rule the evolution of living organisms[10]. Viable values of the system parameters are encoded in a series of genes or chromosomes. A finite population of these chromosomes is allowed to breed, mutate and cross over to create the next generation. Genes which encode bad solutions to the problem are gradually eliminated. In the following generations the predominant gene is that which encodes the better solution.

Table 6.4 shows a comparison of fits obtained for the potassium and sodium ISEs by the three different approaches;

The results show good agreement on the values of the cell potential and slope for both electrodes with all three approaches. Furthermore, the values for selectivity coefficient for the main interferent are very close for both electrodes (i.e. around 0.18 for potassium interference on the ammonium electrode and 0.14 for the value of ammonium interference on the potassium electrode). Even the low-valued selectivity coefficients are modelled to around the same value in each case, which is surprising given their relatively minor effect on the fit. The worst case is for the sodium interference on the potassium electrode ($K^{pot}_{K^+,Na^+}$), for which a value could not be obtained with *solver*. However, examination of the values obtained with the other methods show this to be the smallest coefficient with least effect on the fit. These results show that *solver* can obtain good estimates of electrode parameters using the array-FIA calibration design. However, the genetic algorithm performs better and has the added advantage of being an unsupervised search technique (i.e. requires no prior knowledge of the problem). However, considering the ease with which *solver* can be used, it did perform creditably well in this particular task.

Table 6.2; Matrix of Ion-Activities in Calibration Solutions[9,10].

Activities (Molar)				
Solution	**NH_4^+**	**Na^+**	**K^+**	**Ca^{2+}**
1	7.89E-03	7.10E-03	2.37E-03	3.18E-03
2	8.46E-03	2.54E-03	4.23E-04	4.68E-04
3	8.42E-03	8.42E-04	4.21E-03	3.56E-04
4	8.37E-03	4.18E-04	5.02E-04	1.50E-03
5	8.57E-05	6.00E-03	3.43E-03	2.18E-04
6	8.58E-05	4.29E-03	6.86E-04	1.10E-03
7	8.34E-05	1.67E-04	2.50E-03	2.95E-03
8	8.96E-05	2.69E-04	1.79E-04	1.30E-04
9	7.06E-03	7.84E-03	7.06E-03	2.73E-03
10	7.56E-04	8.40E-03	5.04E-03	3.03E-04
11	3.32E-04	8.30E-03	5.81E-04	1.93E-03
12	2.54E-03	8.46E-03	7.61E-04	4.16E-04
13	4.21E-04	8.43E-05	1.69E-03	2.56E-03
14	5.08E-03	8.47E-05	5.93E-03	5.21E-04
15	5.77E-03	8.25E-05	3.30E-04	2.83E-03
16	1.78E-04	8.92E-05	2.68E-04	3.19E-04
17	6.26E-03	6.26E-03	7.83E-03	3.09E-03
18	7.41E-04	4.94E-04	8.23E-03	2.34E-03
19	3.38E-03	6.76E-04	8.45E-03	3.61E-04
20	6.80E-04	2.55E-03	8.50E-03	2.11E-04
21	1.63E-03	7.34E-04	8.16E-05	4.07E-03
22	2.56E-04	3.42E-03	8.54E-05	1.61E-03
23	8.68E-04	4.34E-03	8.68E-05	5.15E-04
24	1.79E-04	3.58E-04	8.95E-05	1.93E-04
25	6.31E-03	5.52E-03	6.31E-04	3.98E-03
26	3.96E-03	5.55E-04	6.34E-03	4.05E-03
27	2.44E-04	8.13E-04	3.25E-04	4.46E-03
28	5.69E-04	8.12E-05	8.12E-04	4.45E-03
29	5.13E-03	5.13E-03	5.98E-04	5.41E-05
30	2.62E-03	6.99E-04	2.62E-03	5.87E-05
31	7.04E-04	1.76E-03	1.76E-03	6.05E-05
32	5.37E-04	4.48E-04	8.95E-05	6.46E-05

Table 6.3; Matrix of Electrodes Responses to Calibration Solutions[9,10].

Measured Potentials / mV				
Solution	**NH_4^+**	**Na^+**	**K^+**	**Ca^{2+}**
1	1.30E+02	1.41E+02	1.43E+02	6.67E+01
2	1.32E+02	1.18E+02	1.17E+02	4.55E+01
3	1.32E+02	1.08E+02	1.54E+02	4.01E+01
4	1.34E+02	7.93E+01	1.22E+02	5.70E+01
5	8.32E+01	1.49E+02	1.50E+02	3.37E+01
6	5.99E+01	1.36E+02	1.13E+02	4.92E+01
7	7.82E+01	7.86E+01	1.41E+02	5.86E+01
8	4.82E+01	6.89E+01	8.15E+01	2.31E+01
9	1.30E+02	1.44E+02	1.58E+02	5.92E+01
10	9.89E+01	1.43E+02	1.54E+02	4.16E+01
11	7.25E+01	1.44E+02	1.07E+02	5.90E+01
12	1.12E+02	1.46E+02	1.16E+02	3.49E+01
13	8.57E+01	6.49E+01	1.32E+02	5.14E+01
14	1.31E+02	8.49E+01	1.57E+02	4.00E+01
15	1.29E+02	4.99E+01	1.13E+02	5.93E+01
16	6.36E+01	4.28E+01	9.74E+01	3.56E+01
17	1.31E+02	1.42E+02	1.65E+02	6.95E+01
18	1.06E+02	1.02E+02	1.67E+02	6.28E+01
19	1.26E+02	9.97E+01	1.61E+02	3.87E+01
20	1.06E+02	1.25E+02	1.64E+02	3.38E+01
21	1.02E+02	8.55E+01	9.27E+01	6.15E+01
22	6.78E+01	1.20E+02	7.00E+01	5.18E+01
23	9.21E+01	1.26E+02	8.07E+01	4.30E+01
24	5.85E+01	5.85E+01	6.85E+01	2.81E+01
25	1.31E+02	1.29E+02	1.22E+02	6.38E+01
26	1.26E+02	1.00E+02	1.61E+02	6.34E+01
27	6.57E+01	8.83E+01	9.36E+01	6.36E+01
28	8.11E+01	5.86E+01	1.18E+02	6.44E+01
29	1.24E+02	1.48E+02	1.19E+02	2.06E+01
30	1.14E+02	9.85E+01	1.45E+02	2.11E+01
31	9.07E+01	1.19E+02	1.34E+02	2.20E+01
32	7.88E+01	8.56E+01	7.64E+01	2.15E+01

Table 6.4; Comparison of Electrode Characteristics for Valinomycin (K^+) and tetramethylacetate p-t-butylcalix[4]arene (Na^+) based ion-selective electrodes obtained by a (i) genetic algorithm followed by simplex (GA-Simplex), (ii) simplex only, and (iii) solver, using the data in Tables 6.2 and 6.3. The sum of the squared residuals (SSR) for each method is also shown. (SSR(8) refers to the squared residuals for the 8 calibration solutions and SSR(32) refers to the squared residuals over the whole solution set).

Electrode Parameter	GA-simplex[10]	Simplex[9]	Solver
Ammonium ISE			
E^0/mV	225.8	225.8	225.1
S/mV/decade	45.4	45.5	45.2
$K^{pot}_{NH_4^+K^+}$	0.185	0.185	0.182
$K^{pot}_{NH_4^+Na^+}$	9.36×10^{-4}	2.09×10^{-3}	5.49×10^{-4}
$K^{pot}_{NH_4^+Ca^{++}}$	6.46×10^{-3}	4.19×10^{-3}	6.04×10^{-3}
SSR (8)	6.313	6.507	6.405
SSR (32)	270.2	228.29	223.3
Potassium ISE			
E^0/mV	270.2	270.5	270.3
S/mV/decade	51.4	51.5	51.5
$K^{pot}_{K^+NH_4^+}$	0.143	0.143	0.140
$K^{pot}_{K^+Na^+}$	$<1.0\times10^{-6}$	4.53×10^{-4}	0.00
$K^{pot}_{K^+Ca^{++}}$	5.36×10^{-3}	5.32×10^{-3}	7.33×10^{-3}
SSR (8)	29.17	30.04	28.97
SSR (32)	497.7	496.3	481.8

Example 2 : Modelling of Ion-Selective Electrode Dynamic Response in Flow-Injection Analysis.

We have also used *solver* to look at the dynamic responses obtained with PVC membrane electrodes in a flow-injection analysis set-up similar to that used in the previous example. One approach is to use a logistic/sigmoid model to characterise the rising portion of the ISE response peak. The equation used is;

$$E(t) = \left[\frac{a}{\left(1 + \exp[b(t-c)]\right)^{e}} \right] + d \qquad \textbf{(6.3)}$$

where;

a= Peak height (mV).
b= Slope coefficient quantifying the rate of increase of the membrane potential.
c = Time from beginning of the peak to the inflexion of the rise (seconds).
d = Baseline offset (mV).
e = Symmetry parameter for the sigmoid.
E(t) = Electrode response at time t (mV).
t = Time (seconds).

This model can give some indication of the rate of ion-uptake at the membrane surface as the sample plug passes and enables comparisons to be made for different experimental situations (varying concentration of the primary ion, effect of interferents, injection volume, flow rate etc.). The model parameters in turn can be used as inputs in a further optimisation of the instrumental operating conditions (e.g. optimise a combination of a, b, and c in terms of flow rate and injection volume). Figure 6.5 shows fits obtained to two valinomycin electrode responses to potassium injections at differing flow rates (1.0 and 0.5 ml/min). The model parameters returned by *solver* for each flow rate are compared in table 6.5.

Figure 6.5; Fit obtained with sigmoid model for the rising portion of FIA peaks obtained with a potassium PVC membrane electrode at 1.0 and 0.5 ml/min flow rates (see table 6.5). Carrier composition : 5 X 10^{-2} M $MgCl_2$, 10^{-6} M KCl. Injection volume 150 µl.

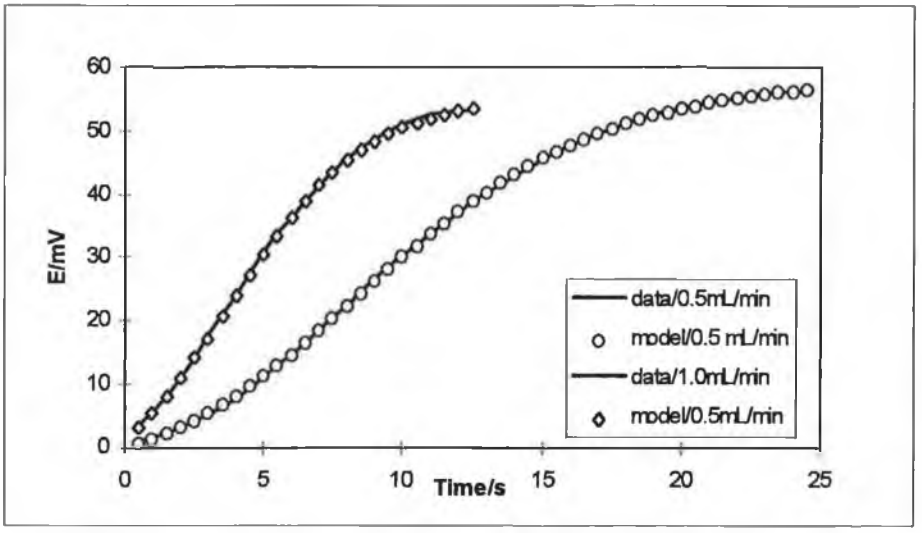

Table 6.5; Model parameters for Sigmoid model of FIA peak rise obtained with Valinomycin ISE in an FIA system at two different Flow Rates (see Figure 6.5). Carrier composition: 5x10^{-2} M $MgCl_2$, 10^{-6} M KCl ; Sample composition: 5x10^{-2} M $MgCl_2$, 10^{-4} M KCl; injection volume: 150 µL.

Model parameters	1.0 ml/min	0.5 ml/min
a / mV	5.70E+01	5.93E+01
b / mV per decade	-1.78E-01	-1.03E-01
c / sec.	4.84E+00	9.59E+00
d / mV	-9.62E-01	-1.14E+00
e	7.49E+00	4.16E+00

From these results we can deduce that increasing the flow rate causes a slight reduction in the peak height (a), an increase in the slope of the rise (given by the increased magnitude of b), a reduced time to the rise inflexion (c almost doubles), and

a less symmetrical rise in terms of the sigmoid model (larger value for e). Characterising peaks in this manner can be very useful for instrumental optimisation purposes as mentioned above and for describing peak shapes in terms of a few simple parameters. This characterisation can be useful for processing large numbers of peaks and for identifying the possible presence of impurities through the definition of a 'typical' analyte peak as possessing these parameters within certain limits.

Example 3: Modelling Chromatography Peaks.

Chromatography (and flow-injection) peaks are characterised by a Gaussian-type shape distorted by tailing which occurs on the falling portion of the peak. Models such as the exponentially modified Gaussian[13,14,15,16] and the tanks-in-series[17,18] have been developed in order to allow this distortion of the standard Gaussian peak shape to be described mathematically. This has important applications in the area of data storage (results can be described mathematically rather than be stored as relatively large ASCII files), and in the analysis of peak purity (e.g. by comparing the shape parameters of experimental peaks to that of a typical peak obtained with the analyte under normal conditions).

Exponentially modified Gaussian model:

The exponentially modified Gaussian function (EMG) is the result of the convolution of a Gaussian function and an exponential decay. In EXCEL this is achieved as follows;

Y(n) represents an unconvoluted Gaussian data array of n points calculated according to equation 6.1. The difference $\Delta Y(m)$ between a point Y(m) and the previous point Y(m-1) is easily obtained by subtracting the appropriate cells. The convoluted set of points, EMG(m) is derived from the Y(m) array as follows;

$$EMG(m) = EMG(m-1) + \left[\frac{Y(m) - EMG(m-1)}{A}\right] \qquad \textbf{(6.4)}$$

$$\text{where } A = \left[\frac{1}{1-\exp(-W_2/\tau)}\right]W_1 \qquad \textbf{(6.5)}$$

for;

τ = time constant of the exponential decay (where a time dependent function is being modelled). W_1 and W_2 = weighting factors, with W_2 normally set at unity and *m* is the data index in the array.

On the spreadsheet, the Gaussian equation (6.1) is first used to create a Gaussian data array over the range of interest. The first point on this array is then set equal to the first convoluted point (EMG(1)). The second EMG point (EMG(2)) can then be calculated via equations 6.4 and 6.5. This procedure is repeated for the entire Gaussian array using the 'edit-fill-down' command in EXCEL.

Tanks in series model:

In this approach, the flow system is regarded as behaving as a series of mixing chambers which serve to distort the initial ideal square wave concentration profile of the sample plug as it travels to the detector. The equation used in this instance is;

$$f(t) = H\left[\left(\frac{1}{T_i(t/T_i)^{N-1}}\right)\times\left(\frac{1}{(N-1)!}\right)\exp(-t/T_i)\right] \qquad \textbf{(6.6)}$$

where:

T_i = Mean residence time of an element of fluid in any one mixing tank (i).

N = number of tanks.

t = Time (x-axis index).

H = scaling factor.

Figure 6.6a-d illustrates the superior performance of the EMG model in describing an experimental HPLC peak. Figure 6.6a shows the best fit obtained with the Gaussian model using *solver* while figure 6.6b and 6.6c shows the equivalent best-fit obtained with the EMG and tanks-in series models respectively. Figure 6.6d compares the residual errors obtained with each model expressed as a percentage of the response maximum and while there is some structure in the EMG residuals, the error is clearly much smaller than that obtained with the other models. The inability of the Gaussian model to cope with the peak tail is demonstrated by the comparatively large residual error for points 22-30 which is much reduced for the EMG residuals.

Figure 6.6: Comparison of (a) Gaussian, (b) exponentially modified Gaussian (EMG), (c) tanks-in series models to an experimental HPLC peak and (d) the residuals obtained for each fit (expressed as a % of the peak maximum). The unit 'Bit-number' refers to the number returned by the I/O card on digitisation of the detector signal.

(a)

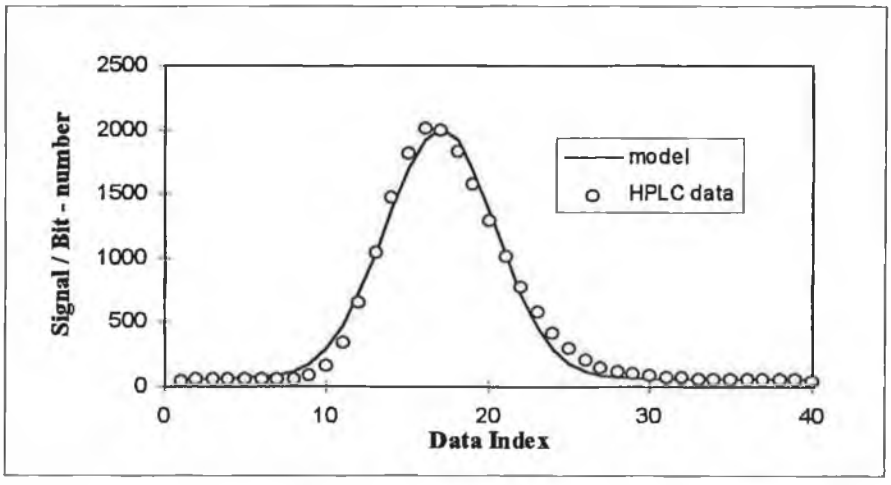

(b)

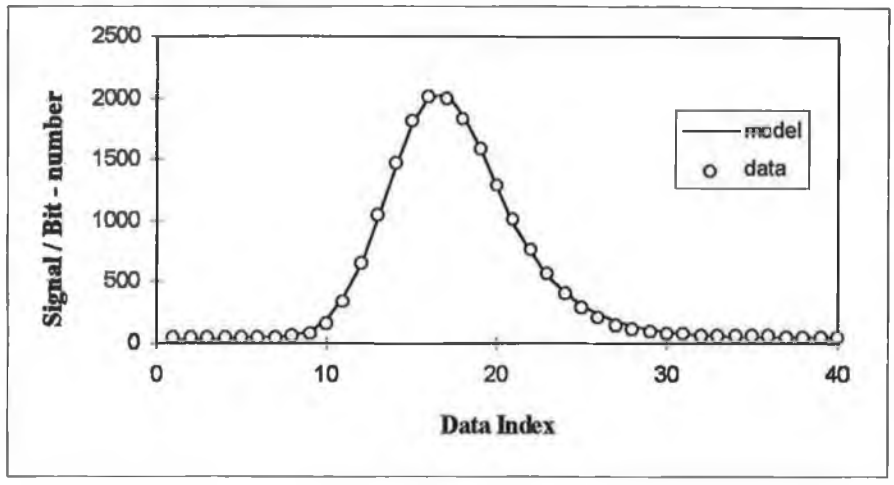
2500
2000
1500
1000
500
0
Signal / Bit - number
0
10
20
30
40
Data Index
model
data

(c)

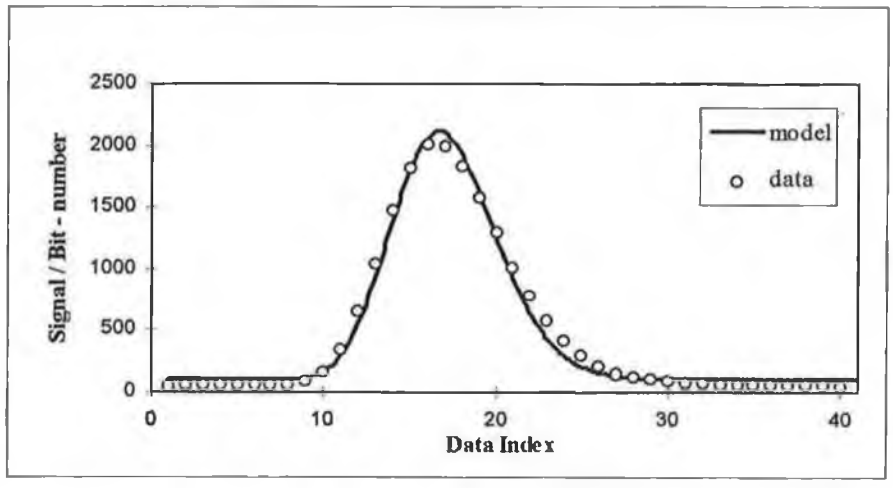
2500
2000
1500
1000
500
0
Signal / Bit - number
0
10
20
30
40
Data Index
model
data

(d)

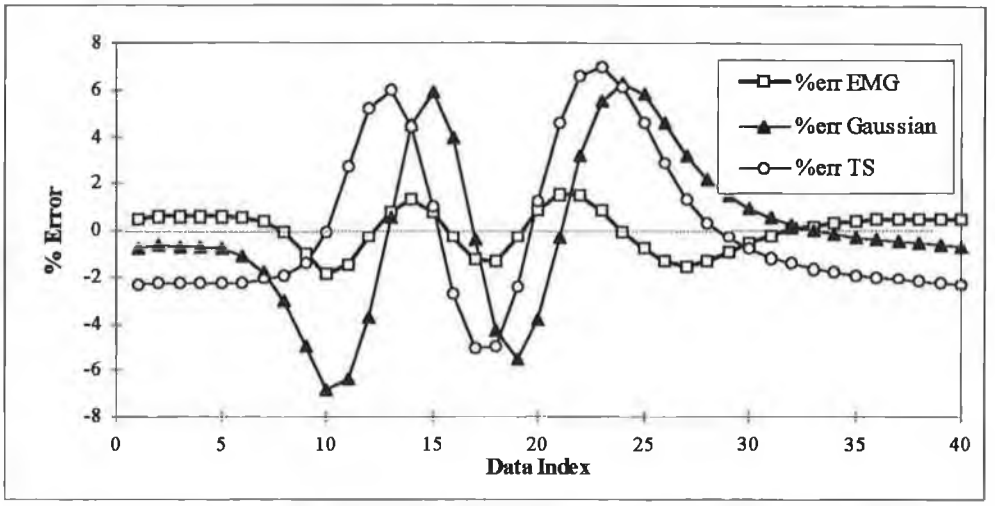

6.5 Conclusion.

In conclusion, *solver* may be used as a tool for mathematical modelling of experimental data. While it is not on a par with custom-written software packages for this purpose such as Mathlab or Mathcad, or with more complex search methods such as genetic algorithms, it is nevertheless, quite a useful aid to data interpretation and an excellent means for introducing non-linear curve fitting into research and teaching. It demonstrates the part that spreadsheet based packages have to play in the interpretation of analytical data. Given the fact that EXCEL is readily available, and familiar to most research and undergraduate students, it can be expected to be quickly adopted by many workers for such applications.

6.6 Bibliography.

[1] J. Zupan; *Data handling in science and technology, Vol.5, PCs for Chemists*; Elsevier Press, New York 1990.

[2] B. Fennema, R.J. Forster, J.G. Vos, G. Hughes, D. Diamond; Trends in Anal. Chem., 12 (1993) 1.

[3] F. J. Sáez de Viteri, D. Diamond; Anal. Proc. Inc. Anal. Comm., 31 (1994) 229.

[4] O. Parker, G. Brennan, *Spreadsheet Chemistry*; Prentice hall, Englewood Cliffs, N. J., 1991.

[5] H. Freiser; *Concepts and Calculations in Analytical Chemistry-a spreadsheet approach*, CRC Press, Boca Raton, 1992.

[6] **S. Walsh**, D.Diamond; Talanta, 42 (1995) 561.

[7] W. Press, B. Flannery, S. Teulolsky, W. Vetterling; *Neumerical Recipes*, Cambridge University Press, New York, 1990.

[8] G. Hostetter, M. Santina, P. D'Carpio-Montalvo; *Analytical, Numerical and Computational Methods for Science and Engineering*, Prentice Hall, Englewood Cliffs, N.J., 1991.

[9] F. J. Sáez de Viteri, D. Diamond; Analyst, 119 (1994) 749.

[10] M. Hartnett; Phd Thesis, Dublin City University, 1994.

[11] D. Diamond, G. Svehla, E. Seward, M.A. McKervey; Anal. Chim. Acta., 204 (1988) 223.

[12] A. Cadogan, D. Diamond, M.R. Smyth, M. Deasy, M.A. McKervey, S.J. Harris; Analyst, 114 (1989) 1551.

[13] E. Grushka; Anal. Chem., 44 (1972) 1733.

[14] J. Foley, J. Dorsey; Anal. Chem., 55 (1983) 73.

[15] R. Delley; Anal. Chem., 57 (1985) 388.

[16] A. Berthod; Anal. Chem., 63 (1991) 1879.

[17] J. Ruzicka, E.H. Hansen; *Flow Injection analysis,* Wiley, New York, 1988.

[18] O. Lee, G. Dumont, P. Tournier, A. Wade; Anal. Chem., 66 (1994) 971.